JOURNAL OF PETROLOGY

Journal of Petrology, 2015, Vol. 56, No. 3, 441–492
doi: 10.1093/petrology/egv006
Advance Access Publication Date: 18 March 2015
Original Article

The Role of Subducted Basalt in the Source of Island Arc Magmas: Evidence from Seafloor Lavas of the Western Aleutians

Gene M. Yogodzinski[1]*, Shaun T. Brown[1,2], Peter B. Kelemen[3], Jeff D. Vervoort[4], Maxim Portnyagin[5], Kenneth W. W. Sims[6], Kaj Hoernle[5], Brian R. Jicha[7] and Reinhard Werner[5]

[1]Department of Earth & Ocean Sciences, University of South Carolina, 701 Sumter St., EWSC617, Columbia, SC 29208, USA, [2]Earth Sciences Division, Lawrence Berkeley National Laboratory, 1 Cyclotron RD, MS 70A-4418, Berkeley, CA 94720, USA, [3]Lamont–Doherty Earth Observatory, Earth Institute at Columbia University, 61 Route 9W, Palisades, NY 10964, USA, [4]School of the Environment, Washington State University, Pullman, WA 99163, USA, [5]GEOMAR Helmholtz Centre for Ocean Research Kiel, Germany, [6]Department of Geology & Geophysics, University of Wyoming, 1000 East University Avenue, Laramie, WY 82071-2000, USA and [7]Department of Geoscience, University of Wisconsin–Madison, 1215 West Dayton Street, Madison, WI 53706, USA

*Corresponding author. E-mail: gyogodzin@geol.sc.edu

Received April 10, 2014; Accepted February 3, 2015

ABSTRACT

Discovery of seafloor volcanism west of Buldir Volcano, the westernmost emergent volcano in the Aleutian arc, demonstrates that surface expression of active Aleutian volcanism falls below sea level just west of 175·9°E longitude, but is otherwise continuous from mainland Alaska to Kamchatka. Lavas dredged from newly discovered seafloor volcanoes up to 300 km west of Buldir have end-member geochemical characteristics that provide new insights into the role of subducted basalt as a source component in Aleutian magmas. Western Aleutian seafloor lavas define a highly calc-alkaline series with 50–70% SiO_2. Most samples have Mg-numbers [Mg# = Mg/(Mg + Fe)] greater than 0·60, with higher MgO and lower FeO* compared with average Aleutian volcanic rocks at all silica contents. Common basalts and basaltic andesites in the series are primitive, with average Mg# values of 0·67 (±0·02, $n = 99$, 1SD), and have Sr concentrations (423 ± 29 ppm, $n = 99$) and La/Yb ratios (4·5 ± 0·4, $n = 29$) that are typical of island arc basaltic lavas. A smaller group of basaltic samples is more evolved and geochemically more enriched, with higher and more variable Sr and La/Yb (average Mg# = 0·61 ± 0·1, $n = 31$; Sr = 882 ± 333 ppm, $n = 31$; La/Yb = 9·1 ± 0·9, $n = 16$). None of the geochemically enriched basalts or basaltic andesites has low Y (<15 ppm) or Yb (<1·5 ppm), so none show the influence of residual or cumulate garnet. In contrast, most western seafloor andesites, dacites and rhyodacites have higher Sr (>1000 ppm) and are adakitic, with strongly fractionated trace element patterns (Sr/Y = 50–350, La/Yb = 8–35, Dy/Yb = 2·0–3·5) with low relative abundances of Nb and Ta (La/Ta > 100), consistent with an enhanced role for residual or cumulate garnet + rutile. All western seafloor lavas have uniformly radiogenic Hf and Nd isotopes, with $\varepsilon_{Nd} = 9{\cdot}1 \pm 0{\cdot}3$ ($n = 31$) and $\varepsilon_{Hf} = 14{\cdot}5 \pm 0{\cdot}6$ ($n = 27$). Lead isotopes are variable and decrease with increasing SiO_2 from basalts with $^{206}Pb/^{204}Pb = 18{\cdot}51 \pm 0{\cdot}05$ ($n = 11$) to dacites and rhyodacites with $^{206}Pb/^{204}Pb = 18{\cdot}43 \pm 0{\cdot}04$ ($n = 18$). Western seafloor lavas form a steep trend in $^{207}Pb/^{204}Pb$–$^{206}Pb/^{204}Pb$ space, and are collinear with lavas from emergent Aleutian volcanoes, which mostly have $^{206}Pb/^{204}Pb > 18{\cdot}6$ and $^{207}Pb/^{204}Pb > 15{\cdot}52$. High MgO and Mg# relative to silica, flat to decreasing abundances of incompatible elements, and decreasing Pb isotope ratios with increasing SiO_2 rule out an origin for the dacites and rhyodacites by fractional crystallization. The physical setting of some samples (erupted through Bering Sea oceanic lithosphere) rules out an origin for their garnet + rutile trace element signature by melting in the deep crust. Adakitic trace element patterns in the dacites and rhyodacites are therefore interpreted as the product of melting of mid-ocean ridge basalt (MORB) eclogite in the subducting oceanic crust. Western seafloor andesites, dacites and rhyodacites define a geochemical end-member that is isotopically like MORB, with strongly fractionated Ta/Hf, Ta/Nd, Ce/Pb, Yb/Nd and Sr/Y. This eclogite component appears to be present in lavas throughout the arc. Mass-balance modeling indicates that it may contribute 36–50% of the light rare earth elements and 18% of the Hf that is present in Aleutian volcanic rocks. Close juxtaposition of high-Mg# basalt, andesite and dacite implies widely variable temperatures in the western Aleutian mantle wedge. A conceptual model explaining this shows interaction of hydrous eclogite melts with mantle peridotite to produce buoyant diapirs of pyroxenite and pyroxenite melt. These diapirs reach the base of the crust and feed surface volcanism in the western Aleutians, but are diluted by extensive melting in a hotter mantle wedge in the eastern part of the arc.

Key words: island arc; isotope; trace element; major element; calc-alkaline; subduction; magnesian andesite; mantle; adakite

INTRODUCTION

The distinctive geochemical signatures observed in rocks produced by subduction magmatism provide an important source of information about the role of subduction systems in the evolution of the solid Earth. The creation of intermediate composition magmas with high Mg relative to Fe [molar Mg/(Mg + Fe), or Mg# >0·50] distinguishes subduction zones from all other tectonic settings in which magmatism is widespread. Trace element patterns in subduction-related magmatic rocks are equally distinctive. The most persistent aspects of these patterns are expressed as enrichments in large ion lithophile elements (K, U, Cs, Rb, Ba), and depletions in middle and heavy rare earth elements (MREE and HREE; Dy, Er, Yb, Lu) and in high field strength elements (HFSE; Ta, Nb, Zr, Hf) compared with mid-ocean ridge basalts (MORB; Pearce & Norry, 1979; Kay, 1980; Gill, 1981). These aspects of subduction-related magmatic systems are broadly significant in the context of solid Earth evolution, because the same geochemical patterns are present in continental crust, and because subduction magmatism is widely inferred to play a key role in the creation of continents (Kelemen, 1995; Rudnick, 1995; Rudnick & Fountain, 1995; Taylor & McLennan, 1995; Wedepohl, 1995).

The subduction-related geochemical characteristics just described are evident in both oceanic subduction zones (island arcs) and continental (Andean-style) systems. For studies aimed at understanding the origins of subduction zone magmas, the advantage of island arc systems stems from the relatively young, thin crust of the overriding plate, and from the common presence of primitive magmas (Mg# >0·60) in oceanic settings. As a result, island arc magmas are less likely to have been significantly affected by shallow processes in crustal-level magma chambers. Island arcs therefore provide our best opportunity to characterize and model the subduction zone processes that initiate arc magma genesis.

A key challenge for this research is to understand the source of island arc magmas, which is known to be a mixture of sub-arc mantle and subduction recycled components that include oceanic basalt, seawater and marine sediment (Armstrong, 1971; Kay *et al.*, 1978; Kay, 1980; Gill, 1981; Arculus & Powell, 1986; Wheller *et al.*, 1987; Morris *et al.*, 1990; Hawkesworth *et al.*, 1993; Plank & Langmuir, 1993; Elliott *et al.*, 1997; Saha *et al.*, 2005). The complex nature of the arc magma source makes it difficult to distinguish trace element signatures imparted by magmatic processes from those that are inherited from recycled, continentally derived sediment. This point is well illustrated by Ba/La, which is nearly always elevated in arc magmas compared with MORB. This difference may be interpreted to result from sediment addition to the arc magma source (Kay, 1980), or as the product of selective transport of Ba over La in aqueous fluids (Tatsumi *et al.*, 1986). These different ideas about processes can lead to very different conclusions about the source of excess Ba in arc lavas, which may be interpreted to lie largely or entirely in sediment in one case, or seawater-altered basalt in the other.

One approach to identifying source components in island arc magmas has been to focus on high-charge elements, such as Th, the REE and HFSE, which have been shown experimentally to be relatively insoluble and therefore not efficiently transported by aqueous fluids (Eggler, 1987; Brenan *et al.*, 1995; Ayers, 1998; Stalder *et al.*, 1998; Kessel *et al.*, 2005). This approach, which aims to simplify the problem by eliminating the aqueous fluids from the source mixture, led to wide acceptance of the idea that high-charge element abundances in arc magmas may be explained as binary mixtures between the sub-arc mantle and a subducted sediment component, which is mobilized in the form of a hydrous, silicate melt (Elliott *et al.*, 1997; Hawkesworth *et al.*, 1997; Class *et al.*, 2000; Walker *et al.*, 2001; Straub *et al.*, 2004; Plank, 2005; Duggen *et al.*, 2007; Singer *et al.*, 2007). Although it is rarely stated, the way this process is modeled implies that subducted basalt makes a negligible contribution of Th, REE and HFSE to arc magmas. A lack of high-charge elements from basalt is also, more explicitly, incorporated in magma source models that call on the selective transport of fluid-mobile elements as the main process controlling trace element patterns in arc magmas (e.g. Perfit *et al.*, 1980; Tatsumi *et al.*, 1986; Miller *et al.*, 1994; Turner *et al.*, 1996; Pearce *et al.*, 1999).

Study of the western part of the oceanic Aleutian arc provides a unique opportunity to unravel the arc magma source, because it is an active island arc in an oblique convergence setting, for which isotopic data indicate that there is little to no subducted sediment in the source of the arc magmas (Yogodzinski *et al.*, 1994, 1995; Kelemen *et al.*, 2003*b*). The western Aleutians therefore provide an opportunity to evaluate the source of high-charge elements in arc magmas, in a place where the source has not been complicated by the addition of recycled continental material.

In a previous contribution (Yogodzinski *et al.*, 2010) we used Hf and Nd isotope data for Aleutian lavas combined with new data on Aleutian–Alaska sediments (Vervoort *et al.*, 2011) to show that sediment-derived Hf is recycled into many Aleutian lavas at a rate similar to that which has been inferred for Pb, Sr and Nd. Here we present new Hf, Nd and Pb isotope and trace element data on an expanded Aleutian sample set, which includes lavas collected by dredging of seafloor volcanoes located west of Buldir Island, the westernmost emergent volcano in the Aleutian arc. The combined datasets display patterns indicating that a significant portion of the Th, Nd and Hf in Aleutian lavas is derived from a geochemical source component that has MORB-like Hf, Nd and Pb isotopes, and a fractionated (adakitic) trace element pattern, with low abundances of Ta, Nb, Y and Yb and elevated Sr, Sr/Y, La/Yb and La/Ta. This source component, which is interpreted to be a hydrous silicate melt derived from subducted, MORB-like basalt in the eclogite facies (e.g. Kelemen *et al.*, 2003*a*, fig. 12), is most clearly expressed in seafloor lavas from the western Aleutians; however, a variety of geochemical patterns, especially expressed in isotope versus trace element ratio plots, indicate that the same component is present in lavas from all parts of the Aleutian arc, as inferred previously (Kay, 1980; Myers & Frost, 1994; Yogodzinski *et al.*, 1995; Yogodzinski & Kelemen, 1998; Kelemen *et al.*, 2003*b*). These results imply that the physical conditions for melting of subducted oceanic crust must exist throughout the Aleutian subduction system, and provide a revised approach to quantifying elemental budgets in the source of subduction-related magmas.

SAMPLES AND DATA

The focus of this study is on late Pleistocene and Holocene age volcanic rocks from seafloor volcanoes located west of Buldir Island (Fig. 1). We present new whole-rock geochemical data for samples collected by dredging from the US R.V. *Thompson* during the 2005 Western Aleutian Volcano Expedition (WAVE), and with the German R.V. *Sonne*, during the June 2009 SO201-1b cruise, under the German–Russian KALMAR project. Sample names, locations and rock types are provided in Table 1.

An important outcome of the WAVE and KALMAR cruises was the discovery of areas of active seafloor volcanism west of Buldir Island, the location of the westernmost emergent volcano in the Aleutian arc (Fig. 1). Most of the samples collected during the WAVE and Aleutian segments of the KALMAR cruise were dredged from the Ingenstrem Depression—a fault-bounded rectangular basin, approximately 60 km long by 10–15 km wide and 2000 m deep, which sits along the crest of the Aleutian ridge, between Attu and Buldir islands (Fig. 1). Seafloor mapping reveals the presence of many small volcanic cones and associated lava flows, in and around the margins of the Ingenstrem Depression (Fig. 2a). The largest cones have base diameters of 2–4 km and are 300–600 m in height. Most appear to be undeformed, constructional volcanic features. Spatial analysis of bathymetric data indicates that there are ~134 volcanic cones in the Ingenstrem Depression, which constitute a combined volume of ~10 km^3—a volume similar to that of single, small, emergent calc-alkaline volcanoes found throughout the arc (White *et al.*, 2007). Western Aleutian seafloor lavas were also dredged from volcanic cones at an unnamed location 300 km west of Buldir Island, which we refer to as the Western Cones area (Fig. 1). This area includes five small cones, aligned along a volcanic front for a distance of ~70 km (Fig. 2b). The largest of the cones, which has a base diameter of 5–10 km and is 600 m high, is similar in size to emergent volcanoes in the western Aleutians, such as Buldir, Kiska and Little Sitkin.

We show here that volcanic rocks from the Ingenstrem Depression and Western Cones have geochemical characteristics that distinguish them from common Aleutian volcanic rocks, and we refer to them collectively throughout this paper as the western Aleutian seafloor lavas, or simply the western seafloor lavas. For these samples we present whole-rock major and trace element data, and isotope ratios for Pb, Nd and Hf. Additional whole-rock trace element and Pb isotope data for lavas collected from emergent Aleutian volcanoes located throughout the arc, for which Hf and Nd isotopes were previously reported (Yogodzinski *et al.*, 2010) are included in the Supplementary Data (supplementary data are available for downloading at http://www.petrology.oxfordjournals.org).

New trace element and Pb, Hf and Nd isotope data are also presented for Adak and Komandorsky area magnesian andesites, which were originally studied by Kay (1978) and later named adakites by Defant & Drummond (1990). These Miocene age rocks were collected from northern Adak Island at the foot of Mt. Moffett, and in dredges from the Komandorsky Straits area (Fig. 1) west of the Komandorsky Islands

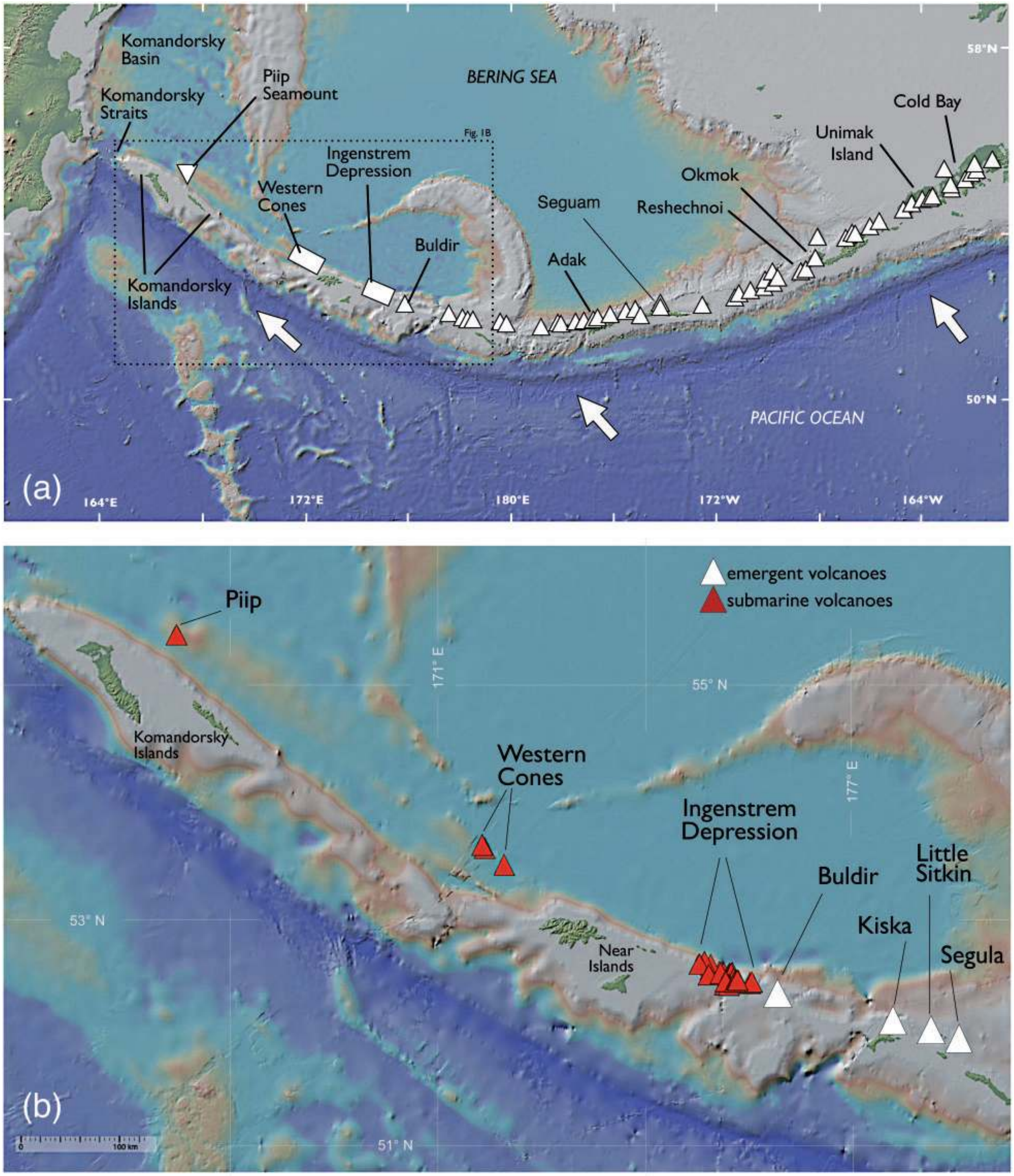

Fig. 1. Maps of the North Pacific and Bering Sea region showing the geographical locations mentioned in text. (a) The whole Aleutian island arc, from the Cold Bay area at the tip of the Alaska Peninsula in the east to the Aleutian–Kamchatka junction in the west. White triangles mark locations of emergent volcanoes. White rectangles mark areas of Western Aleutian seafloor volcanism in the Ingenstrem Depression and at an unnamed location referred to in this paper as the Western Cones area. The inverted white triangle at the western end of the map area marks the location of Piip Seamount. White arrows show the Pacific–North America plate convergence direction. (b) The western Aleutian area only, from Segula volcano in the east to Piip Seamount in the west. White triangles are emergent volcanoes. Red triangles are seafloor volcanoes. (Note the position of the western Aleutian volcanic front, which is offset to the north of the Near and Komandorsky Islands, which mark the axis of thickened arc crust of the western Aleutian ridge.)

Table 1: Sample information

Sample ID	IGSN	Cruise	Location	Rock	Lat. (°N)	Long. (°E)	Depth (m)
TN182_13_005	GMY00004P	WAVE	Ing. Dep.	BA	52·4716	175·3297	−791
TN182_09_003	GMY000043	WAVE	Ing. Dep.	B	52·4343	175·1453	−461
TN182_09_002	GMY000042	WAVE	Ing. Dep.	B	52·4343	175·1453	−461
TN182_09_004	GMY000044	WAVE	Ing. Dep.	B	52·4343	175·1453	−461
TN182_09_005	GMY000045	WAVE	Ing. Dep.	B	52·4343	175·1453	−461
TN182_09_001	GMY000041	WAVE	Ing. Dep.	B	52·4343	175·1453	−461
SO201-1b-21-004		KALMAR	Ing. Dep.	B	52·4690	175·3440	−570
SO201-1b-21-005		KALMAR	Ing. Dep.	B	52·4690	175·3440	−570
SO201-1b-14-007		KALMAR	Ing. Dep.	B	52·5320	175·2150	−1321
SO201-1b-18-002		KALMAR	Ing. Dep.	B	52·5020	175·2220	−967
SO201-1b-14-008		KALMAR	Ing. Dep.	B	52·5320	175·2150	−1321
TN182_06_001	GMY000038	WAVE	Ing. Dep.	B	52·5357	175·0853	−1084
TN182_12_002	GMY00004K	WAVE	Ing. Dep.	B	52·4588	175·2941	−790
TN182_12_001	GMY00004J	WAVE	Ing. Dep.	B	52·4588	175·2941	−790
SO201-1b-14-001		KALMAR	Ing. Dep.	B	52·5320	175·2150	−1321
SO201-1b-15-003		KALMAR	Ing. Dep.	B	52·5130	175·1940	−878
TN182_07_003	GMY00003B	WAVE	Ing. Dep.	B	52·5301	175·2449	−1567
TN182_07_001	GMY000039	WAVE	Ing. Dep.	B	52·5301	175·2449	−1567
SO201-1b-15-001		KALMAR	Ing. Dep.	B	52·5130	175·1940	−878
TN182_08_003	GMY00003M	WAVE	Ing. Dep.	B	52·4842	175·2772	−770
TN182_07_011	GMY00003J	WAVE	Ing. Dep.	B	52·5301	175·2449	−1567
SO201-1b-15-005		KALMAR	Ing. Dep.	B	52·5130	175·1940	−878
SO201-1b-20-012		KALMAR	Ing. Dep.	B	52·4780	175·2970	−795
SO201-1b-16-006		KALMAR	Ing. Dep.	B	52·5140	175·2100	−1015
TN182_08_012	GMY00003V	WAVE	Ing. Dep.	B	52·4842	175·2772	−770
TN182_08_011	GMY00003U	WAVE	Ing. Dep.	B	52·4842	175·2772	−770
SO201-1b-16-007		KALMAR	Ing. Dep.	B	52·5140	175·2100	−1015
TN182_07_007	GMY00003F	WAVE	Ing. Dep.	B	52·5301	175·2449	−1567
TN182_08_009	GMY00003S	WAVE	Ing. Dep.	B	52·4842	175·2772	−770
TN182_07_008	GMY00003G	WAVE	Ing. Dep.	B	52·5301	175·2449	−1567
TN182_08_005	GMY00003O	WAVE	Ing. Dep.	B	52·4842	175·2772	−770
SO201-1b-15-002		KALMAR	Ing. Dep.	B	52·5130	175·1940	−878
TN182_08_013	GMY00003W	WAVE	Ing. Dep.	B	52·4842	175·2772	−770
TN182_08_010	GMY00003T	WAVE	Ing. Dep.	B	52·4842	175·2772	−770
TN182_08_016	GMY00003Z	WAVE	Ing. Dep.	B	52·4842	175·2772	−770
TN182_07_006	GMY00003E	WAVE	Ing. Dep.	B	52·5301	175·2449	−1567
TN182_07_002	GMY00003A	WAVE	Ing. Dep.	B	52·5301	175·2449	−1567

(Continued)

(Scholl *et al.*, 1976; Kay, 1978; Yogodzinski *et al.*, 1995). These samples have distinctive trace element and isotopic characteristics, and are considered key geochemical end-members in several published models of Aleutian magma genesis (Kay, 1980; Myers & Frost, 1994; Yogodzinski *et al.*, 1995; Yogodzinski & Kelemen, 1998; Kelemen *et al.*, 2003*b*).

ANALYTICAL METHODS

Major elements

Rock samples were reduced to powders prior by grinding in agate containers following procedures described by Bryant *et al.* (2010). Samples were prepared for X-ray fluorescence (XRF) analysis by mixing 3·5 g of dry rock powder with 7 g of Li-tetraborate flux. The rock–flux mixtures were melted and quenched in graphite crucibles at 1050°C. The cooled glass beads were ground in a ring mill using a tungsten carbide container, and the resulting powders were fused and quenched in graphite for a second time. One surface of each bead was then flattened on a diamond lap. Finishing of the bead surfaces and XRF analysis was done at the Washington State University Geoanalytical Laboratory. The XRF data are reported on an anhydrous basis with totals recalculated to 100% to improve precision for the major elements. Analytical totals, loss on ignition (LOI) and analytical precision are also reported (Table 2).

Trace elements

Sample digestion procedures for whole-rock trace element analysis by inductively coupled plasma mass spectrometry (ICP-MS) at the University of South Carolina were adapted from the hydrothermal decomposition method of Krogh (1973). Approximately 40 mg of agate-ground rock powder was weighed into 3 ml Teflon capsules. The capsules were covered with loosely fitted lids and positioned in the Teflon inserts of Parr-style steel bombs, containing 5 ml of an HF–HNO_3 mixture (3:1). The bombs were assembled and held in an oven at 150°C for 4–5 days. The digested samples were transferred to 15 ml Teflon capsules using 4–6 ml of 15N HNO_3. The samples were then evaporated to incipient dryness on a hotplate at ~90°C. The dissolution in 15N HNO_3 and evaporation steps were repeated twice more. Samples were then heated gently overnight in 6 ml of a

Table 1: Continued

Sample ID	IGSN	Cruise	Location	Rock	Lat. (°N)	Long. (°E)	Depth (m)
TN182_08_014	GMY00003X	WAVE	Ing. Dep.	B	52·4842	175·2772	−770
SO201-1b-20-007		KALMAR	Ing. Dep.	B	52·4780	175·2970	−795
TN182_08_006	GMY00003P	WAVE	Ing. Dep.	B	52·4842	175·2772	−770
TN182_08_015	GMY00003Y	WAVE	Ing. Dep.	B	52·4842	175·2772	−770
TN182_08_001	GMY00003K	WAVE	Ing. Dep.	B	52·4842	175·2772	−770
TN182_08_002	GMY00003L	WAVE	Ing. Dep.	B	52·4842	175·2772	−770
TN182_08_007	GMY00003Q	WAVE	Ing. Dep.	B	52·4842	175·2772	−770
TN182_08_008	GMY00003R	WAVE	Ing. Dep.	B	52·4842	175·2772	−770
SO201-1b-14-006		KALMAR	Ing. Dep.	B	52·5320	175·2150	−1321
TN182_08_004	GMY00003N	WAVE	Ing. Dep.	B	52·4842	175·2772	−770
SO201-1b-09-002		KALMAR	Ing. Dep.	B	52·5650	174·9440	−880
TN182_13_004	GMY00004O	WAVE	Ing. Dep.	BA	52·4716	175·3297	−791
TN182_13_001	GMY00004L	WAVE	Ing. Dep.	BA	52·4716	175·3297	−791
SO201-1b-09-001		KALMAR	Ing. Dep.	BA	52·5650	174·9440	−880
TN182_13_002	GMY00004M	WAVE	Ing. Dep.	BA	52·4716	175·3297	−791
TN182_13_003	GMY00004N	WAVE	Ing. Dep.	BA	52·4716	175·3297	−791
SO201-1b-09-005		KALMAR	Ing. Dep.	BA	52·5650	174·9440	−880
SO201-1b-10-003		KALMAR	Ing. Dep.	BA	52·5650	174·9560	−980
SO201-1b-10-006		KALMAR	Ing. Dep.	BA	52·5650	174·9560	−980
SO201-1b-10-001		KALMAR	Ing. Dep.	BA	52·5650	174·9560	−980
SO201-1b-10-005		KALMAR	Ing. Dep.	BA	52·5650	174·9560	−980
SO201-1b-10-004		KALMAR	Ing. Dep.	BA	52·5650	174·9560	−980
SO201-1b-20-009		KALMAR	Ing. Dep.	BA	52·4780	175·2970	−795
TN182_05_002	GMY000036	WAVE	Ing. Dep.	BA	52·5202	174·9189	−539
TN182_05_001	GMY000035	WAVE	Ing. Dep.	BA	52·5202	174·9189	−539
SO201-1b-09-007		KALMAR	Ing. Dep.	BA	52·5650	174·9440	−880
SO201-1b-09-003		KALMAR	Ing. Dep.	BA	52·5650	174·9440	−880
TN182_11_004	GMY00004F	WAVE	Ing. Dep.	A	52·4599	175·1580	−398
TN182_10_003	GMY000049	WAVE	Ing. Dep.	A	52·4290	175·2030	−581
TN182_10_002	GMY000048	WAVE	Ing. Dep.	A	52·4290	175·2030	−581
TN182_10_001	GMY000047	WAVE	Ing. Dep.	A	52·4290	175·2030	−581
SO201-1b-09-008		KALMAR	Ing. Dep.	A	52·5650	174·9440	−880
SO201-1b-09-010		KALMAR	Ing. Dep.	A	52·5650	174·9440	−880
SO201-1b-09-011		KALMAR	Ing. Dep.	A	52·5650	174·9440	−880
SO201-1b-09-014		KALMAR	Ing. Dep.	A	52·5650	174·9440	−880
SO201-1b-10-010		KALMAR	Ing. Dep.	A	52·5650	174·9440	−880
SO201-1b-10-011		KALMAR	Ing. Dep.	A	52·5650	174·9440	−880

(continued)

4:1 mixture of 18 MΩ H_2O and 15 N HNO_3. For most samples these steps produced clear solutions, free of visible precipitates. Additional dissolution and drying steps were needed to produce clear solutions for some samples. The solutions were transferred to HDPE bottles and diluted 2000 times the initial powder weight with 18 MΩ H_2O water containing 25 ppb In and 1% HNO_3 by volume. The final solutions were ~80 ml with 2·5% HNO_3 and containing ~500 ppm of dissolved rock.

Concentrations of 26 trace elements were measured at the University of South Carolina on a Varian 820MS quadrupole ICP-MS system. Instrument settings, which are summarized in Table 3, were established to control oxide formation while maintaining a count rate of 200 000 c.p.s. per ppb for Th in a 5 ppb tuning solution, prior to each analytical run. In-run ThO/Th was typically 0·05–0·07 for most standards and unknowns. Average, in-run sensitivity for all elements measured on a BCR-2 rock standard solution is 346 000 c.p.s. per ppb. Sensitivities for all elements are listed in Table 4.

Blank solutions were measured at the beginning and end of each analytical run. Unknowns were bracketed by the USGS reference standard AGV-1, which was analyzed at the start of each run and after every five unknown solutions. Average blanks were subtracted from the raw count rates after correcting for small differences in sample weight and dilution. Count rates for each element were normalized to the internal indium standard. Drift corrections were made using interpolated values measured for the bracketing AGV-1 standards. Drift-corrected count rates for unknown solutions were quantified to ppm rock concentrations against the same AGV-1 solutions as used to make the drift corrections. A correction was applied to the ^{157}Gd peak to remove the effects of the oxide interference from ^{141}Pr. Results for USGS rock standards (BHVO-1, DNC-1, W-2) run as unknowns, with comparisons to reference values from Kelley *et al*. (2003) and from the GeoReM database, are shown in Table 4. Data reported here are corrected against final results for the BCR-2 rock standard, which was included in all runs. Repeat analyses of USGS standards run as unknowns indicate that the average precision for most elements is 2·2–3·2% (Table 4). Standard values used for AGV-1 and BCR-2 (Table 4) are from Kelley *et al.* (2003) and preferred values from the GeoREM database. Results of ICP-MS trace element analyses on unknowns are reported in Table 5.

Table 1: Continued

Sample ID	IGSN	Cruise	Location	Rock	Lat. (°N)	Long. (°E)	Depth (m)
TN182_01_004	GMY00002L	WAVE	Ing. Dep.	A	52·6056	174·9473	−734
TN182_05_003	GMY000037	WAVE	Ing. Dep.	A	52·5650	174·9440	−880
TN182_11_003	GMY00004E	WAVE	Ing. Dep.	A	52·4599	175·1580	−398
TN182_11_001	GMY00004C	WAVE	Ing. Dep.	A	52·4599	175·1580	−398
TN182_11_005	GMY00004G	WAVE	Ing. Dep.	A	52·4599	175·1580	−398
TN182_11_002	GMY00004D	WAVE	Ing. Dep.	A	52·4599	175·1580	−398
TN182_10_004	GMY00004A	WAVE	Ing. Dep.	A	52·4290	175·2030	−581
SO201-1b-20-005		KALMAR	Ing. Dep.	A	52·4780	175·2970	−795
SO201-1b-09-012		KALMAR	Ing. Dep.	A	52·5650	174·9440	−880
70B-29		KALMAR	Ing. Dep.	D	52·6342	174·8567	−750
TN182_03_004	GMY00002U	WAVE	Ing. Dep.	D	52·6342	174·8567	−730
SO201-1b-20-011		KALMAR	Ing. Dep.	D	52·4780	175·2970	−795
TN182_03_001	GMY00002R	WAVE	Ing. Dep.	D	52·6342	174·8567	−730
TN182_03_005	GMY00002V	WAVE	Ing. Dep.	D	52·6342	174·8567	−730
SO201-1b-20-004		KALMAR	Ing. Dep.	D	52·4780	175·2970	−795
TN182_03_008	GMY00002Y	WAVE	Ing. Dep.	D	52·6342	174·8567	−730
TN182_03_007	GMY00002X	WAVE	Ing. Dep.	D	52·6342	174·8567	−730
SO201-1b-20-008		KALMAR	Ing. Dep.	D	52·4780	175·2970	−795
TN182_03_006	GMY00002W	WAVE	Ing. Dep.	D	52·6342	174·8567	−730
TN182_03_002	GMY00002S	WAVE	Ing. Dep.	D	52·6342	174·8567	−730
SO201-1b-11-002		KALMAR	Ing. Dep.	D	52·5450	175·0730	−1058
TN182_03_010	GMY000030	WAVE	Ing. Dep.	D	52·6342	174·8567	−730
TN182_03_009	GMY00002Z	WAVE	Ing. Dep.	D	52·6342	174·8567	−730
TN182_03_003	GMY00002T	WAVE	Ing. Dep.	D	52·6342	174·8567	−730
TN182_07_009	GMY00003H	WAVE	Ing. Dep.	D	52·5301	175·2449	−1567
SO201-1b-13-008		KALMAR	Ing. Dep.	D	52·5360	175·1330	−804
SO201-1b-11-008		KALMAR	Ing. Dep.	D	52·5450	175·0730	−1058
TN182_07_010	GMY00003I	WAVE	Ing. Dep.	D	52·5301	175·2449	−1567
TN182_07_004	GMY00003C	WAVE	Ing. Dep.	D	52·5301	175·2449	−1567
TN182_07_005	GMY00003D	WAVE	Ing. Dep.	D	52·5301	175·2449	−1567
TN182_04_002	GMY000032	WAVE	Ing. Dep.	D	52·6131	174·7802	−250
SO201-1b-13-002		KALMAR	Ing. Dep.	D	52·5360	175·1330	−804
TN182_04_004	GMY000034	WAVE	Ing. Dep.	D	52·6131	174·7802	−250
TN182_01_002	GMY00002J	WAVE	Ing. Dep.	D	52·6056	174·9473	−734
TN182_01_006	GMY00002N	WAVE	Ing. Dep.	D	52·6056	174·9473	−734
TN182_01_008	GMY00002P	WAVE	Ing. Dep.	D	52·6056	174·9473	−734
TN182_01_001	GMY00002I	WAVE	Ing. Dep.	D	52·6056	174·9473	−734

(continued)

Isotopes (Nd, Hf, Pb)

Isotope ratios for Hf, Nd and Pb reported in this paper were determined in laboratories at Washington State University (WSU), the Woods Hole Oceanographic Institution (WHOI), and the University of South Carolina (SCAR). Results reported are corrected to a common set of reference values for isotope standards that are routinely measured in each laboratory. The reference values are shown in the notes at the bottom of Table 6. Analytical procedures used in these laboratories and external precision based on repeat analyses of standards are summarized below. References to publications containing additional analytical information are also provided.

At WSU, samples prepared for Hf and Nd isotope analysis were dissolved in 10:1 HF–HNO_3 mixtures in Parr-style bombs at 160°C for 5–7 days. Following primary decomposition in HF–HNO_3, the samples were treated successively with orthoboric acid and HCl to convert fluoride to chloride complexes. The Hf and Nd were purified using well-established ion chromatography techniques that have been described elsewhere (Patchett & Tatsumoto, 1980; Patchett & Ruiz, 1987; Vervoort & Patchett, 1996; Vervoort & Blichert-Toft; 1999; Münker *et al.*, 2001). Measurements of Hf and Nd isotope ratios at WSU were done on a ThermoFinnigan Neptune multi-collector (MC)-ICP-MS system. Instrumental mass bias was corrected with an exponential law using $^{179}Hf/^{177}Hf = 0{\cdot}7325$ and $^{146}Nd/^{144}Nd = 0{\cdot}7219$. Analyses of the JMC475 Hf and La Jolla Nd standards run throughout the course of this study yielded average values of $^{176}Hf/^{177}Hf = 0{\cdot}282149 \pm 10$ (2SD, $n = 79$) and $^{143}Nd/^{144}Nd = 0{\cdot}511834 \pm 14$ (2SD, $n = 70$). The Hf and Nd isotopic composition of samples are reported relative to the accepted values for these standards ($^{176}Hf/^{177}Hf = 0{\cdot}282160$, Vervoort & Blichert-Toft, 1999; $^{143}Nd/^{144}Nd = 0{\cdot}511859$, Lugmair & Carlson, 1978). Samples for Pb isotope analysis at WSU were prepared from whole-rock powders that were leached by sonicating in 6M HCl followed by rinsing in 18 MΩ H_2O. The leaching step was repeated until the solutions were clear. The leached samples were dissolved in an HF–HNO_3 mixture in sealed Teflon capsules at ~180°C on a hot plate for 24 h. Lead was separated using 0·45 ml Teflon columns and BioRad AG1-X8 anion

Table 1: Continued

Sample ID	IGSN	Cruise	Location	Rock	Lat. (°N)	Long. (°E)	Depth (m)
TN182_01_003	GMY00002K	WAVE	Ing. Dep.	D	52·6056	174·9473	−734
TN182_04_001	GMY000031	WAVE	Ing. Dep.	D	52·6131	174·7802	−250
TN182_04_003	GMY000033	WAVE	Ing. Dep.	D	52·6131	174·7802	−250
TN182_01_005	GMY00002M	WAVE	Ing. Dep.	D	52·6056	174·9473	−734
TN182_01_007	GMY00002O	WAVE	Ing. Dep.	D	52·6056	174·9473	−734
SO201-1b-34-004		KALMAR	W. Cone	RD	53·6240	171·6700	−2829
SO201-1b-36-010		KALMAR	W. Cone	RD	53·4800	171·9540	−3974
SO201-1b-36-004		KALMAR	W. Cone	RD	53·4800	171·9540	−3974
SO201-1b-36-012		KALMAR	W. Cone	RD	53·4800	171·9540	−3974
SO201-1b-36-006		KALMAR	W. Cone	RD	53·4800	171·9540	−3974
SO201-1b-36-007		KALMAR	W. Cone	RD	53·4800	171·9540	−3974
SO201-1b-35-002		KALMAR	W. Cone	RD	53·6490	171·6340	−3955
SO201-1b-36-002		KALMAR	W. Cone	RD	53·4800	171·9540	−3974
SO201-1b-36-001		KALMAR	W. Cone	RD	53·4800	171·9540	−3974
SO201-1b-34-002		KALMAR	W. Cone	RD	53·6240	171·6700	−2829
SO201-1b-34-003		KALMAR	W. Cone	RD	53·6240	171·6700	−2829
SO201-1b-33-001		KALMAR	W. Cone	RD	53·6480	171·6350	−3457
SO201-1b-36-009		KALMAR	W. Cone	RD	53·4800	171·9540	−3974
SO201-1b-36-014		KALMAR	W. Cone	RD	53·4800	171·9540	−3974
SO201-1b-36-005		KALMAR	W. Cone	RD	53·4800	171·9540	−3974
SO201-1b-36-011		KALMAR	W. Cone	RD	53·4800	171·9540	−3974
SO201-1b-36-003		KALMAR	W. Cone	RD	53·4800	171·9540	−3974
SO201-1b-35-005		KALMAR	W. Cone	RD	53·6490	171·6340	−3955
SO201-1b-35-003		KALMAR	W. Cone	RD	53·6490	171·6340	−3955
SO201-1b-34-001		KALMAR	W. Cone	RD	53·6240	171·6700	−2829
SO201-1b-35-001		KALMAR	W. Cone	RD	53·6490	171·6340	−3955
SO201-1b-35-004		KALMAR	W. Cone	RD	53·6490	171·6340	−3955
SO201-1b-36-008		KALMAR	W. Cone	RD	53·4800	171·9540	−3974
ADK04L7			Adak	MA	51·9636	−176·7078	+2
V3841Y2			Kom. Str.	MA	55·668	165·182	−1440
V3841Y3			Kom. Str.	MA	55·668	165·182	−1440
V3842Y2			Kom. Str.	MA	55·682	165·184	−1200
V3842Y3			Kom. Str.	MA	55·669	165·184	−880

IGSN is the international geo sample number. Locations: Ing. Dep., Ingenstrem Depression; W. Cone, Western Cones; Adak, Adak Island; Kom. Str., Komandorsky Straits. Rock types: B, basalt; BA, basaltic andesite; A, andesite; D, dacite; RD, rhyodacite; MA, magnesian andesite/adakite. Negative longitude locations are in the western hemisphere. Negative depth values are below sea level. Sample 70B-29 is from Scholl *et al.* (1976), with location approximately the same as for TN182_03 samples. Sample ADK04L7 is a Miocene-age magnesian andesite (adakite) collected at the base of Mt. Moffett in the same location as ADK-53 from Kay (1978). Samples with V38 identifiers are Miocene-age magnesian andesites (adakites) of Yogodzinski *et al.* (1995) collected from locations close to sample 70B-49 of Scholl *et al.* (1976) and Kay (1978).

exchange resin. The samples were loaded in 0·5M HBr and eluted with 6·0M HCl. Lead samples were then evaporated and treated with concentrated HNO_3 to destroy residual organic materials. Lead isotope measurements were made on the ThermoFinnigan Neptune MC-ICP-MS system using Tl (^{203}Tl/^{205}Tl = 0·41867) to correct for mass bias (White *et al.*, 2000). Final Pb isotope values were normalized relative to the values for NBS981 of Galer and Abouchami (1998). The 2σ external reproducibility of the Pb isotope measurements based on repeat analysis of NBS981 averaged ± 0·0021 (^{206}Pb/^{204}Pb), ±0·0018 (^{207}Pb/^{204}Pb), and ±0·0046 for (^{208}Pb/^{204}Pb) for multiple analytical sessions.

At WHOI, samples were prepared for Pb and Nd isotope analysis from rock powders leached for ~1 h in hot 6·2N HCl, and then rinsed repeatedly with 18 MΩ H_2O. The leached powders were dissolved in a concentrated HF–$HClO_4$ mixture, followed by conversion of fluorides to chlorides by drying down three times in 6·2N HCl. Separation of Nd was done by ion-exchange chromatography in a DOWEX 50 resin, followed by HDEHP-coated Teflon powder (Taras & Hart, 1987). Separation of Pb followed the HBr–HNO_3 procedure of Abouchami *et al.* (1999) using a single column pass. Measurements at WHOI were made on a ThermoFinnigan Neptune MC-ICP-MS system. Neodymium isotope ratios were corrected for instrumental mass bias relative to ^{146}Nd/^{144}Nd = 0·7219 using an exponential law. External precision based on repeat analyses of the La Jolla standard, and after normalization to reference values, is ±15–25 ppm (2σ). Lead isotope ratios were measured using the Tl-normalized method with standard–sample bracketing, following the procedures of White *et al.* (2000). Instrumental mass bias was corrected relative to ^{203}Tl/^{205}Tl = 0·41891. External precision based on repeat analyses of the NBS981 standard is variable from ±17 ppm for ^{207}Pb/^{204}Pb to 117 ppm for ^{208}Pb/^{204}Pb (2σ).

At SCAR, isotope analyses were done on ~200 mg of rock powder that was leached in HCl at ~120°C for 60 min, and then rinsed in 18 MΩ H_2O. Initial sample digestion followed the method described previously for ICP-MS trace element analyses. The digested samples

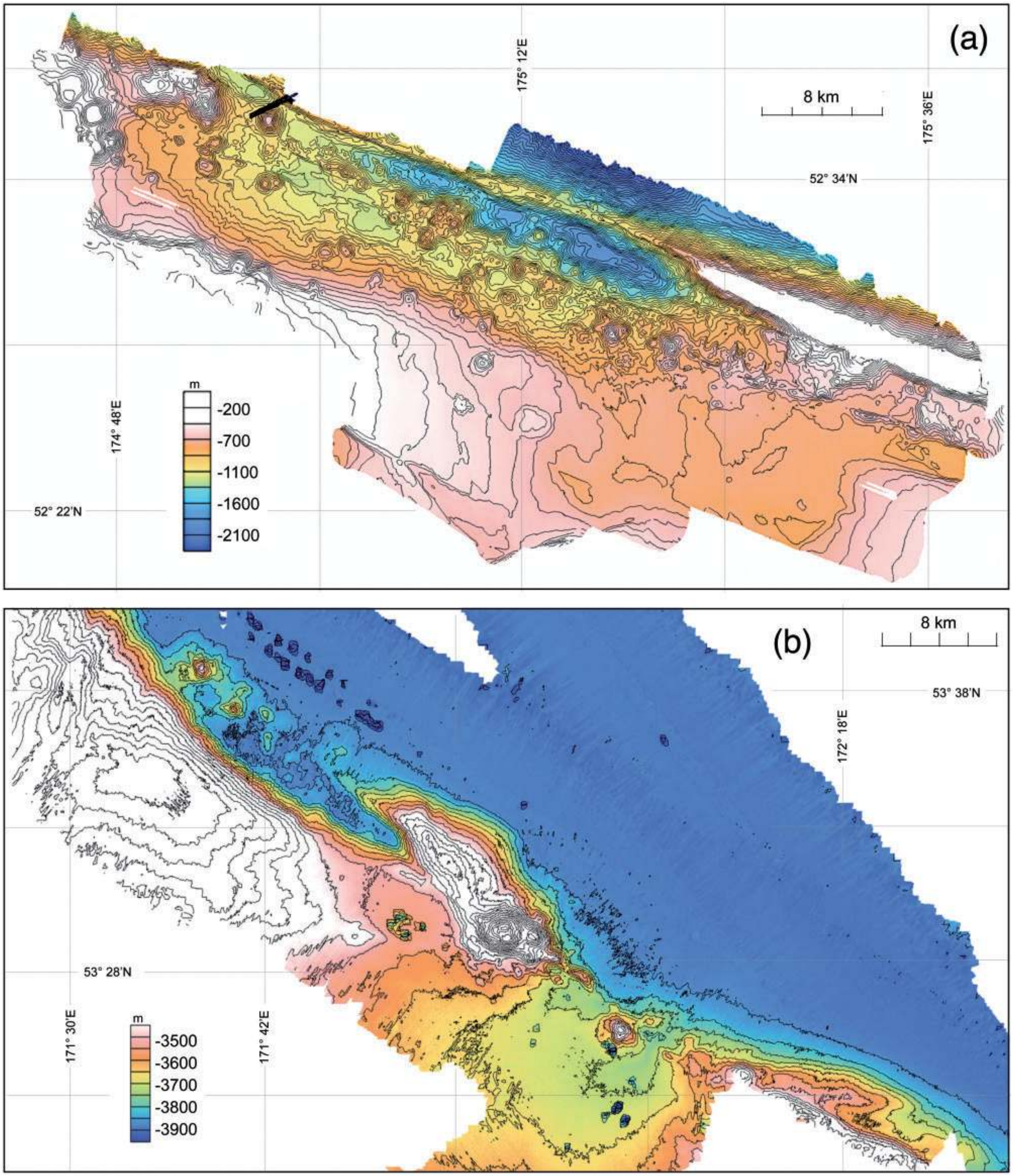

Fig. 2. Seafloor bathymetric maps of showing portions of the western Aleutian arc: (a) the Ingenstrem Depression; (b) the Western Cones area. Contour intervals are 50 m. Regional scale locations of these maps are shown in Fig. 1. Multi-beam data used to produce these figures were recorded on R.V. *Thompson* cruise TN182 and R.V. *Sonne* cruise SO201-1b (Werner & Hauff, 2009).

were transferred to 15 ml PFA capsules using 4–6 ml of 15N HNO_3. The samples were then evaporated to incipient dryness on a hotplate at ~90°C, then re-dissolved in 6N HCl, and evaporated again to incipient dryness. This step was repeated twice more, to convert fluorides to chlorides. The samples were then dissolved in 2 ml of 6N HCl and centrifuged at 40 000 r.p.m. for 10 min. Lead was extracted first, using conventional HBr–HNO_3

Table 2: Whole-rock XRF results

	SiO_2	TiO_2	Al_2O_3	FeO*	MnO	MgO	CaO	Na_2O	K_2O	P_2O_5	LOI	Mg#	Analytical total	Sc	V	Ga	Cr	Ni	Cu	Zn	Rb	Sr	Y	Zr	Ba	Ce
± precision:	0·19	0·012	0·082	0·18	0·002	0·073	0·043	0·036	0·015	0·003				2	5	3	3	4	7	3	2	5	1	4	12	8
TN182_09_003	50·30	0·87	18·10	8·25	0·19	8·80	9·33	3·21	0·77	0·18	0·60	0·66	100·62	32	250	22	266	162	64	89	12	403	18	91	281	24
TN182_09_002	50·33	0·86	18·21	8·27	0·17	8·66	9·33	3·22	0·77	0·18	0·35	0·65	100·80	32	245	20	260	158	62	80	13	404	19	92	277	18
TN182_09_004	50·35	0·86	18·28	8·02	0·18	8·69	9·40	3·27	0·77	0·18	0·87	0·66	98·65	36	242	21	262	152	77	98	12	400	20	91	275	25
TN182_09_005	50·36	0·86	18·07	8·14	0·18	9·00	9·25	3·23	0·74	0·17	0·21	0·66	100·91	32	243	22	277	160	55	78	13	400	18	91	274	18
TN182_09_001	50·41	0·86	18·17	7·97	0·18	8·85	9·36	3·25	0·77	0·17	0·29	0·66	99·59	32	239	20	254	152	77	87	12	398	20	91	277	23
SO201-1b-21-004	50·64	0·83	17·70	7·94	0·16	9·28	9·39	3·22	0·68	0·17	0·36	0·68	99·48	32	225	20	347	174	71	71	12	409	20	97	260	20
SO201-1b-21-005	50·65	0·83	17·66	7·94	0·16	9·30	9·39	3·22	0·68	0·17	0·34	0·68	99·46	31	226	19	345	173	72	73	13	407	19	97	257	17
SO201-1b-14-007	50·72	0·77	15·99	7·90	0·16	10·76	9·57	2·98	0·89	0·25	0·32	0·71	99·43	29	216	17	647	243	79	73	16	540	18	102	389	32
SO201-1b-18-002	51·12	0·83	17·73	7·92	0·16	8·65	9·48	3·23	0·73	0·15	0·33	0·66	100·33	32	229	19	329	141	66	76	12	385	20	93	229	17
SO201-1b-14-008	51·19	0·86	16·53	8·18	0·16	8·16	10·52	3·18	0·96	0·27	0·58	0·64	100·57	33	251	19	231	79	86	73	16	598	20	104	371	39
TN182_06_001	51·31	0·93	17·72	7·62	0·16	8·58	9·12	3·55	0·81	0·20	0·44	0·67	99·86	27	218	21	250	141	62	78	11	447	18	111	226	22
TN182_12_002	51·33	0·83	18·09	7·96	0·16	8·39	9·06	3·27	0·74	0·16	0·26	0·65	100·81	30	217	19	257	140	60	77	12	396	18	96	238	18
TN182_12_001	51·45	0·84	18·20	7·68	0·17	8·25	9·14	3·37	0·74	0·16	0·44	0·66	99·12	31	217	21	247	129	142	89	12	394	19	96	247	20
SO201-1b-14-001	51·59	0·88	16·88	7·87	0·16	7·58	10·63	3·15	0·99	0·26	0·39	0·63	97·28	32	251	19	190	59	92	71	16	581	18	101	363	33
SO201-1b-15-003	51·72	0·74	15·92	7·66	0·15	10·11	9·60	2·99	0·86	0·25		0·70	99·54	29	210	18	557	211	62	70	14	577	18	102	365	34
TN182_07_003	51·75	0·79	18·33	7·56	0·16	7·93	9·08	3·40	0·83	0·17	0·92	0·65	100·42	29	216	21	182	115	74	85	13	435	19	100	282	21
TN182_07_001	51·76	0·79	18·17	7·65	0·16	8·06	9·03	3·41	0·79	0·17	0·51	0·65	99·91	29	213	19	183	117	68	76	13	428	19	98	277	19
SO201-1b-15-001	51·78	0·77	16·40	7·57	0·15	8·92	10·21	3·04	0·89	0·26		0·68	99·56	31	219	19	384	135	84	67	13	598	18	101	369	33
TN182_08_003	51·78	0·72	17·77	7·21	0·15	9·72	8·74	3·15	0·61	0·16	0·20	0·71	99·51	26	194	21	359	223	56	72	11	406	16	89	221	16
TN182_07_011	51·79	0·78	18·27	7·58	0·16	8·07	9·02	3·35	0·81	0·17	0·69	0·65	100·36	29	216	20	194	118	52	72	14	428	17	96	277	20
SO201-1b-15-005	51·79	0·78	16·37	7·62	0·15	8·89	10·15	3·04	0·94	0·26		0·68	98·93	29	222	18	376	137	72	69	13	597	17	102	381	35
SO201-1b-20-012	51·80	0·81	17·23	7·58	0·15	9·35	8·86	3·27	0·77	0·17	0·61	0·69	99·88	27	213	20	358	200	63	76	13	397	18	93	254	17
SO201-1b-16-006	51·81	0·78	16·35	7·60	0·16	8·92	10·12	3·06	0·95	0·26		0·68	99·47	29	218	18	387	139	82	73	15	591	18	103	377	36
TN182_08_012	51·85	0·72	17·71	7·27	0·15	9·59	8·63	3·22	0·68	0·16	0·29	0·70	99·61	24	193	19	366	223	60	73	11	404	16	91	228	12
TN182_08_011	51·87	0·73	17·80	7·27	0·16	9·39	8·71	3·23	0·68	0·16	0·43	0·70	100·35	24	195	22	370	214	56	72	12	414	16	92	232	15
SO201-1b-16-007	51·88	0·78	16·38	7·65	0·16	8·72	10·14	3·07	0·96	0·26	0·49	0·67	99·86	30	222	18	370	129	84	71	16	599	18	105	378	37
TN182_07_007	51·89	0·79	18·36	7·42	0·16	7·97	9·07	3·37	0·80	0·17	0·49	0·66	100·38	28	220	20	186	113	69	80	14	429	17	98	282	23
TN182_08_009	51·90	0·79	18·33	7·33	0·16	8·10	9·03	3·38	0·81	0·17	0·54	0·66	100·25	30	218	22	192	123	52	72	13	428	18	97	278	18
TN182_07_008	51·90	0·79	18·42	7·33	0·16	7·91	9·05	3·46	0·81	0·17	0·75	0·66	100·01	29	216	21	183	112	62	79	13	431	18	99	283	21
TN182_08_005	51·92	0·72	18·26	7·23	0·16	8·69	8·99	3·23	0·64	0·16	0·26	0·68	100·57	26	193	21	313	174	50	72	12	429	16	88	224	14
SO201-1b-15-002	51·92	0·78	16·34	7·55	0·15	9·00	10·08	3·03	0·89	0·26		0·68	100·27	31	223	19	372	136	68	65	13	600	18	104	378	33
TN182_08_013	51·93	0·72	17·89	7·14	0·16	9·30	8·81	3·22	0·68	0·16	0·30	0·70	99·36	26	196	18	339	203	54	70	12	414	15	90	226	20
TN182_08_010	51·93	0·72	18·03	7·24	0·16	8·96	8·91	3·26	0·64	0·16	0·23	0·69	100·06	27	195	20	334	187	72	82	10	425	17	91	232	20
TN182_08_016	51·94	0·73	18·19	7·39	0·16	8·75	8·92	3·18	0·57	0·16	0·20	0·68	101·01	22	195	21	328	177	44	83	9	431	16	89	230	16
TN182_07_006	51·96	0·79	18·39	7·30	0·16	7·93	9·10	3·40	0·79	0·17	0·54	0·66	100·20	29	215	21	182	119	59	74	13	429	18	98	281	20
TN182_07_002	52·01	0·73	17·16	7·49	0·16	9·10	9·12	3·14	0·92	0·16	0·99	0·68	99·16	29	202	19	326	178	61	79	14	404	18	100	292	25
TN182_08_014	52·08	0·72	18·15	7·14	0·16	8·78	8·92	3·25	0·64	0·17	0·86	0·69	99·34	28	194	19	300	179	76	85	11	428	17	90	229	18
SO201-1b-20-007	52·08	0·80	16·88	7·66	0·16	9·58	8·68	3·24	0·74	0·17	1·00	0·69	99·10	27	207	18	354	209	65	75	12	378	18	92	249	18
TN182_08_006	52·09	0·73	18·09	7·25	0·16	8·79	8·88	3·23	0·61	0·16	0·60	0·68	99·39	26	197	20	315	183	56	75	11	424	16	91	230	12
TN182_08_015	52·12	0·73	18·18	7·15	0·15	8·82	8·89	3·22	0·59	0·15	0·44	0·69	100·79	26	195	20	311	185	47	71	10	429	16	90	230	18
TN182_08_001	52·13	0·73	17·89	7·19	0·16	9·04	8·75	3·24	0·70	0·17	0·12	0·69	100·44	25	196	21	321	199	57	73	12	417	16	93	238	17
TN182_08_002	52·17	0·73	18·23	7·11	0·15	8·70	8·85	3·31	0·63	0·12	0·20	0·69	100·43	26	197	21	310	180	28	71	10	430	15	90	232	15
TN182_08_007	52·17	0·73	18·01	7·07	0·16	9·07	8·82	3·18	0·64	0·16	0·38	0·70	100·52	26	197	20	328	196	50	70	11	423	16	91	237	20
TN182_08_008	52·21	0·76	18·13	7·46	0·16	8·20	9·01	3·22	0·69	0·17	0·35	0·66	100·49	27	204	20	270	149	56	71	11	434	17	92	240	14
SO201-1b-14-006	52·26	0·72	16·47	7·38	0·15	9·22	9·49	3·06	0·97	0·26	0·48	0·69	100·34	26	201	18	534	178	75	71	16	592	17	109	393	34
TN182_08_004	52·31	0·73	18·03	7·01	0·15	8·83	8·78	3·32	0·68	0·17	0·56	0·69	100·50	27	195	19	319	188	66	74	12	423	18	95	238	21
SO201-1b-09-002	52·72	1·07	18·49	7·96	0·14	5·49	9·86	3·24	0·85	0·18	0·63	0·55	99·08	32	276	21	37	18	81	73	10	1375	19	88	207	38
TN182_13_004	53·13	0·74	18·08	7·26	0·15	7·59	8·71	3·38	0·80	0·18	0·42	0·65	100·97	26	203	20	215	132	49	73	14	470	16	100	291	17
TN182_13_001	53·19	0·75	18·16	7·17	0·15	7·40	8·77	3·43	0·81	0·18	0·18	0·65	100·64	26	199	20	210	122	63	77	14	470	18	101	297	20
SO201-1b-09-001	53·21	1·03	18·61	7·77	0·13	5·31	9·81	3·24	0·73	0·15	0·81	0·55	97·95	30	264	22	25	16	47	74	10	1372	17	87	209	31

(continued)

Table 2: Continued

	SiO_2	TiO_2	Al_2O_3	FeO*	MnO	MgO	CaO	Na_2O	K_2O	P_2O_5	LOI	Mg#	Analytical total	Sc	V	Ga	Cr	Ni	Cu	Zn	Rb	Sr	Y	Zr	Ba	Ce
± precision:	0·19	0·012	0·082	0·18	0·002	0·073	0·043	0·036	0·015	0·003				2	5	3	3	4	7	3	2	5	1	4	12	8
TN182_13_002	53·25	0·74	18·16	7·16	0·15	7·39	8·78	3·38	0·81	0·18	0·35	0·65	100·51	26	203	21	213	126	56	74	14	467	16	99	292	15
TN182_13_003	53·26	0·74	18·06	7·20	0·15	7·57	8·71	3·35	0·79	0·18	0·40	0·65	101·24	27	201	20	219	134	47	75	14	468	16	100	292	21
TN182_13_005	53·54	0·75	18·08	6·94	0·16	7·41	8·76	3·36	0·83	0·18	0·29	0·66	100·30	27	203	22	207	122	25	73	14	468	17	99	294	17
SO201-1b-09-005	53·79	1·00	18·45	7·51	0·14	5·02	9·70	3·33	0·87	0·20	0·74	0·54	98·59	29	251	21	17	12	65	73	11	1362	18	95	222	42
SO201-1b-10-003	53·91	0·97	18·44	7·93	0·14	4·82	9·37	3·28	0·93	0·21		0·52	99·01	26	243	19	18	13	52	73	12	1319	18	99	225	38
SO201-1b-10-006	54·01	0·98	18·75	7·47	0·16	4·77	9·38	3·34	0·93	0·19	0·88	0·53	98·78	26	246	22	16	15	69	70	11	1320	18	97	232	34
SO201-1b-10-001	54·03	0·96	18·42	7·66	0·19	4·83	9·55	3·27	0·90	0·19		0·53	99·18	26	237	21	13	14	64	74	11	1302	18	100	224	36
SO201-1b-10-005	54·12	0·96	18·34	7·56	0·14	4·88	9·64	3·25	0·92	0·19	0·98	0·54	99·14	28	240	22	13	12	62	74	13	1293	17	99	222	35
SO201-1b-10-004	54·16	0·96	18·50	7·70	0·14	4·74	9·35	3·32	0·95	0·19		0·52	98·84	26	240	21	15	11	37	74	13	1312	18	100	230	34
SO201-1b-20-009	54·78	0·79	18·27	6·72	0·15	6·39	8·02	3·79	0·93	0·17	0·88	0·63	99·34	24	183	20	202	95	12	67	14	391	18	108	266	22
TN182_05_002	55·82	0·71	18·35	6·12	0·15	5·81	8·25	3·64	0·97	0·18	0·71	0·63	99·59	21	165	21	148	87	38	69	15	777	15	110	279	23
TN182_05_001	55·84	0·70	18·40	6·14	0·14	5·79	8·13	3·68	0·99	0·18	0·69	0·63	99·30	22	163	21	141	84	62	77	15	775	16	112	277	26
SO201-1b-09-007	56·04	0·78	18·22	7·17	0·15	4·11	9·27	3·32	0·79	0·17	0·97	0·51	98·34	21	192	22	5	7	69	73	10	1072	17	89	178	25
SO201-1b-09-003	56·38	0·79	19·13	6·97	0·14	3·57	8·53	3·50	0·82	0·18	0·73	0·48	98·35	15	185	20	5	7	71	73	10	1137	16	94	187	26
TN182_11_004	58·05	0·61	18·52	5·46	0·13	4·72	7·28	4·09	0·96	0·17	0·87	0·61	99·10	18	136	19	95	61	52	71	14	509	16	112	266	20
TN182_10_003	58·32	0·80	17·77	6·67	0·16	3·10	7·78	3·10	1·97	0·32	1·35	0·45	99·15	16	183	23	5	22	50	80	22	1287	17	184	433	59
TN182_10_002	58·42	0·80	17·86	6·45	0·14	3·08	7·82	3·13	1·97	0·33	1·27	0·46	99·26	16	190	22	5	20	45	81	21	1279	16	182	423	53
TN182_10_001	58·54	0·80	17·72	6·65	0·13	3·04	7·78	3·23	1·80	0·32	0·74	0·45	98·53	18	184	23	5	15	67	96	20	1246	17	178	415	59
SO201-1b-09-008	58·57	1·10	15·02	5·60	0·11	5·29	7·97	3·51	2·24	0·59	0·91	0·63	98·54	18	175	19	132	107	63	78	49	1776	22	306	426	91
TN182_11_003	60·20	0·76	17·08	4·99	0·11	4·05	7·05	3·60	1·86	0·29	1·40	0·59	99·22	14	141	21	29	67	48	64	16	1803	14	185	357	64
TN182_11_001	60·23	0·77	17·07	4·84	0·10	4·17	7·06	3·61	1·87	0·29	1·57	0·61	98·01	16	141	22	29	69	68	69	17	1741	14	183	349	65
TN182_11_005	60·23	0·76	17·02	5·01	0·10	4·09	7·06	3·58	1·86	0·29	1·47	0·59	98·82	14	142	24	31	69	52	65	16	1769	14	183	353	60
TN182_11_002	60·24	0·77	16·93	4·87	0·11	4·31	7·14	3·52	1·82	0·29	1·34	0·61	99·26	14	144	23	37	78	47	66	16	1752	13	179	349	55
TN182_10_004	61·14	0·90	15·51	4·52	0·09	4·02	7·39	3·64	2·30	0·48	1·40	0·61	98·40	15	163	24	46	61	46	71	42	2256	18	228	622	98
SO201-1b-09-010	61·21	0·49	18·36	4·71	0·11	3·11	6·64	4·30	0·88	0·19	0·30	0·54	99·36	12	100	21	25	15	19	58	11	636	14	113	252	21
SO201-1b-10-010	61·67	0·52	17·36	5·34	0·11	3·23	7·01	3·56	1·07	0·12	1·10	0·52	98·90	16	147	20	36	32	48	59	8	838	10	68	125	9
SO201-1b-10-011	62·00	0·48	17·99	4·73	0·09	2·88	6·38	4·05	1·26	0·16	1·08	0·52	98·25	13	112	20	19	26	89	55	15	868	11	102	216	25
SO201-1b-09-011	62·16	0·52	18·08	4·65	0·10	2·00	6·75	3·99	1·52	0·22	0·25	0·43	98·70	11	117	22	9	8	20	58	22	1107	12	113	439	36
SO201-1b-20-005	62·32	0·79	15·52	4·51	0·08	4·49	6·97	3·71	1·39	0·22	1·15	0·64	98·53	17	133	22	89	76	38	55	14	1755	13	126	219	39
TN182_05_003	62·46	0·60	16·89	4·12	0·09	3·23	6·97	3·98	1·40	0·26	0·30	0·58	99·98	13	117	22	68	54	24	56	16	1429	12	128	428	44
TN182_01_004	62·85	0·55	16·54	4·53	0·10	4·00	6·02	4·11	1·13	0·17	0·41	0·61	98·43	15	114	20	123	68	45	64	13	741	13	102	263	19
SO201-1b-09-012	62·90	0·60	16·73	4·35	0·06	3·51	6·55	4·00	1·10	0·21	0·74	0·59	98·40	15	122	22	47	43	30	44	11	1445	12	102	324	37
SO201-1b-09-014	62·91	0·60	16·75	4·27	0·06	3·50	6·54	4·05	1·11	0·21	0·72	0·59	99·27	14	121	21	50	46	32	46	11	1459	13	104	338	33
70B-29	63·00	0·52	17·5	4·1	0·06	2·9	5·9	3·8	1·2	0·11		0·70														
TN182_03_004	63·57	0·53	17·21	4·08	0·10	2·91	6·23	3·99	1·20	0·19	0·94	0·56	98·95	12	106	20	25	32	33	65	9	969	12	107	282	35
SO201-1b-20-011	63·67	0·62	16·14	3·86	0·07	3·62	6·45	4·02	1·40	0·16	0·84	0·63	98·51	12	107	20	69	57	21	40	10	1259	11	107	201	23
TN182_03_001	63·70	0·59	16·88	4·21	0·09	2·96	6·20	3·99	1·22	0·17	0·38	0·56	99·42	13	113	21	28	34	40	62	11	1088	11	107	243	23
TN182_03_005	63·74	0·60	16·85	4·14	0·08	2·94	6·26	4·02	1·19	0·18	0·31	0·56	100·20	13	112	22	25	34	39	63	11	1160	11	108	233	24
SO201-1b-20-004	63·83	0·61	15·99	3·88	0·07	3·73	6·34	4·03	1·36	0·16	1·15	0·63	97·95	14	106	21	78	57	16	39	10	1242	11	105	197	23
TN182_03_008	63·90	0·58	17·00	3·99	0·08	2·90	6·18	3·98	1·22	0·18	0·35	0·56	99·66	13	112	19	25	33	15	49	11	1069	11	107	240	23
TN182_03_007	63·95	0·60	16·82	3·91	0·08	3·01	6·25	4·00	1·19	0·18	0·25	0·58	100·08	13	114	22	30	33	17	54	11	1143	11	106	232	22
SO201-1b-20-008	63·95	0·60	16·03	3·87	0·07	3·52	6·34	4·05	1·40	0·16	0·87	0·62	98·88	12	105	20	67	55	24	41	11	1271	11	103	208	21
TN182_03_006	64·00	0·60	16·90	3·92	0·08	2·92	6·21	4·00	1·20	0·18	0·23	0·57	100·67	13	115	24	28	35	13	53	11	1164	11	108	233	27
TN182_03_002	64·01	0·59	16·83	3·90	0·08	3·00	6·22	3·95	1·23	0·18	0·41	0·58	99·88	13	112	22	28	34	22	55	9	1140	11	106	231	24
SO201-1b-11-002	64·06	0·50	16·38	3·97	0·09	3·68	5·92	4·01	1·24	0·15	1·22	0·62	99·22	12	94	18	112	71	13	51	16	862	11	103	248	20
TN182_03_010	64·08	0·60	16·86	3·86	0·08	2·92	6·18	4·05	1·20	0·18	0·34	0·57	99·31	13	109	20	26	36	13	49	11	1147	11	107	233	19
TN182_03_009	64·15	0·58	16·95	3·80	0·08	2·82	6·13	4·07	1·23	0·18	0·26	0·57	100·39	12	111	24	25	32	19	43	11	1119	10	108	238	23
TN182_03_003	64·19	0·58	16·91	3·82	0·07	2·81	6·10	4·16	1·17	0·19	0·21	0·57	100·15	8	107	22	23	31	11	36	8	1113	10	106	240	24
TN182_07_009	64·32	0·54	16·08	3·71	0·08	3·62	6·14	3·89	1·45	0·17	1·63	0·64	98·50	12	100	20	64	69	48	56	20	1409	10	120	234	31
SO201-1b-13-008	64·39	0·46	17·00	3·32	0·08	3·24	5·91	4·06	1·35	0·20	0·59	0·63	98·41	9	73	20	55	64	17	50	11	949	11	131	333	24

(continued)

Table 2: Continued

	SiO_2	TiO_2	Al_2O_3	FeO*	MnO	MgO	CaO	Na_2O	K_2O	P_2O_5	LOI	Mg#	Analytical total	Sc	V	Ga	Cr	Ni	Cu	Zn	Rb	Sr	Y	Zr	Ba	Ce
± precision:	0·19	0·012	0·082	0·18	0·002	0·073	0·043	0·036	0·015	0·003				2	5	3	3	4	7	3	2	5	1	4	12	8
SO201-1b-11-008	64·40	0·48	16·62	3·60	0·09	3·48	5·85	4·14	1·18	0·15		0·63	98·89	10	89	18	94	66	16	49	13	878	10	104	254	20
TN182_07_010	64·41	0·54	16·12	3·73	0·08	3·60	6·11	3·84	1·41	0·17	1·82	0·63	98·71	12	101	22	64	67	32	53	20	1418	9	118	238	29
TN182_07_004	64·74	0·52	16·26	3·46	0·07	3·42	6·09	3·98	1·29	0·17	0·32	0·64	99·69	11	96	21	57	63	14	43	12	1446	9	117	239	30
TN182_07_005	64·85	0·51	16·27	3·59	0·08	3·36	5·97	3·90	1·31	0·17	2·05	0·63	98·58	8	94	21	57	60	44	48	20	1449	9	120	242	34
TN182_04_002	65·24	0·59	16·06	3·81	0·07	2·95	5·95	3·90	1·29	0·14	0·22	0·58	98·47	12	107	20	36	45	18	46	7	1245	10	95	144	17
SO201-1b-13-002	65·27	0·45	16·60	3·18	0·08	3·11	5·68	4·03	1·42	0·18		0·64	97·86	9	73	20	45	59	15	51	16	996	10	127	285	27
TN182_04_004	65·35	0·58	15·81	3·68	0·07	3·30	5·92	3·84	1·32	0·14	0·62	0·62	99·63	13	106	22	66	55	28	47	8	1248	9	97	147	18
TN182_01_002	65·57	0·55	15·82	3·71	0·08	2·98	5·42	4·06	1·66	0·16	0·77	0·59	97·39	11	100	20	46	54	36	55	14	1039	10	121	274	31
TN182_01_006	65·84	0·54	15·95	3·54	0·07	2·79	5·33	4·10	1·69	0·16	0·65	0·58	99·13	10	100	22	42	49	38	52	14	1060	11	123	282	26
TN182_01_008	65·86	0·54	15·88	3·55	0·07	2·90	5·34	4·06	1·64	0·16	1·43	0·59	97·63	11	97	21	42	52	46	60	14	1066	10	119	282	25
TN182_01_001	65·94	0·53	15·96	3·36	0·07	2·90	5·35	4·08	1·65	0·16	0·84	0·61	99·86	12	98	22	41	51	58	65	15	1077	10	123	286	31
TN182_01_003	65·99	0·54	15·96	3·46	0·07	2·80	5·32	4·03	1·67	0·16	0·64	0·59	99·82	11	100	22	41	52	38	55	14	1080	9	123	282	27
TN182_04_001	66·16	0·55	15·64	3·31	0·07	3·07	5·66	4·00	1·41	0·14	0·78	0·62	99·21	12	93	20	58	57	47	52	8	1265	9	104	161	18
TN182_04_003	66·30	0·55	15·65	3·28	0·07	3·05	5·64	3·93	1·39	0·14	0·66	0·62	98·85	8	92	20	63	58	23	45	9	1256	9	100	157	20
TN182_01_005	66·33	0·55	15·74	3·29	0·07	2·97	5·57	3·91	1·44	0·13	0·90	0·62	99·07	8	94	20	55	54	29	45	9	1262	9	101	163	19
TN182_01_007	66·39	0·41	16·37	2·90	0·07	2·85	5·28	4·17	1·41	0·14	0·66	0·64	97·56	11	66	18	61	55	40	52	14	973	9	109	252	26
SO201-1b-34-004	68·99	0·53	15·10	1·95	0·03	2·13	5·12	4·30	1·71	0·14		0·66	97·35	6	55	21	51	30	29	38	11	1589	7	127	218	23
SO201-1b-34-003	69·00	0·52	15·12	1·94	0·04	2·15	5·10	4·24	1·76	0·13	2·73	0·66	98·17	7	56	21	52	32	25	36	11	1597	6	127	216	27
SO201-1b-36-007	69·01	0·44	15·53	1·74	0·04	1·82	4·45	4·59	2·26	0·13		0·65	97·64	4	39	21	37	23	7	36	13	1457	5	125	128	16
SO201-1b-36-009	69·02	0·44	15·58	1·70	0·05	1·82	4·44	4·75	2·08	0·13		0·65	97·90	5	42	22	36	24	6	26	27	1457	5	126	131	19
SO201-1b-36-010	69·03	0·44	15·57	1·70	0·04	1·82	4·44	4·71	2·13	0·13		0·65	98·13	5	41	22	38	25	6	27	27	1459	7	125	122	18
SO201-1b-36-006	69·04	0·44	15·49	1·72	0·03	1·82	4·42	4·58	2·35	0·12		0·65	97·20	4	41	21	36	21	8	32	21	1440	7	124	116	17
SO201-1b-34-002	69·05	0·53	15·09	1·94	0·03	2·13	5·11	4·29	1·68	0·14	2·37	0·66	97·88	7	54	20	49	31	36	37	11	1605	7	129	219	27
SO201-1b-36-004	69·07	0·44	15·55	1·69	0·02	1·83	4·41	4·70	2·15	0·12	2·65	0·66	97·50	5	38	20	38	23	7	30	30	1451	6	124	124	19
SO201-1b-34-001	69·07	0·53	15·09	1·95	0·03	2·15	5·13	4·30	1·60	0·14	2·03	0·68	98·20	6	54	20	51	33	31	38	10	1608	7	129	213	27
SO201-1b-36-012	69·08	0·44	15·56	1·71	0·03	1·81	4·44	4·62	2·18	0·13		0·64	98·67	5	42	22	36	23	7	31	11	1458	6	127	123	18
SO201-1b-36-008	69·11	0·44	15·61	1·64	0·03	1·80	4·43	4·69	2·14	0·12	2·41	0·64	98·00	6	41	22	38	23	4	28	28	1461	6	125	120	22
SO201-1b-36-001	69·12	0·44	15·61	1·68	0·02	1·88	4·41	4·76	1·97	0·11		0·66	98·60	5	42	21	36	21	4	29	28	1461	6	125	119	23
SO201-1b-36-014	69·14	0·44	15·59	1·71	0·10	1·82	4·37	4·85	1·86	0·11		0·64	99·17	5	41	23	37	44	12	25	5	1471	6	126	127	16
SO201-1b-36-002	69·15	0·44	15·54	1·67	0·03	1·80	4·41	4·62	2·22	0·13	2·67	0·66	98·24	5	42	21	37	21	8	34	16	1455	6	124	121	18
SO201-1b-36-011	69·16	0·44	15·55	1·74	0·03	1·85	4·38	4·86	1·87	0·12		0·65	99·70	5	42	21	37	25	4	19	5	1475	5	126	125	20
SO201-1b-36-005	69·19	0·44	15·53	1·67	0·03	1·79	4·42	4·64	2·17	0·12	2·59	0·66	98·17	6	41	20	35	22	7	31	10	1461	6	125	126	19
SO201-1b-36-003	69·52	0·44	15·72	1·49	0·03	1·96	4·14	4·65	1·97	0·08	2·99	0·69	98·88	6	43	23	37	25	4	26	15	1469	6	127	115	19
SO201-1b-35-005	69·69	0·44	14·98	1·82	0·04	2·18	4·87	4·22	1·65	0·10		0·68	98·56	7	50	21	60	38	31	33	6	1470	6	98	92	14
SO201-1b-35-002	69·73	0·44	15·02	1·80	0·03	2·15	4·86	4·22	1·65	0·10	1·86	0·66	97·96	6	49	20	55	37	30	34	5	1468	6	97	85	12
SO201-1b-35-003	69·74	0·41	15·01	1·78	0·03	2·14	4·56	4·22	2·01	0·10	2·67	0·68	97·55	7	50	19	48	37	13	30	31	1329	5	94	78	12
SO201-1b-35-001	69·82	0·41	14·98	1·79	0·03	2·15	4·56	4·19	1·97	0·10	2·71	0·68	97·52	6	47	21	46	37	17	30	29	1324	5	92	76	12
SO201-1b-35-004	70·11	0·43	14·99	1·78	0·03	1·82	4·71	4·21	1·80	0·11	2·62	0·64	98·48	6	47	21	42	19	11	36	7	1286	7	102	129	9
SO201-1b-33-001	70·12	0·42	14·97	1·77	0·03	1·82	4·70	4·11	1·95	0·11	2·59	0·66	97·85	5	45	21	40	19	12	39	7	1279	7	101	128	14
ADK04L7	56·35	0·84	15·51	6·03	0·09	6·23	9·91	3·00	1·62	0·42			99·90	21	181	18	341	173	33	61	17	1788	10	150	477	79
V3841Y2	59·70	0·89	15·43	3·38	0·04	4·76	7·48	3·69	2·08	0·39	0·24															
V3841Y3	60·05	0·92	15·52	3·40	0·05	4·52	6·94	3·63	2·22	0·43	0·24															
V3842Y2	60·85	0·83	15·53	3·70	0·05	4·94	7·62	3·83	2·23	0·40	0·28		100·27	12	87	19	168	134	47	53	17	2573	8	183	357	83
V3842Y3	58·88	0·89	15·71	3·37	0·05	4·44	7·32	3·48	2·12	0·38	0·58															

Major element oxide concentrations are in weight per cent on an anhydrous basis and normalized to totals of 100%. Trace elements are in ppm. Analytical precision is at the 2σ level. Additional details about the XRF method may be found at the website of the Washington State University Geoanalytical Laboratory (http://environment.wsu.edu/facilities/geolab/technotes). Major element data for sample 70B-29 are from Scholl *et al.* (1976). Major element data for samples V3841Y2, V3841Y3 and V3842Y3 are from Yogodzinski *et al.* (1995).

Table 3: ICP-MS instrument settings

Flow parameters (l min^{-1})	
Plasma flow	17
Auxiliary flow	1·70
Sheath gas	0·25
Nebulizer flow	1·00
Ion optics (V)	
First extraction lens	−2
Second extraction lens	−173
Third extraction lens	−201
Corner lens	−221
Mirror lens—left	33
Mirror lens—right	23
Mirror lens—bottom	37
Entrance lens	0
Fringe bias	−2·3
Entrance plate	−40
Pole bias	0
Scanning	
Scan mode	peak hopping
Points/peak	1
Scans/replicate	15
Replicates/sample	3
Dwell time (μs)	10000
Sampling/autosampler (s)	
Sample uptake	60
Stabilization delay	150
Rinse	180
Other settings	
Sampling depth (mm)	5·0–5·5
RF power (kW)	1·40
Pump rate (r.p.m.)	4–6

Varian model 820 quadrupole ICP mass spectrometer settings used for whole-rock trace element measurements.

methods, with 0·1 ml of anion exchange resin (BioRad AG-1 8X) in Teflon micro-columns. Washes left from the Pb chemistry were dried and re-dissolved in 2·5N HCl. The REE were separated from these using ~5 ml of cation exchange resin (Dowex 50W-8X) in Teflon columns. Measurements at SCAR were made on the ThermoFinnigan Neptune Plus MC-ICP-MS system, in the Center for Elemental Mass Spectrometry. Isotope ratios for Nd were corrected for instrumental mass bias relative to ^{146}Nd/^{144}Nd = 0·7219 using an exponential law. Repeat analyses of the La Jolla standard, which were made at the same time as analyses of the samples, produced an average of ^{143}Nd/^{144}Nd = 0·511835 ± 11 (2σ, $n = 8$). Lead isotope ratios were measured using the Tl-normalization method with standard–sample bracketing, following the procedures of White *et al.* (2000). Thalium spiking was done to produce ^{205}Tl–^{208}Pb ratios in the sample solutions as close as possible to those of the NBS981 Pb isotope standard. Instrumental mass bias was corrected relative to ^{203}Tl/^{205}Tl = 0·41891. The 2σ external precision, based on repeat analyses of the NBS981 standard, is ±0·0016 for ^{206}Pb/^{204}Pb, ±0·0021 for ^{207}Pb/^{204}Pb, and ±0·0063 for ^{208}Pb/^{204}Pb (2σ).

^{40}Ar/^{39}Ar geochronology

Incremental heating experiments for ^{40}Ar/^{39}Ar age dating were undertaken on groundmass from five Ingenstrem Depression lavas. Groundmass separates were prepared, weighed, and then irradiated at the Oregon State University TRIGA reactor in the Cadmium-Lined In-Core Irradiation Tube for 1 h. All age data presented here are calculated relative to 28·02 Ma for the Fish Canyon sanidine monitor (Renne *et al.*, 1998); the decay constants used are those of Steiger & Jäger (1977). Furnace incremental heating experiments were performed on 200 mg of groundmass following the methods of Jicha *et al.* (2012). All argon isotope analyses were done using a MAP 215-50; the data were reduced using ArArCalc software version 2.5 (http://earthref.org/ArArCALC/). The age uncertainties reported in Table 7 and Fig. 3 reflect analytical contributions (including J uncertainty) at the 2σ level.

RESULTS

^{40}Ar/^{39}Ar ages

Results from the incremental heating experiments are summarized in Table 7. Representative age spectra and isochrons and complete analyses for each experiment are shown in Fig. 3 and in the online Supplementary Data. All experiments define statistically acceptable plateaux comprising >97% of the gas released, and have isochrons with trapped ^{40}Ar/^{36}Ar ratios that are indistinguishable from the atmospheric ^{40}Ar/^{36}Ar ratio of 295·5 (Steiger & Jäger, 1977). Thus, we consider the plateau ages to give the best estimate of the time elapsed since eruption. Ages of the Ingenstrem Depression lavas range from 17 to 521 ka (Table 7). Large uncertainties associated with several of the ^{40}Ar/^{39}Ar ages are a result of young samples with relatively low K$_2$O contents and that therefore contain little radiogenic ^{40}Ar.

Major elements

Seafloor lavas from the Ingenstrem Depression and Western Cones areas are primarily basalts, dacites and rhyodacites. Basaltic andesites and andesites are present among the dredge samples, but they are relatively few in number and are more geochemically variable than lavas with both higher and lower silica. This pattern of geochemical variability is well illustrated for K$_2$O, which generally increases systematically with increasing silica in the seafloor lavas, but is highly variable between 55 and 63% SiO$_2$ (Fig. 4a). The samples are widely variable in SiO$_2$ (50–70%) but all have Mg# values greater than 0·55 (Fig. 4b). As a result, the Ingenstrem and Western Cones lavas describe a highly calc-alkaline igneous series based on the criteria of Miyashiro (1974), who defined calc-alkalinity in the context of whole-rock FeO*/MgO relative to SiO$_2$ (Fig. 4b). Zimmer *et al.* (2010) defined the tholeiitic index (THI) as an alternative measure of calc-alkalinity. On this basis, which considers the relative FeO* and MgO abundances without regard to SiO$_2$, the Ingenstrem and Western Cones lavas are also highly calc-alkaline, with a THI of 0·6, which is low (a more Fe-depleted series) compared with the values of 0·7–1·1 that are commonly observed in arc volcanic rocks igneous series (THI values >1 show enrichment in Fe and so are tholeiitic;

Table 4: Standard results for whole-rock ICP-MS trace elements

Element	Mass	Primary standard	Primary standard		Standard run as unknown				Standard run as unknown			Standard run as unknown			
		AGV1	BCR-2	BCR-2 Sens/ 1000	BHVO-1 Ref. values*	BHVO-1 Ref. values†	BHVO-1 Mean (*n* = 20)	BHVO-1 %RSD	DNC-1 Ref. values*	DNC-1 Mean (*n* = 20)	DNC-1 %RSD	W-2 Ref. values*	W-2 Ref. values†	W-2 Mean (*n* = 20)	W-2 %RSD
Rb	85	66·6	46·9	344	9·2	9·19	9·41	6·3	3·9	4·06	16·8	22·0	21·00	18·71	4·4
Sr	88	660	340	407	399	396	396	3·0	145	145	3·1	197	196	198	3·0
Y	89	19·0	37	334	27·1	26	26·6	1·8	17·7	17·5	2·0	21·9	22	21·9	1·9
Zr	90	231	184	340	184	174	168	1·0	36·9	34·0	2·2	93	92	89	5·2
Nb	93	14·6	12·6	262	19·7	18·6	18·7	1·4	1·47	1·52	1·1	7·7	7·5	7·3	2·7
Cs	133	1·26	1·1	381	0·097	0·101	0·091	3·3	0·207	0·198	2·9	0·902	0·920	0·857	4·2
Ba	137	1200	677	406	133	133	129	1·8	103·3	100	2·1	172	172	169	1·9
La	139	38·7	24·9	381	15·7	15·5	15·3	2·4	3·56	3·68	2·8	10·1	10·8	10·6	2·3
Ce	140	69	52·9	412	37·8	38·1	37·6	1·9	8·11	8·14	2·2	22·8	23·4	23·1	2·4
Pr	141	8·5	6·7	418	5·4	5·42	5·28	1·4	1·12	1·08	1·7	3·0	3·00	2·98	2·2
Nd	146	32·3	28·7	408	24·8	24·7	24·6	1·6	4·98	4·93	1·5	12·9	13·0	13·0	2·0
Sm	147	5·82	6·58	392	6·1	6·12	6·06	1·9	1·43	1·41	1·9	3·2	3·30	3·30	2·3
Eu	153	1·73	1·96	414	1·98	2·09	1·98	1·7	0·57	0·573	2·2	1·10	1·08	1·08	2·0
Gd	157	4·9	6·75	417	6·56	6·33	6·17	2·0	2·11	2·01	2·6	3·73	3·66	3·72	3·3
Tb	159	0·706	1·07	382	0·948	0·96	0·942	1·7	0·399	0·377	2·1	0·632	0·62	0·620	2·6
Dy	163	3·78	6·41	364	5·37	5·31	5·26	2·3	2·76	2·72	2·6	3·83	3·79	3·86	2·8
Ho	165	0·698	1·28	359	1·01	0·98	0·95	1·7	0·62	0·602	2·1	0·80	0·79	0·78	3·0
Er	166	1·87	3·66	359	2·38	2·55	2·38	1·6	1·87	1·76	1·7	2·17	2·22	2·12	2·6
Tm	169	0·265	0·54	337		0·33	0·321	1·8		0·276	2·1		0·33	0·315	3·2
Yb	172	1·7	3·38	351	2·01	2	1·98	2·5	1·97	1·90	2·1	1·98	2	2·06	3·1
Lu	175	0·262	0·503	330	0·29	0·27	0·274	2·9	0·32	0·290	2·4	0·30	0·31	0·304	3·3
Hf	178	5·17	4·90	309	4·49	4·46	4·29	1·7	0·995	0·943	2·9	2·48	2·45	2·42	5·6
Ta	181	0·87	0·74	284	1·21	1·21	1·10	1·9	0·095	0·083	2·2	0·50	0·47	0·44	3·9
Pb	208	37	11	188	2·06	2·4	2·12	3·7	6·2	5·90	4·2	7·70	7·7	7·88	6·0
Th	232	6·5	5·7	204	1·25	1·23	1·16	1·9	0·24	0·229	5·8	2·10	2·17	2·12	4·7
U	238	1·92	1·69	201	0·408	0·409	0·417	2·3	0·05	0·055	7·5	0·490	0·510	0·510	2·9
Average				346				2·2			3·2				3·2

*Reference values from Kelley *et al.* (2003).

†July 1011 GeoREM preferred reference values.

Table 5: Whole-rock ICP-MS trace element results (ppm)

	Rb	Sr	Y	Zr	Nb	Cs	Ba	La	Ce	Pr	Nd	Sm	Eu	Gd	Tb	Dy	Ho	Er	Tm	Yb	Lu	Hf	Ta	Pb	Th	U
TN182_09_003	12·1	399	19·2	93·0	1·37	0·43	281	9·0	21·3	3·16	14·7	3·67	1·15	3·70	0·575	3·44	0·703	1·92	0·285	1·89	0·293	2·66	0·096	2·74	1·17	0·66
TN182_09_002	13·5	408	19·8	91·8	1·50	0·42	275	8·9	21·1	3·03	14·2	3·60	1·13	3·56	0·549	3·27	0·647	1·79	0·271	1·84	0·275	2·40	0·093	3·34	1·08	0·61
TN182_09_004	12·2	402	19·5	96·0	1·40	0·43	282	9·4	22·0	3·26	14·9	3·63	1·17	3·81	0·576	3·49	0·712	1·93	0·291	1·94	0·296	2·72	0·096	2·83	1·18	0·67
TN182_09_005	11·7	401	19·0	89·7	1·34	0·40	273	9·0	21·1	3·13	14·4	3·59	1·14	3·63	0·574	3·40	0·688	1·87	0·284	1·88	0·289	2·54	0·091	2·70	1·14	0·64
TN182_09_001	11·6	443	17·4	90·7	1·18	0·40	231	7·0	18·2	2·61	12·3	3·08	1·00	3·12	0·482	2·85	0·576	1·60	0·245	1·66	0·252	2·45	0·074	3·09	0·85	0·50
SO201-1b-21-004	10·8	410	18·8	97·2	1·62	0·41	258	8·5	20·7	3·04	14·2	3·49	1·11	3·53	0·549	3·22	0·646	1·76	0·272	1·76	0·270	2·59	0·097	4·03	1·02	0·53
SO201-1b-21-005	10·7	396	18·0	94·7	1·59	0·39	249	8·0	19·9	2·91	13·6	3·32	1·06	3·41	0·514	3·09	0·620	1·73	0·259	1·71	0·260	2·50	0·098	2·69	0·99	0·52
SO201-1b-14-007	14·2	539	17·2	102	1·97	0·45	400	14·3	33·2	4·70	21·3	4·75	1·39	3·99	0·588	3·21	0·612	1·68	0·244	1·65	0·251	2·82	0·126	3·47	1·84	0·95
SO201-1b-18-002	11·2	385	19·1	92·3	1·61	0·35	229	7·0	18·1	2·75	13·3	3·46	1·11	3·49	0·555	3·29	0·666	1·83	0·273	1·86	0·280	2·50	0·097	2·76	0·87	0·48
SO201-1b-14-008	14·8	610	19·2	109	2·38	0·37	389	15·1	36·1	5·18	23·3	5·28	1·55	4·59	0·654	3·53	0·655	1·76	0·252	1·67	0·254	2·95	0·147	2·99	1·79	0·90
TN182_06_001	11·4	439	18·3	110	2·86	0·29	228	8·4	21·3	3·17	14·9	3·75	1·19	3·62	0·555	3·32	0·648	1·74	0·255	1·71	0·252	3·00	0·171	3·36	0·99	0·54
TN182_12_002	11·7	379	18·8	96·4	1·55	0·40	238	7·3	18·5	2·87	13·5	3·48	1·12	3·58	0·547	3·25	0·660	1·83	0·282	1·90	0·290	2·75	0·106	2·67	0·94	0·51
TN182_12_001	10·3	393	18·8	95·9	1·56	0·40	239	7·4	18·8	2·84	13·4	3·46	1·12	3·54	0·556	3·28	0·658	1·82	0·274	1·89	0·288	2·71	0·103	8·50	0·95	0·50
SO201-1b-14-001	14·2	585	17·5	106	2·55	0·39	355	13·9	33·0	4·82	21·8	4·92	1·46	4·41	0·630	3·47	0·654	1·78	0·251	1·65	0·247	2·77	0·150	3·51	1·71	0·84
SO201-1b-15-003	12·7	577	16·9	102	2·01	0·37	375	14·4	34·5	4·92	22·1	4·90	1·43	4·11	0·583	3·07	0·582	1·57	0·223	1·49	0·230	2·73	0·123	3·32	1·71	1·09
TN182_07_003	13·0	432	18·7	98·8	1·21	0·43	289	8·7	21·3	3·11	14·3	3·53	1·12	3·42	0·531	3·15	0·638	1·77	0·268	1·83	0·280	2·71	0·077	5·90	1·25	0·65
TN182_07_001	11·8	428	18·8	100	1·19	0·43	279	8·7	20·9	3·13	14·3	3·57	1·11	3·54	0·554	3·21	0·672	1·84	0·277	1·88	0·293	2·83	0·082	3·17	1·32	0·67
SO201-1b-15-001	12·4	593	17·2	102	2·21	0·13	375	14·3	34·4	4·92	22·3	4·99	1·45	4·26	0·598	3·16	0·590	1·59	0·224	1·53	0·226	2·72	0·130	2·34	1·69	0·91
TN182_08_003	8·8	398	15·5	85·3	1·14	0·16	223	6·5	16·8	2·40	11·2	2·86	0·930	2·81	0·435	2·62	0·518	1·42	0·222	1·47	0·227	2·28	0·071	2·65	0·82	0·54
TN182_07_011	12·5	416	17·8	93·4	1·11	0·41	272	8·3	20·5	2·94	13·6	3·36	1·09	3·28	0·515	3·01	0·611	1·69	0·256	1·75	0·264	2·56	0·070	3·41	1·18	0·64
SO201-1b-15-005	11·1	592	17·2	103	2·23	0·38	378	14·7	34·9	5·03	22·5	5·07	1·47	4·36	0·597	3·18	0·601	1·62	0·229	1·56	0·234	2·74	0·132	3·07	1·73	0·90
SO201-1b-20-012	11·3	385	17·3	91·7	1·77	0·40	243	7·8	19·2	2·80	13·1	3·29	1·06	3·30	0·504	3·01	0·598	1·63	0·249	1·70	0·258	2·48	0·104	3·33	1·19	0·60
SO201-1b-16-006	13·7	605	17·6	104	2·37	0·43	380	14·6	35·2	4·92	22·7	5·05	1·46	4·22	0·603	3·21	0·600	1·58	0·225	1·55	0·232	2·71	0·135	3·75	1·74	0·90
TN182_08_012*	11·2	391	16·4	89·6	1·08	0·40	228	7·0	17·4	2·61	12·3	3·09	0·994	3·14	0·493	2·93	0·601	1·64	0·250	1·70	0·260	2·54	0·074	2·64	0·87	0·53
TN182_08_011	10·6	409	16·5	87·6	1·11	0·40	222	6·9	17·1	2·58	12·1	3·03	0·978	3·05	0·475	2·83	0·571	1·58	0·240	1·64	0·248	2·45	0·074	2·77	0·85	0·51
SO201-1b-16-007	14·8	610	18·3	104·8	2·34	0·40	386	14·9	35·4	5·13	23·0	5·13	1·49	4·32	0·598	3·25	0·608	1·60	0·234	1·55	0·240	2·72	0·132	3·76	1·72	0·88
TN182_07_007	11·6	408	18·8	100·8	1·22	0·43	278	8·8	21·0	3·09	14·2	3·48	1·12	3·50	0·537	3·22	0·647	1·81	0·274	1·85	0·284	2·74	0·081	3·19	1·28	0·66
TN182_08_009	11·5	448	18·2	96·3	1·27	0·40	248	7·7	19·4	2·87	13·4	3·32	1·08	3·30	0·516	3·10	0·620	1·72	0·264	1·82	0·274	2·63	0·079	3·65	0·92	0·56
TN182_07_008	12·9	430	18·4	96·3	1·15	0·43	284	8·6	21·3	3·07	14·3	3·54	1·14	3·47	0·545	3·21	0·648	1·80	0·272	1·85	0·285	2·72	0·075	3·98	1·27	0·67

(continued)

Table 5: Continued

	Rb	Sr	Y	Zr	Nb	Cs	Ba	La	Ce	Pr	Nd	Sm	Eu	Gd	Tb	Dy	Ho	Er	Tm	Yb	Lu	Hf	Ta	Pb	Th	U
TN182_08_005	11·1	383	15·9	86·5	1·06	0·38	216	6·6	16·6	2·46	11·5	2·87	0·94	2·83	0·448	2·67	0·538	1·49	0·228	1·55	0·234	2·32	0·066	3·10	0·80	0·56
SO201-1b-15-002	12·1	599	17·2	104·1	2·27	0·14	379	14·5	34·8	4·95	22·5	4·99	1·45	4·23	0·600	3·17	0·601	1·61	0·232	1·52	0·233	2·74	0·134	2·12	1·74	0·92
TN182_08_013	13·0	408	17·6	94·2	1·26	0·42	243	7·5	18·3	2·74	13·2	3·28	1·05	3·39	0·506	3·05	0·608	1·70	0·260	1·77	0·270	2·64	0·077	3·50	0·91	0·57
TN182_08_010	11·6	443	17·4	90·7	1·18	0·40	231	7·0	18·2	2·61	12·3	3·08	1·00	3·12	0·482	2·85	0·576	1·60	0·245	1·66	0·252	2·45	0·074	3·09	0·85	0·50
TN182_08_016	11·2	410	17·0	90·6	1·15	0·40	234	7·1	17·7	2·61	12·4	3·13	1·01	3·15	0·482	2·87	0·589	1·63	0·247	1·70	0·263	2·52	0·076	2·95	0·88	0·54
TN182_07_006	12·6	418	18·3	96·6	1·18	0·41	283	8·4	20·5	3·03	14·0	3·45	1·10	3·33	0·516	3·11	0·625	1·74	0·263	1·80	0·279	2·68	0·076	3·64	1·23	0·65
TN182_07_002	13·6	405	16·8	99·8	1·38	0·42	284	8·9	21·7	3·13	14·5	3·50	1·09	3·30	0·505	2·93	0·575	1·58	0·238	1·61	0·245	2·66	0·085	3·31	1·41	0·68
TN182_08_014*	11·9	448	17·1	96·1	1·17	0·45	242	7·5	18·6	2·79	13·2	3·24	1·04	3·32	0·515	3·01	0·627	1·72	0·261	1·77	0·270	2·71	0·082	3·00	0·96	0·84
SO201-1b-20-007	12·5	410	19·5	102·8	2·00	0·43	276	8·5	21·0	3·10	14·6	3·65	1·16	3·69	0·570	3·37	0·675	1·85	0·280	1·91	0·292	2·78	0·116	3·48	1·31	0·68
TN182_08_006	8·3	411	17·5	87·7	1·14	0·34	226	7·2	18·3	2·66	12·6	3·18	1·04	3·22	0·497	2·93	0·595	1·64	0·252	1·71	0·263	2·41	0·073	4·07	0·88	1·49
TN182_08_015	9·4	445	17·2	91·4	1·23	0·39	235	7·2	18·0	2·67	12·5	3·21	1·04	3·34	0·490	2·92	0·593	1·63	0·252	1·70	0·264	2·50	0·076	2·65	0·89	0·53
TN182_08_001	11·6	433	17·7	94·5	1·21	0·43	242	7·4	18·9	2·77	12·9	3·30	1·06	3·35	0·511	3·02	0·622	1·68	0·265	1·75	0·278	2·59	0·081	3·66	0·93	0·56
TN182_08_002	11·2	394	16·1	87·0	1·06	0·39	220	6·7	16·9	2·50	11·8	2·97	0·97	2·95	0·460	2·74	0·557	1·55	0·233	1·60	0·240	2·39	0·066	3·09	0·82	0·67
TN182_08_007	10·0	441	17·5	89·5	1·20	0·39	232	7·2	18·2	2·71	12·6	3·17	1·03	3·19	0·497	2·99	0·598	1·64	0·254	1·70	0·263	2·51	0·078	3·76	0·90	0·58
TN182_08_008	11·1	413	16·6	89·1	1·10	0·38	224	6·9	17·3	2·57	12·1	3·06	1·00	3·02	0·473	2·85	0·578	1·58	0·245	1·68	0·250	2·46	0·070	3·39	0·84	0·51
SO201-1b-14-006	16·1	582	17·5	106·9	2·07	0·46	390	14·3	34·9	4·84	21·7	4·82	1·42	4·15	0·573	3·08	0·584	1·57	0·239	1·56	0·236	2·83	0·121	4·26	1·75	0·92
TN182_08_004	11·5	441	18·3	97·2	1·19	0·41	242	7·4	18·6	2·77	13·1	3·29	1·08	3·28	0·513	3·08	0·621	1·71	0·260	1·74	0·267	2·63	0·075	3·43	0·89	0·56
SO201-1b-09-002	8·8	1377	17·7	97·9	1·29	0·18	204	14·7	36·3	5·02	21·8	4·72	1·47	4·48	0·646	3·56	0·679	1·82	0·257	1·63	0·238	2·94	0·080	3·34	1·12	0·55
TN182_13_004	12·5	459	17·2	103·3	1·68	0·51	291	8·9	21·2	3·11	14·1	3·40	1·10	3·38	0·513	3·01	0·602	1·65	0·256	1·71	0·267	2·85	0·109	3·25	1·23	0·64
TN182_13_001	13·5	476	17·2	101·6	1·68	0·51	292	8·8	21·0	3·04	14·0	3·38	1·07	3·33	0·505	2·98	0·603	1·67	0·252	1·71	0·267	2·82	0·109	3·17	1·23	0·65
SO201-1b-09-001	8·5	1306	17·1	86·5	1·14	0·15	202	14·1	34·1	4·65	20·0	4·29	1·34	3·85	0·549	3·10	0·587	1·56	0·223	1·45	0·208	2·64	0·073	2·25	0·98	0·50
TN182_13_002	13·2	428	15·8	95·2	1·51	0·47	274	7·8	19·2	2·78	12·8	3·10	0·99	2·98	0·460	2·79	0·552	1·52	0·234	1·60	0·246	2·61	0·096	3·57	1·10	0·60
TN182_13_003	14·8	462	17·0	99·4	1·63	0·50	285	8·4	20·6	2·95	13·5	3·24	1·04	3·18	0·486	2·89	0·577	1·60	0·245	1·67	0·256	2·70	0·100	3·89	1·17	0·63
TN182_13_005	13·8	444	16·7	96·6	1·58	0·49	282	8·3	20·1	2·93	13·4	3·23	1·05	3·11	0·476	2·86	0·575	1·60	0·247	1·65	0·254	2·64	0·101	3·70	1·13	0·62
SO201-1b-09-005	10·1	1367	17·5	104·1	1·31	0·22	225	15·5	38·2	5·31	23·2	4·94	1·51	4·54	0·654	3·57	0·680	1·80	0·256	1·65	0·241	3·11	0·080	3·17	1·20	0·62
SO201-1b-10-003	11·3	1315	18·0	99·3	1·25	0·32	228	15·0	37·5	5·08	21·8	4·69	1·43	4·18	0·587	3·25	0·617	1·65	0·238	1·53	0·228	2·97	0·078	3·66	1·16	0·64
SO201-1b-10-006	9·7	1306	17·4	99·4	1·15	0·19	225	15·2	36·3	5·00	22·0	4·67	1·43	4·16	0·585	3·22	0·620	1·67	0·236	1·56	0·232	3·09	0·078	2·72	1·16	0·60
SO201-1b-10-001	9·4	1282	18·1	98·9	1·17	0·18	228	14·8	36·3	4·99	21·6	4·70	1·38	4·09	0·593	3·23	0·620	1·68	0·237	1·56	0·235	2·95	0·074	2·81	1·13	0·60
SO201-1b-10-005	10·2	1269	16·9	101·7	1·25	0·22	221	14·7	35·7	5·09	22·0	4·72	1·45	4·38	0·624	3·48	0·661	1·79	0·253	1·64	0·241	3·10	0·080	5·32	1·21	0·60
SO201-1b-10-004	11·2	1282	17·7	100·4	1·23	0·32	225	14·5	35·9	4·86	21·1	4·59	1·37	4·01	0·583	3·21	0·601	1·62	0·234	1·52	0·230	2·91	0·078	3·26	1·13	0·56
SO201-1b-20-009	13·5	390	18·3	111·1	1·97	0·09	267	8·4	21·0	2·88	13·2	3·31	1·03	3·30	0·506	2·98	0·594	1·63	0·246	1·69	0·255	2·87	0·127	1·79	1·28	0·66

(continued)

Table 5: Continued

	Rb	Sr	Y	Zr	Nb	Cs	Ba	La	Ce	Pr	Nd	Sm	Eu	Gd	Tb	Dy	Ho	Er	Tm	Yb	Lu	Hf	Ta	Pb	Th	U
TN182_05_002	13·7	779	16·0	113·8	1·54	0·55	283	10·8	24·7	3·54	15·6	3·52	1·14	3·31	0·496	2·83	0·564	1·55	0·231	1·59	0·245	3·19	0·105	3·45	1·18	0·73
TN182_05_001	14·4	767	16·3	115·0	1·68	0·52	291	11·0	25·9	3·55	15·3	3·40	1·10	3·17	0·482	2·77	0·538	1·52	0·229	1·56	0·240	3·02	0·103	4·04	1·19	0·74
SO201-1b-09-007	8·5	1067	15·6	97·6	1·23	0·27	178	10·0	24·8	3·57	16·0	3·66	1·19	3·52	0·541	3·12	0·607	1·66	0·243	1·61	0·244	2·93	0·083	3·39	1·01	0·50
SO201-1b-09-003	8·4	1133	15·0	102·2	1·31	0·23	182	10·6	26·1	3·66	16·3	3·56	1·17	3·43	0·513	2·93	0·567	1·57	0·230	1·53	0·234	2·94	0·082	3·30	1·03	0·50
TN182_11_004	14·6	506	15·7	110·1	1·44	0·58	267	8·6	20·6	2·95	13·2	3·04	0·98	2·92	0·446	2·60	0·518	1·45	0·224	1·52	0·232	2·89	0·092	4·21	0·97	0·69
TN182_10_003	22·4	1240	18·8	195·1	1·49	0·41	443	25·7	60·2	8·14	34·6	6·82	1·88	5·37	0·704	3·47	0·621	1·67	0·229	1·53	0·222	5·43	0·087	5·26	3·61	1·75
TN182_10_002	20·0	1253	18·5	191·0	1·46	0·40	429	25·0	59·9	8·06	33·9	6·77	1·84	4·98	0·720	3·46	0·626	1·66	0·232	1·51	0·230	5·32	0·087	5·45	3·67	1·82
TN182_10_001	18·7	1291	17·1	184·8	1·37	0·33	415	24·4	57·3	7·61	32·0	6·50	1·80	4·88	0·661	3·29	0·603	1·60	0·221	1·47	0·218	5·30	0·085	4·32	3·51	1·61
SO201-1b-09-008	45·8	1740	21·6	326·8	3·51	0·47	417	35·1	91·0	13·13	57·1	11·22	3·00	8·57	1·108	5·06	0·823	2·01	0·259	1·58	0·222	8·45	0·218	5·17	2·48	1·92
TN182_11_003	17·7	1843	15·5	197·6	1·89	0·46	379	28·2	65·2	8·68	35·8	6·46	1·76	4·80	0·628	2·98	0·523	1·41	0·196	1·30	0·194	5·71	0·112	6·83	3·73	1·62
TN182_11_001*	16·3	1675	15·6	183·2	1·68	0·46	352	26·7	58·9	7·51	31·7	6·51	1·85	4·85	0·619	3·19	0·583	1·43	0·198	1·20	0·196	5·48	0·113	5·35	3·60	1·33
TN182_11_005	18·7	1819	15·9	196·3	1·87	0·45	372	27·4	64·1	8·55	35·2	6·44	1·74	4·69	0·624	2·89	0·522	1·41	0·200	1·31	0·192	5·45	0·108	6·76	3·60	1·45
TN182_11_002	16·7	1603	14·2	180·7	1·54	0·39	335	24·5	58·4	7·69	31·6	5·77	1·59	4·12	0·550	2·70	0·485	1·26	0·179	1·20	0·177	5·31	0·097	5·82	3·26	1·33
TN182_10_004	43·4	2257	20·6	245·6	1·66	0·64	647	42·0	102·1	14·13	62·1	12·27	3·25	9·11	1·071	4·54	0·709	1·73	0·205	1·28	0·178	6·92	0·103	6·11	3·51	2·29
SO201-1b-09-010	6·9	618	12·9	123·0	2·41	0·13	251	8·9	21·5	2·98	12·9	2·78	0·90	2·66	0·402	2·32	0·462	1·32	0·201	1·38	0·217	3·11	0·148	3·59	0·99	0·66
SO201-1b-10-010	6·6	800	9·0	71·0	0·72	0·08	120	4·3	10·6	1·57	7·2	1·77	0·66	1·84	0·288	1·70	0·340	0·95	0·143	0·94	0·142	1·97	0·049	3·06	0·54	0·41
SO201-1b-10-011	14·5	879	10·2	116·4	1·48	0·29	218	10·3	23·7	3·16	13·0	2·58	0·85	2·28	0·337	1·91	0·371	1·05	0·159	1·07	0·170	3·01	0·098	11·19	1·53	0·80
SO201-1b-09-011	14·6	1063	10·8	126·3	1·20	0·38	428	15·5	37·0	5·25	22·8	4·54	1·32	3·51	0·455	2·23	0·394	1·04	0·146	0·96	0·145	3·30	0·078	4·36	1·88	1·06
SO201-1b-20-005	12·0	1721	12·4	138·1	1·46	0·23	214	16·0	39·0	5·42	22·9	4·47	1·34	3·63	0·504	2·59	0·461	1·24	0·172	1·10	0·162	4·01	0·093	4·03	1·60	0·78
TN182_05_003	12·4	1370	14·2	145·2	1·31	0·13	472	20·3	49·7	6·93	30·7	6·32	1·78	4·71	0·616	2·93	0·501	1·33	0·172	1·15	0·168	3·97	0·090	4·39	2·19	0·91
TN182_01_004	12·8	743	12·8	104·7	1·59	0·48	276	9·1	21·4	2·86	12·3	2·66	0·87	2·59	0·377	2·18	0·425	1·19	0·179	1·23	0·190	2·80	0·102	3·92	1·23	0·70
SO201-1b-09-012	9·3	1445	11·3	115·3	1·28	0·09	333	14·8	35·5	5·10	22·3	4·47	1·35	3·62	0·478	2·36	0·418	1·09	0·153	0·98	0·148	3·19	0·079	3·18	1·57	0·77
SO201-1b-09-014	9·7	1462	11·2	114·5	1·26	0·09	342	14·8	35·7	5·16	22·6	4·57	1·33	3·67	0·487	2·45	0·427	1·13	0·157	1·00	0·151	3·28	0·083	3·55	1·63	0·80
TN182_03_004*	7·8	937	12·2	111·0	1·31	0·44	295	11·9	28·3	4·04	17·8	3·74	1·14	3·11	0·426	2·24	0·420	1·12	0·162	1·09	0·167	3·13	0·090	5·35	1·36	0·82
70B-29	14·4	1013	12·4	116·6	1·38	0·53	297	11·9	28·4	4·02	17·7	3·76	1·15	3·10	0·433	2·25	0·420	1·14	0·165	1·11	0·170	3·32	0·090	4·96	1·39	0·77
SO201-1b-20-011	9·3	1236	10·5	113·0	1·20	0·07	200	9·3	23·1	3·41	15·3	3·34	1·03	2·85	0·407	2·16	0·398	1·07	0·152	0·98	0·145	3·18	0·076	2·31	1·22	0·60
TN182_03_001*	7·9	1104	12·4	113·7	1·18	0·24	246	11·3	27·5	3·89	17·3	3·73	1·16	3·08	0·433	2·33	0·440	1·20	0·170	1·15	0·172	3·26	0·083	4·11	1·28	0·64
TN182_03_005	11·8	1130	12·2	114·7	1·35	0·13	251	11·5	27·1	3·91	17·1	3·58	1·09	2·97	0·420	2·19	0·406	1·10	0·159	1·06	0·162	3·21	0·083	4·76	1·26	0·68
SO201-1b-20-004	9·1	1243	10·3	112·2	1·18	0·09	196	9·1	22·5	3·32	14·9	3·23	1·01	2·81	0·395	2·08	0·390	1·04	0·148	0·96	0·142	3·10	0·075	2·09	1·14	0·54
TN182_03_008	11·4	1117	11·7	113·8	1·37	0·22	254	10·6	25·7	3·61	16·0	3·42	1·04	2·83	0·398	2·11	0·395	1·07	0·153	1·04	0·156	3·14	0·084	5·80	1·21	0·70

(continued)

Table 5: Continued

	Rb	Sr	Y	Zr	Nb	Cs	Ba	La	Ce	Pr	Nd	Sm	Eu	Gd	Tb	Dy	Ho	Er	Tm	Yb	Lu	Hf	Ta	Pb	Th	U
TN182_03_007	7·6	1049	11·6	111·2	1·22	0·12	208	9·8	24·8	3·47	15·4	3·37	1·04	2·84	0·393	2·10	0·395	1·07	0·157	1·01	0·150	3·22	0·080	3·51	1·16	0·49
SO201-1b-20-008	9·6	1236	10·2	112·4	1·19	0·08	201	9·1	22·7	3·35	15·0	3·26	1·01	2·82	0·395	2·10	0·384	1·03	0·146	0·96	0·145	3·13	0·075	2·58	1·14	0·68
TN182_03_006	12·0	1122	11·6	111·3	1·21	0·13	232	10·6	25·9	3·65	16·1	3·38	1·04	2·78	0·383	2·10	0·388	1·05	0·154	1·02	0·154	3·18	0·079	4·01	1·20	0·64
TN182_03_002	10·3	1126	12·2	114·0	1·34	0·33	246	11·1	26·2	3·75	16·8	3·48	1·07	3·01	0·412	2·16	0·406	1·08	0·157	1·06	0·158	3·16	0·083	4·61	1·23	0·67
SO201-1b-11-002	14·7	860	10·2	110·9	1·61	0·59	249	8·4	19·3	2·62	11·1	2·36	0·80	2·25	0·339	1·92	0·371	1·05	0·156	1·05	0·161	2·88	0·102	4·72	1·23	0·64
TN182_03_010	7·0	1023	11·3	108·3	1·15	0·12	203	9·5	24·4	3·41	15·4	3·28	1·01	2·76	0·380	2·06	0·395	1·03	0·151	1·00	0·152	3·12	0·077	3·12	1·16	0·47
TN182_03_009	12·6	1085	11·4	112·9	1·36	0·24	249	10·6	25·3	3·63	15·9	3·33	1·03	2·81	0·393	2·07	0·386	1·05	0·150	1·02	0·154	3·16	0·083	5·03	1·20	0·72
TN182_03_003*	8·8	1096	12·2	115·9	1·30	0·11	263	11·6	27·5	4·00	17·2	3·79	1·20	3·31	0·443	2·45	0·470	1·24	0·177	1·05	0·174	3·29	0·092	5·25	1·36	0·93
TN182_07_009	19·9	1365	9·5	125·4	1·29	0·45	252	13·3	31·3	4·25	17·7	3·36	1·02	2·63	0·355	1·80	0·322	0·85	0·125	0·82	0·122	3·48	0·082	5·18	1·52	0·80
SO201-1b-13-008	9·1	912	10·2	138·9	1·69	0·33	325	11·2	26·4	3·64	15·5	3·15	0·97	2·61	0·366	1·94	0·363	1·00	0·148	1·02	0·162	3·59	0·109	4·23	1·78	0·84
SO201-1b-11-008	12·3	867	9·8	110·3	1·59	0·57	254	8·5	19·4	2·61	10·9	2·32	0·78	2·15	0·324	1·84	0·362	1·01	0·151	1·02	0·155	2·94	0·106	4·65	1·27	0·65
TN182_07_010	15·7	1476	10·6	133·8	1·25	0·43	240	13·7	32·5	4·42	18·8	3·71	1·13	2·86	0·395	2·02	0·364	0·99	0·139	0·91	0·140	3·89	0·089	3·96	1·60	0·73
TN182_07_004	11·4	1436	10·1	127·8	1·31	0·20	253	13·5	32·3	4·34	18·2	3·50	1·07	2·77	0·377	1·89	0·333	0·92	0·131	0·87	0·129	3·55	0·080	3·74	1·53	0·81
TN182_07_005	19·7	1384	10·1	129·1	1·26	0·47	256	13·9	32·8	4·35	18·3	3·52	1·07	2·73	0·371	1·88	0·341	0·93	0·128	0·87	0·133	3·62	0·083	5·25	1·59	0·83
TN182_04_002	3·8	1242	10·7	108·0	0·90	0·08	114	6·9	18·5	2·54	11·5	2·57	0·86	2·36	0·341	1·91	0·369	0·99	0·144	0·94	0·140	3·21	0·061	2·86	0·92	0·32
SO201-1b-13-002	15·9	1018	9·4	139·5	1·57	0·55	293	10·9	25·6	3·54	14·9	3·01	0·93	2·48	0·350	1·83	0·343	0·94	0·140	0·93	0·147	3·65	0·101	4·91	1·75	0·84
TN182_04_004	7·8	1207	9·8	103·9	0·87	0·22	160	8·2	19·9	2·84	12·5	2·66	0·86	2·28	0·326	1·81	0·338	0·91	0·132	0·89	0·131	3·07	0·061	3·52	0·99	0·51
TN182_01_002*	14·5	1054	10·7	121·4	1·07	0·42	282	11·7	26·6	3·60	16·5	3·94	1·20	3·14	0·414	2·14	0·395	0·98	0·134	0·83	0·134	3·43	0·079	4·83	1·76	0·81
TN182_01_006	15·3	1081	10·2	126·4	1·03	0·41	284	11·5	28·1	3·91	17·5	3·59	1·07	2·89	0·382	1·87	0·336	0·88	0·124	0·83	0·124	3·30	0·066	5·55	1·66	0·81
TN182_01_008	10·8	1022	10·5	131·3	1·41	0·61	264	10·0	24·2	3·16	13·3	2·72	0·88	2·28	0·328	1·81	0·348	0·94	0·145	0·97	0·156	3·66	0·098	6·01	1·52	0·67
TN182_01_001	16·6	1081	10·4	128·9	1·09	0·44	301	11·6	28·0	3·91	17·0	3·60	1·07	2·87	0·392	1·96	0·339	0·91	0·133	0·88	0·128	3·50	0·071	5·49	1·71	0·83
TN182_01_003	11·8	1014	10·1	127·2	0·97	0·39	263	11·2	27·7	3·84	16·9	3·58	1·05	2·79	0·373	1·86	0·337	0·87	0·126	0·81	0·125	3·51	0·067	5·18	1·67	0·77
TN182_04_001	5·8	1262	9·8	114·1	0·91	0·25	153	8·6	21·0	2·93	12·9	2·80	0·91	2·34	0·332	1·81	0·344	0·93	0·132	0·89	0·132	3·39	0·065	6·07	1·08	0·47
TN182_04_003	7·9	1241	9·5	110·3	0·89	0·25	165	8·6	20·6	2·94	12·8	2·72	0·88	2·28	0·331	1·76	0·335	0·90	0·127	0·86	0·129	3·26	0·063	3·30	1·06	0·56
TN182_01_005*	8·7	1215	9·7	108·7	0·90	0·27	173	8·8	21·1	3·04	13·0	2·86	0·98	2·45	0·352	1·96	0·379	0·98	0·140	0·86	0·137	3·23	0·066	5·18	1·14	0·53
TN182_01_007	13·5	978	9·3	115·1	0·95	0·38	269	10·2	24·5	3·50	15·3	3·21	0·95	2·61	0·348	1·73	0·312	0·83	0·118	0·79	0·116	3·15	0·064	4·77	1·55	0·73
SO201-1b-34-004	10·7	1561	6·0	120·3	0·93	0·16	216	11·2	26·7	3·64	15·5	2·96	0·92	1·82	0·266	1·23	0·207	0·52	0·069	0·44	0·067	3·37	0·064	4·75	1·67	0·69
SO201-1b-34-003	9·7	1380	5·4	107·6	0·85	0·14	189	9·9	23·6	3·18	13·6	2·56	0·81	1·73	0·234	1·08	0·182	0·45	0·061	0·40	0·059	3·01	0·057	4·25	1·49	0·62
SO201-1b-36-007	11·7	1304	4·5	107·2	0·77	0·11	113	7·4	18·0	2·44	10·6	2·15	0·70	1·54	0·204	0·94	0·154	0·38	0·052	0·32	0·046	3·06	0·055	4·15	1·27	0·53
SO201-1b-36-009	28·8	1552	5·5	126·4	0·93	0·16	135	8·6	21·1	2·86	12·5	2·54	0·83	1·83	0·243	1·13	0·186	0·46	0·063	0·40	0·056	3·60	0·066	4·71	1·47	0·63

(continued)

Table 5: Continued

	Rb	Sr	Y	Zr	Nb	Cs	Ba	La	Ce	Pr	Nd	Sm	Eu	Gd	Tb	Dy	Ho	Er	Tm	Yb	Lu	Hf	Ta	Pb	Th	U
SO201-1b-36-010	28·2	1551	5·4	126·9	0·91	0·18	127	8·5	20·8	2·84	12·3	2·50	0·82	1·82	0·241	1·11	0·183	0·45	0·060	0·39	0·056	3·56	0·065	3·66	1·44	0·61
SO201-1b-36-006	22·0	1532	5·2	128·1	0·92	0·15	123	8·3	20·3	2·77	12·0	2·43	0·79	1·85	0·232	1·07	0·177	0·43	0·058	0·37	0·053	3·59	0·065	4·20	1·43	0·61
SO201-1b-34-002	10·2	1536	5·9	120·6	0·93	0·16	208	11·1	26·5	3·55	15·1	2·87	0·89	1·91	0·257	1·20	0·201	0·50	0·066	0·43	0·065	3·32	0·064	5·21	1·65	0·68
SO201-1b-36-004	31·7	1533	5·3	127·2	0·90	0·15	130	8·6	21·0	2·85	12·3	2·50	0·81	1·81	0·236	1·08	0·177	0·43	0·058	0·37	0·053	3·56	0·064	3·62	1·44	0·62
SO201-1b-34-001	9·4	1475	5·7	115·7	0·89	0·15	198	10·5	24·9	3·37	14·3	2·69	0·84	1·80	0·244	1·13	0·190	0·47	0·065	0·42	0·061	3·19	0·061	4·58	1·56	0·65
SO201-1b-36-012	11·0	1426	5·0	119·6	0·86	0·12	115	7·8	19·2	2·61	11·4	2·31	0·75	1·83	0·222	1·03	0·169	0·41	0·056	0·36	0·051	3·36	0·060	4·40	1·37	0·58
SO201-1b-36-008	29·9	1567	5·3	126·8	0·91	0·17	126	8·5	20·8	2·83	12·3	2·50	0·82	1·83	0·236	1·09	0·177	0·43	0·057	0·37	0·052	3·61	0·065	3·54	1·43	0·61
SO201-1b-36-001	27·3	1411	4·9	117·2	0·85	0·22	112	8·2	20·3	2·75	11·8	2·34	0·74	1·53	0·220	1·02	0·167	0·41	0·053	0·34	0·050	3·24	0·058	3·08	1·29	0·58
SO201-1b-36-014	5·2	1625	5·6	132·1	1·01	0·03	137	8·7	21·0	2·82	12·4	2·55	0·86	1·84	0·251	1·16	0·193	0·47	0·064	0·41	0·059	3·74	0·068	3·60	1·56	0·65
SO201-1b-36-002	17·2	1555	5·3	129·2	0·91	0·13	133	8·7	21·4	2·92	12·6	2·54	0·83	1·82	0·238	1·09	0·178	0·44	0·059	0·37	0·054	3·68	0·066	4·48	1·51	0·65
SO201-1b-36-011	4·7	1591	5·6	128·7	0·95	0·04	131	8·4	20·5	2·81	12·3	2·53	0·84	2·04	0·248	1·16	0·190	0·47	0·063	0·40	0·057	3·67	0·066	3·16	1·52	0·64
SO201-1b-36-005	10·2	1592	5·4	130·3	0·92	0·13	135	8·8	21·5	2·94	12·7	2·56	0·83	1·91	0·240	1·11	0·181	0·44	0·059	0·38	0·054	3·66	0·065	4·29	1·48	0·63
SO201-1b-36-003	16·8	1677	6·3	139·4	1·04	0·15	129	9·6	22·8	3·21	14·0	2·89	0·92	2·03	0·280	1·30	0·214	0·52	0·069	0·45	0·064	3·91	0·071	3·59	1·66	0·64
SO201-1b-35-005	4·8	1412	4·9	91·7	0·64	0·08	88	5·4	13·5	1·83	8·1	1·71	0·60	1·39	0·190	0·95	0·168	0·43	0·059	0·39	0·057	2·65	0·043	3·73	0·62	0·31
SO201-1b-35-002	4·6	1429	4·8	90·3	0·62	0·08	80	5·3	13·3	1·82	8·0	1·69	0·61	1·34	0·185	0·94	0·163	0·42	0·059	0·38	0·056	2·63	0·042	3·56	0·59	0·30
SO201-1b-35-003	29·9	1277	4·8	86·8	0·52	0·10	71	4·1	10·4	1·47	6·7	1·49	0·54	1·26	0·177	0·90	0·161	0·41	0·059	0·39	0·057	2·49	0·037	2·94	0·52	0·29
SO201-1b-35-001	28·4	1294	4·9	87·3	0·53	0·11	73	4·1	10·6	1·50	6·8	1·52	0·56	1·28	0·179	0·92	0·165	0·42	0·060	0·39	0·057	2·52	0·038	3·44	0·52	0·29
SO201-1b-35-004	6·3	1244	5·3	97·4	0·60	0·08	121	5·0	12·8	1·83	8·4	1·88	0·64	1·56	0·209	1·04	0·181	0·46	0·063	0·41	0·062	2·74	0·041	3·41	0·67	0·34
SO201-1b-33-001	7·9	1280	5·4	98·0	0·61	0·09	124	5·1	12·9	1·84	8·4	1·88	0·64	1·50	0·207	1·03	0·178	0·45	0·063	0·41	0·061	2·77	0·041	3·42	0·66	0·36
V3841Y3	10·1	2473	9·9	182·4	3·75	0·08	314	32·4	77·6	10·22	42·2	7·10	2·07	4·34	0·529	2·22	0·342	0·81	0·099	0·61	0·085	4·73	0·226	6·33	3·14	1·10
V3841Y2	10·2	2372	9·6	174·6	3·61	0·08	314	31·4	74·8	9·80	40·2	6·83	2·01	4·20	0·510	2·12	0·334	0·78	0·099	0·60	0·084	4·42	0·213	6·11	2·97	1·02
V3842Y3	23·6	2335	9·6	174·4	3·52	0·20	306	30·3	72·4	9·48	39·1	6·66	1·94	4·06	0·496	2·06	0·322	0·77	0·094	0·57	0·082	4·35	0·203	6·11	2·81	0·96
V3842Y2	15·8	2446	10·4	178·8	3·58	0·12	331	31·5	74·0	9·79	40·8	6·90	2·01	4·33	0·514	2·15	0·345	0·82	0·100	0·65	0·090	4·41	0·208	5·60	2·87	1·02
ADK04L7	15·6	1713	12·3	142·0	3·57	0·24	448	33·4	76·9	9·96	40·7	6·72	1·94	4·93	0·561	2·54	0·439	1·12	0·149	0·99	0·143	4·02	0·211	4·53	2·94	1·19

These data were collected at the University of South Carolina, except samples marked by asterisks (*), indicating data from the Washington State University Geoanalytical Laboratories.

Table 6: Whole-rock Nd, Hf and Pb isotope results

	Laboratory	$^{143}Nd/^{144}Nd$	2σ	ε_{Nd}	$^{176}Hf/^{177}Hf$	2σ	ε_{Hf}	$^{206}Pb/^{204}Pb$	2σ	$^{207}Pb/^{204}Pb$	$2\sigma^{c}$	$^{208}Pb/^{204}Pb$	2σ
TN182_09_001	WHOI (Nd, Pb), WSU (Hf)	0·513082	*	8·8	0·283191	±4	14·4	18·5662	*	15·5177	*	38·1030	*
SO201-1b-14-007	SCAR (Pb)							18·5199	±5	15·5056	±5	38·0380	±17
SO201-1b-14-008	SCAR (Pb)							18·4771	±7	15·4983	±8	37·9865	±24
SO201-1b-15-001	SCAR (Pb)							18·4816	±7	15·4993	±8	37·9906	±27
TN182_08_003	WHOI (Nd, Pb), WSU (Hf)	0·513073	±4	8·6	0·283214	±6	15·2	18·5668	*	15·5203	*	38·1131	*
SO201-1b-16-007	SCAR (Pb)							18·4928	±8	15·5001	±8	38·0031	±26
TN182_08_013	WSU (Nd, Hf, Pb)	0·513079	±9	8·8	0·283179	±6	13·9	18·5583	±6	15·5110	±5	38·0816	±14
TN182_07_002	WHOI (Nd, Pb), WSU (Hf)	0·513078	*	8·7	0·283201	±5	14·7	18·5396	*	15·5092	*	38·0649	*
TN182_08_014	WHOI (Nd, Pb), WSU (Hf)	0·513096	*	9·1	0·283216	±4	15·2	18·5662	*	15·5177	*	38·1030	*
SO201-1b-14-006	SCAR (Pb)							18·4998	±5	15·4996	±6	38·0061	±18
SO201-1b-09-002	SCAR (Pb)							18·3815	±5	15·4740	±5	37·8513	±17
TN182_13_001	WHOI (Nd, Pb), WSU (Hf)	0·513092	*	9·0	0·283200	±4	14·7	18·5626	*	15·5165	*	38·0972	*
SO201-1b-09-001	SCAR (Pb)							18·3785	±6	15·4716	±7	37·8439	±20
SO201-1b-09-005	SCAR (Pb)							18·3707	±13	15·4745	±16	37·8424	±52
SO201-1b-10-003	SCAR (Pb)							18·3901	±5	15·4742	±5	37·8579	±18
SO201-1b-10-005	SCAR (Pb)							18·3897	±5	15·4755	±6	37·8601	±21
TN182_05_001	WHOI (Nd, Pb), WSU (Hf)	0·513108	*	9·3	0·283212	±5	15·1	18·5332	*	15·5098	*	38·0592	*
SO201-1b-09-007	SCAR (Pb)							18·4023	±5	15·4781	±6	37·8783	±21
TN182_11_004	WSU (Nd, Hf, Pb)	0·513109	±9	9·3	0·283186	±7	14·2	18·5317	±6	15·5077	±6	38·0497	±12
TN182_10_003	WSU (Nd, Hf, Pb)	0·513107	±8	9·3	0·283188	±6	14·3	18·4735	±8	15·4888	±6	37·9483	±16
TN182_10_002	WSU (Nd), WHOI (Pb)	0·513058	±4	8·3				18·4710	*	15·4885	*	37·9479	*
TN182_10_001	WHOI (Nd, Pb), WSU (Hf)	0·513071	*	8·6	0·283191	±4	14·4	18·4710	*	15·4884	*	37·9474	*
SO201-1b-09-008	SCAR (Pb)							18·3925	±6	15·4762	±7	37·8537	±24
TN182_11_003	WHOI (Pb), WSU (Nd, Hf)	0·513086	±4	8·9	0·283195	±4	14·5	18·4817	*	15·4862	*	37·9544	*
TN182_11_001	WHOI (Nd, Pb), WSU (Hf)	0·513105	*	9·3	0·283191	±6	14·4	18·4858	*	15·4911	*	37·9697	*
TN182_11_005	WSU (Nd, Hf, Pb)	0·513082	±9	8·8	0·283172	±6	13·7	18·4902	±10	15·4936	±8	37·9752	±20
TN182_10_004	WSU (Nd, Hf, Pb)	0·513090	±10	9·0	0·283240	±6	16·1	18·4402	±10	15·4842	±8	37·9107	±21
SO201-1b-09-010	SCAR (Pb)							18·4652	±6	15·4962	±5	37·9669	±17
SO201-1b-10-010	SCAR (Pb)							18·4148	±5	15·4854	±7	37·8961	±22
SO201-1b-10-011	SCAR (Pb)							18·4836	±7	15·4975	±8	37·9810	±22
SO201-1b-09-011	SCAR (Pb)							18·4769	±7	15·4973	±8	37·9748	±24
SO201-1b-20-005	SCAR (Pb)							18·3508	±7	15·4633	±8	37·7996	±28
TN182_01_004	WSU (Sr, Nd, Hf, Pb)	0·513101	±8	9·2	0·283192	±4	14·4	18·4882	±8	15·4970	±14	37·9878	±14
SO201-1b-09-014	SCAR (Pb)							18·4249	±6	15·4879	±7	37·9211	±22
TN182_03_004	WHOI (Pb) WSU (Nd, Hf)	0·513082	±16	8·8	0·283242	±5	16·2	18·4897	†	15·4961	†	37·9839	†
TN182_03_005	WHOI (Pb) WSU (Nd)	0·513083	±4	8·8				18·4472	†	15·4796	†	37·9149	†
TN182_03_008	WSU (Nd, Hf, Pb)	0·513092	±8	9·0	0·283194	±7	14·5	18·4631	±8	15·4884	±6	37·9434	±18
TN182_03_002	WSU (Nd, Hf, Pb)	0·513097	±11	9·1				18·4542	±8	15·4846	±6	37·9302	±16
TN182_03_009	WSU (Nd, Hf, Pb)	0·513109	±11	9·3	0·283176	±6	13·8	18·4598	±7	15·4844	±6	37·9336	±14
TN182_07_009	WHOI (Nd, Pb), WSU (Hf)	0·513122	†	9·6	0·283210	±4	15·0	18·4206	†	15·4786	†	37·8931	†

(continued)

Table 6: Continued

	Laboratory	$^{143}Nd/^{144}Nd$	2σ	ε_{Nd}	$^{176}Hf/^{177}Hf$	2σ	ε_{Hf}	$^{206}Pb/^{204}Pb$	2σ	$^{207}Pb/^{204}Pb$	2σ	$^{208}Pb/^{204}Pb$	2σ
TN182_07_004	WHOI (Pb) WSU (Hf)				0·283201	±4	14·7	18·4214	†	15·4781	†	37·8920	†
TN182_07_005	WSU (Nd, Hf, Pb)	0·513107	±7	9·3	0·283187	±6	14·2	18·4206	±9	15·4756	±8	37·8855	±19
TN182_04_004	WHOI (Pb)							18·3817	†	15·4698	†	37·8365	†
TN182_01_006	WSU (Nd, Hf, Pb)	0·513114	±9	9·4	0·283176	±6	13·8	18·4233	±7	15·4757	±5	37·8836	±14
TN182_01_001	WHOI (Pb), WSU (Nd, Hf)	0·513087	±4	8·9	0·283186	±6	14·2	18·4446	†	15·4911	†	37·9299	†
TN182_01_003	WSU (Hf, Pb)				0·283168	±6	13·6	18·4245	±12	15·4770	±6	37·8877	±14
TN182_04_003	WSU (Nd, Hf, Pb)	0·513131	±10	9·8	0·283192	±5	14·4	18·3809	±11	15·4666	±9	37·8287	±24
TN182_01_007	WSU (Nd, Hf, Pb)	0·513096	±8	9·1	0·283178	±5	13·9	18·4241	±8	15·4790	±7	37·8920	±18
SO201-1b-33-001	SCAR (Nd, Pb)	0·513122	±9	9·6				18·3379	±4	15·4537	±4	37·7489	±11
SO201-1b-36-003	SCAR (Nd, Pb)	0·513093	±9	9·0				18·4878	±4	15·4979	±4	38·0034	±22
SO201-1b-35-004	SCAR (Nd, Pb)	0·513113	±8	9·4				18·3420	±3	15·4546	±3	37·7577	±9
V3842Y3	WSU	0·513100	±10	9·2	0·283188	±6	14·3	17·8946	±6	15·4175	±6	37·3690	±18
V3842Y3 REP	WSU	0·513075	±10	8·7	0·283186	±10	14·2						
ADK04L7	WSU	0·513100	±10	9·2	0·283183	±8	14·1	18·3355	±10	15·4690	±8	37·7877	±20
TN182_09_001	WHOI (Nd, Pb), WSU (Hf)	0·513082		8·8	0·283191	±4	14·4	18·5662		15·5177		38·1030	
SO201-1b-14-007	SCAR (Pb)							18·5199	±5	15·5056	±5	38·0380	±17

These results are from laboratories at Washington State University (WSU), the University of South Carolina (SCAR) and the Woods Hole Oceanographic Institution (WHOI). Errors shown here from WSU and SCAR are within-run uncertainties calculated as 2σ and expressed as variation in the last decimal place. Internal precision for WHOI analyses is ±5–10 in the last decimal place for $^{143}Nd/^{144}Nd$, ±6–19 for $^{206}Pb/^{204}Pb$, ±5–16 for $^{207}Pb/^{204}Pb$, and ±5–16 and ±11–38 for $^{208}Pb/^{204}Pb$. Nd isotopes are normalized to a reference value for the La Jolla standard of $^{143}Nd/^{144}Nd = 0{\cdot}511859$ (Lugmair & Carlson, 1978). Hf isotopes are normalized to a reference value for JMC475 of $^{176}Hf/^{177}Hf = 0{\cdot}282160$ (Vervoort & Blichert-Toft, 1999). Pb isotopes are normalized to reference values for NBS981 of $^{206}Pb/^{204}Pb = 16{\cdot}9405$, $^{207}Pb/^{204}Pb = 15{\cdot}4963$ and $^{208}Pb/^{204}Pb = 36{\cdot}7219$ (Galer & Abouchami, 1998). Epsilon Hf and Nd values were calculated using chondritic values from Bouvier *et al.* (2008).

Table 7: Summary of $^{40}Ar/^{39}Ar$ groundmass incremental heating experiments

Sample	K/Ca total	$^{40}Ar/^{36}Ar_i \pm 2\sigma$	Isochron age (ka) $\pm 2\sigma$	MSWD	^{39}Ar %	Plateau Age (ka) $\pm 2\sigma$
TN182-01-001	0·34	295·6 ± 1·9	16·2 ± 7·9	0·21	100·0	16·6 ± 4·5
TN182-07-004	0·28	296·1 ± 1·5	60·7 ± 12·8	0·10	100·0	64·1 ± 9·2
TN182-08-014	0·07	291·8 ± 7·4	231·3 ± 191·7	0·22	97·5	133·6 ± 35·2
TN182-03-004	0·20	295·9 ± 1·0	266·1 ± 19·9	0·13	100·0	272·2 ± 14·4
TN182-09-001	0·08	295·8 ± 8·7	513·8 ± 216·1	0·37	100·0	520·8 ± 44·3

Ages calculated relative to 28.02 Ma Fish Canyon sanidine (Renne *et al.*, 1998) using decay constant of Steiger & Jäger (1977).

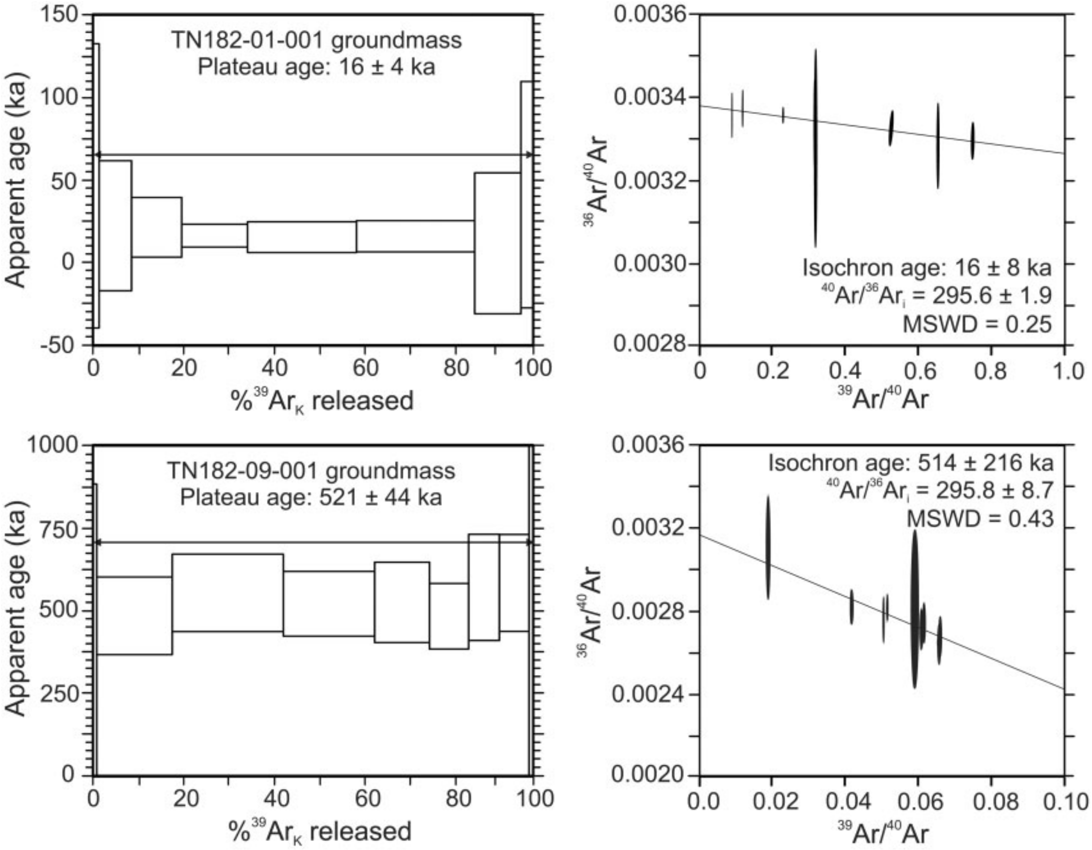

Fig. 3. $^{40}Ar/^{39}Ar$ age plateau and isochron diagrams for two Ingenstrem Depression lavas, showing the various ages ($\pm 2\sigma$ uncertainties) obtained from incremental heating experiments. Arrows indicate steps used to determine plateau ages. Additional age data are provided in Table 7 and online Supplementary Data.

Zimmer *et al.*, 2010). The highly calc-alkaline character of the western Aleutian seafloor lavas is particularly well expressed in the rhyodacites, which have some of the highest silica contents among Aleutian lavas (69–70% SiO_2), but also 2·0–2·5% MgO and very high Mg# values (0·64–0·68). The western seafloor lavas display several other distinctive major element characteristics compared with typical Aleutian lavas, which are also observed in the Miocene Adak and Komandorsky magnesian andesites. The abundance of FeO*, for example, is uniformly low and MgO is generally high at all silica contents in the western seafloor lavas compared with lavas from emergent volcanoes throughout the arc (Fig. 5a and b). Western seafloor lavas with basaltic compositions (SiO_2 <55%) generally have similar Na_2O, CaO and CaO/Al_2O_3 compared with average Aleutian basalts. At higher silica contents Na_2O and K_2O are generally lower (<5·0% and <2%, respectively) and CaO and CaO/Al_2O_3 are higher in the western Aleutian seafloor samples compared with common Aleutian lavas (Figs 5a and 6c–e).

PETROGRAPHY

Observations of approximately 30 petrographic thin sections spanning the range of western seafloor lava compositions show no significant effects of alteration or development of secondary minerals by hydrothermal or weathering processes. Below, we summarize the primary textural and mineralogical characteristics of the samples. Key characteristics described here are

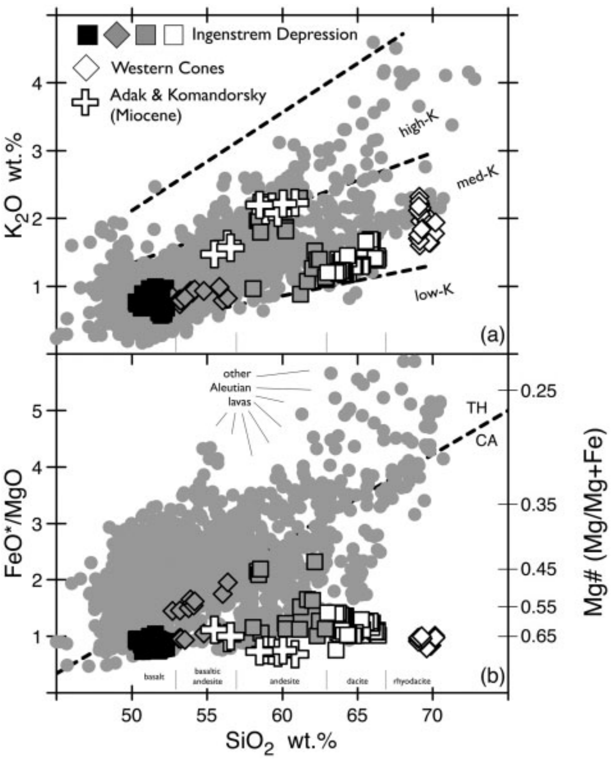

Fig. 4. Major element compositions of Aleutian lavas in terms of weight per cent K_2O and FeO*/MgO vs SiO_2 for samples included in this study (large symbols) compared with other Aleutian lava compositions from the literature (gray circles). Data for western Aleutian seafloor lavas are from Table 2. Black squares, basalts ($<$53% SiO_2); gray diamonds, basaltic andesites (53–57% SiO_2); gray squares, andesites (57–63% SiO_2); white squares, dacites (63–67% SiO_2); white diamonds, rhyodacites (67–70% SiO_2). Crosses, Miocene-age magnesian andesites/adakites from Adak Island and the far western Aleutian Komandorsky area from Table 2 and from Kay (1978) and Kay & Kay (1994). Dashed lines separating low-, medium- and high-K fields in (a) are from Gill (1981). The calc-alkaline–tholeiitic discriminant line (TH/CA) in (b) is from Miyashiro (1974). Gray circles, data for Quaternary age Aleutian volcanic rocks of all compositions compiled by Kelemen *et al.* (2003*b*) and combined with all Aleutian data published subsequently. Geographical coverage of the database is from the Cold Bay area in the east to Piip Seamount in the west (Fig. 1).

also illustrated in photomicrographs provided as Supplementary Data (SD Figs S1–S6).

Western seafloor basalts are variable between olivine-rich and plagioclase-rich petrographic types. Olivine-rich samples contain 10–25 modal % phenocrysts of olivine and clinopyroxene only (SD Fig. S1). Olivine phenocrysts are up to 2·0 mm long and contain inclusions of Cr-spinel. Clinopyroxene phenocrysts are smaller (~0·5 mm long), less abundant, and often glomerocrystic. Plagioclase-rich basalt types are crystal-rich, with 40–60 modal % phenocrysts and microphenocrysts that are mostly plagioclase (up to 2 mm long) with lesser quantities of clinopyroxene and olivine (SD Fig. S2). Remnant phenocrysts of amphibole, largely replaced by opaque minerals, were observed in one basalt sample. The groundmass of the basalts is mostly crystalline and dominated by plagioclase, pyroxene and opaque minerals.

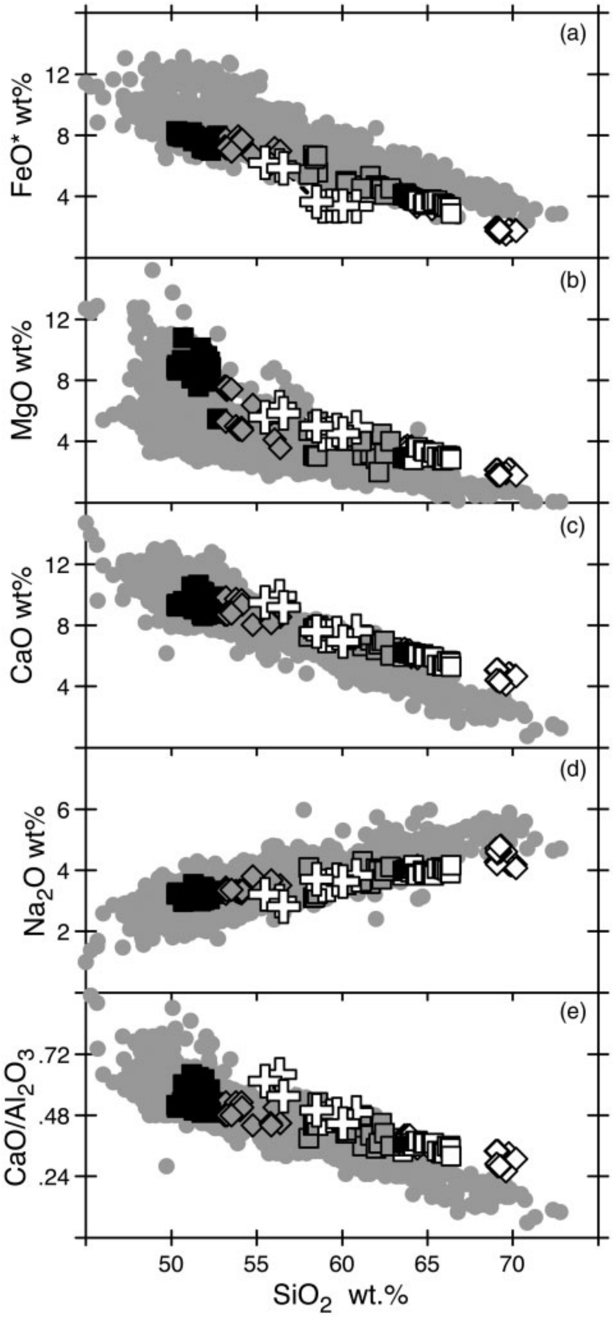

Fig. 5. Major element abundances of Aleutian lavas showing weight per cent FeO*, MgO, CaO, Na_2O and CaO/Al_2O_3 vs SiO_2. The high MgO and low FeO* for western Aleutian seafloor lavas at all SiO_2 contents should be noted. Symbols and data sources here are the same as in Fig. 4.

Most basaltic andesites are crystal-rich, often with 40–60% phenocrysts and microphenocrysts set in a groundmass of plagioclase, pyroxene, opaque minerals and brown glass. The dominant phenocryst mineral is plagioclase. These phenocrysts are generally $<$1·5 mm long, often with cores clouded by inclusions, especially in amphibole-bearing samples. Olivine-bearing basaltic andesites are petrographically similar to the plagioclase-rich basalts described above. Basaltic andesites lacking phenocrysts of olivine commonly

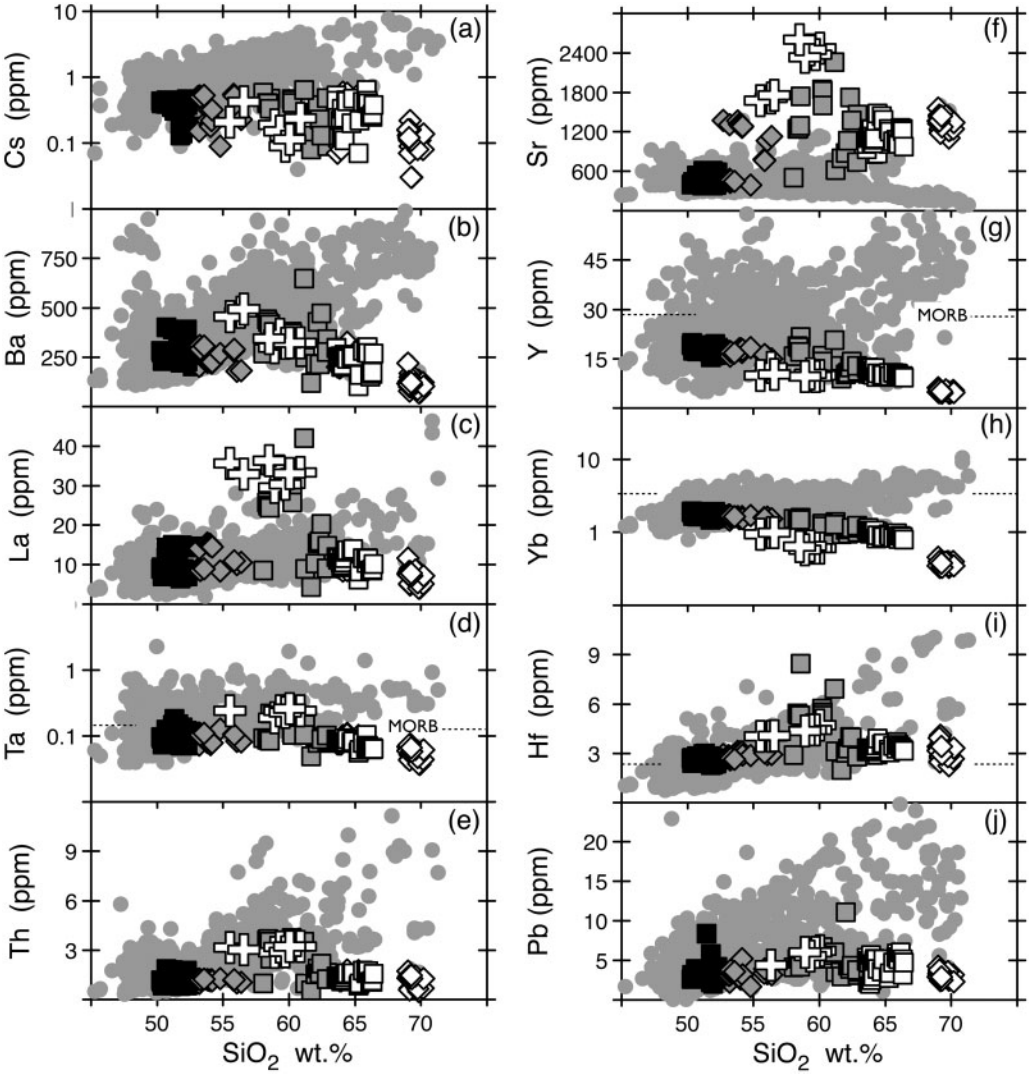

Fig. 6. Incompatible trace element abundances in Aleutian lavas vs SiO_2. The vertical-axis log scale in (a), (d) and (h) should be noted. Trace element abundances for normal MORB, shown by horizontal dashed lines, are from Sun & McDonough (1989). Normal MORB abundances for Cs, Ba, La, Th, Sr and Pb (not shown) are near the lower horizontal axis of the respective graphs. Symbols are the same as in Fig. 4. Trace element data are from Table 5.

contain two-pyroxene glomerocrysts up to 4 mm long with abundant inclusions of opaque minerals (SD Fig. S3). Basaltic andesites lacking phenocrysts of olivine also often contain amphibole phenocrysts up to 2–4 mm long. Most amphibole phenocrysts in basaltic andesites have opaque rims, are variably resorbed and appear to have reacted with the surrounding groundmass (SD Fig. S4).

The most petrographically distinctive western Aleutian seafloor lavas are andesites with 58–60% SiO_2, which have phenocrysts of amphibole and clinopyroxene (10–20%), but contain no phenocrysts or microphenocrysts of plagioclase (SD Figs S5–S8). Amphibole phenocrysts in these lavas are 1–4 mm long and are often needle-like in shape. Amphibole phenocrysts usually have opaque rims, but do not appear resorbed or reacted with the groundmass, which is composed mostly of dense, microlitic plagioclase with pyroxene, opaque minerals and brown glass. Clinopyroxene phenocrysts in these andesites are generally smaller and less abundant than amphibole. Higher silica andesites and dacites (61–66% SiO_2) are primarily plagioclase–amphibole phyric (SD Fig. S9). Some contain phenocrysts of clinopyroxene, but many do not. Most of the high-silica andesites and dacites have modest phenocryst abundances (10–15%) and some are nearly aphyric (SD Fig. S10). The rhyodacites, which are the most siliceous western seafloor lavas (68–70% SiO_2), are aphyric to sparsely phyric with microphenocrysts of plagioclase, amphibole and clinopyroxene (SD Fig. S11). Amphibole microphenocrysts in the rhyodacites are free of opaque rims and are often needle-like in shape.

Trace elements

Western Aleutian seafloor basalts have abundances of incompatible trace elements that are generally similar to those in basalts from other parts of the arc (Fig. 6).

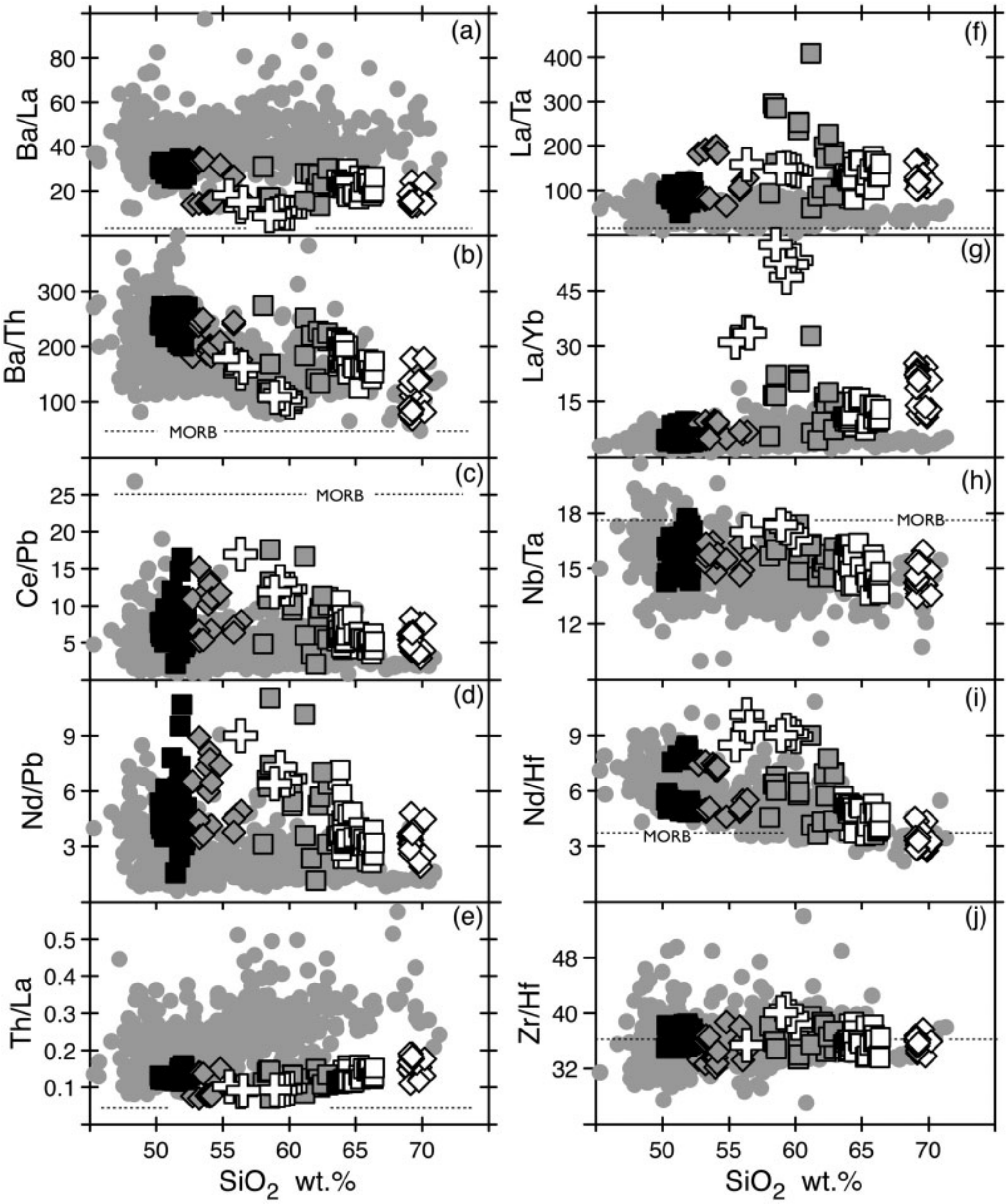

Fig. 7. Incompatible trace element ratios vs weight per cent SiO_2 for Aleutian lavas. Ratios for average normal MORB shown by horizontal dashed lines are from Sun & McDonough (1989). Normal MORB value for Nd/Pb (not shown) is 24·3. Other MORB ratio values for normal MORB not shown are near the lower horizontal axis of the respective graphs. Symbols and data sources are the same as in Fig. 4.

At higher silica, abundances of these elements in the western seafloor lavas are similar to or lower than those of the basalts. This is particularly clear for the dacites and rhyodacites, which have Cs, Ba, Th, Ta, K and La concentrations significantly lower than those for lavas with similar silica contents from the central and eastern Aleutians (Fig. 6). The pattern is less clear in the andesites, which are highly variable and have relatively high abundances for some elements, especially La, and Th (Fig. 6) in addition to K_2O (Fig. 4a). In contrast to the incompatible trace elements in most Aleutian volcanic rocks, which show increasing abundances with increasing SiO_2, incompatible trace elements in western Aleutian seafloor lavas show flat to decreasing abundances of incompatible elements with increasing SiO_2 (Fig. 6). This pattern is, again, less clear for the andesites, which are highly variable for some elements (e.g. Hf, Zr, Dy). The only clear exception to the pattern of flat to decreasing abundances with increasing silica is Sr, which is below 600 ppm for all basalts, but is highly variable and greater than 1000 ppm for most of the higher silica, western seafloor lavas (Fig. 6f). The highest Sr concentrations are seen in the andesites, which have Sr between ~500 and ~2300 ppm.

Incompatible trace element ratios in the western Aleutian seafloor basalts are generally similar to those in basalts from other parts of the arc. This is illustrated in REE patterns for basalts from the Ingenstrem

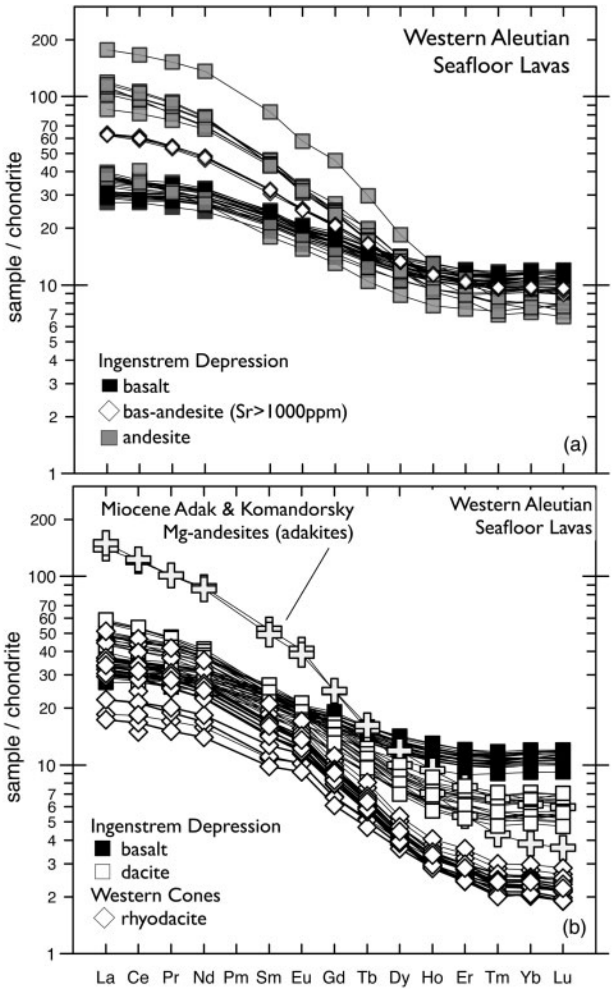

Fig. 8. Chondrite-normalized REE abundances in western Aleutian seafloor lavas and Miocene Mg-andesites/adakites from Adak Island and Komandorsky Straits. Chondritic normalizing values are from Sun & McDonough (1989). Symbols and data sources here are the same as in Fig. 4.

Depression, which lie approximately parallel to those observed in basalts from central and eastern Aleutian volcanoes (La = 4–10 ppm with La/Yb = 3–6; Figs 6c and 7g). This results in a pattern enriched in the light REE (LREE), with La and Ce at ~30 times chondritic values (Fig. 8a). Relative enrichments in Ba and Th in Ingenstrem basalts are slightly lower than is typical for Aleutians basalts (e.g. Ba/La ~35, Th/La ~1·5; Fig. 7a and e). Relative abundances for the HFSE (Ta, Nb, Zr, Hf) in Ingenstrem basalts are also similar to those for basalts throughout the arc, as illustrated by ratios such as La/Ta and Nd/Hf (Fig. 7f and i).

At intermediate and high silica contents the western Aleutian seafloor lavas have the most strongly fractionated trace element patterns among Quaternary-age lavas in the Aleutians. This is most evident in the dacites and rhyodacites, which are progressively depleted in the HREE with increasing silica (Fig. 6g and h), with Lu and Yb abundances no more than 2–3 times chondritic in the rhyodacites (Fig. 8b). The seafloor dacites and rhyodacites have strongly fractionated REE patterns (La/Yb >7; Fig. 7g), but their LREE abundances are not significantly elevated compared with those of basalts (Fig. 8b). All of the western seafloor dacites and rhyodacites would be classified as adakites, based on the criteria of Defant & Drummond (1990). However, relatively low abundances of La, Ce and other LREE, which are similar to or lower than those for many Aleutian basalts (Figs 6c and 8b), distinguish the western seafloor dacites and rhyodacites from Miocene-age

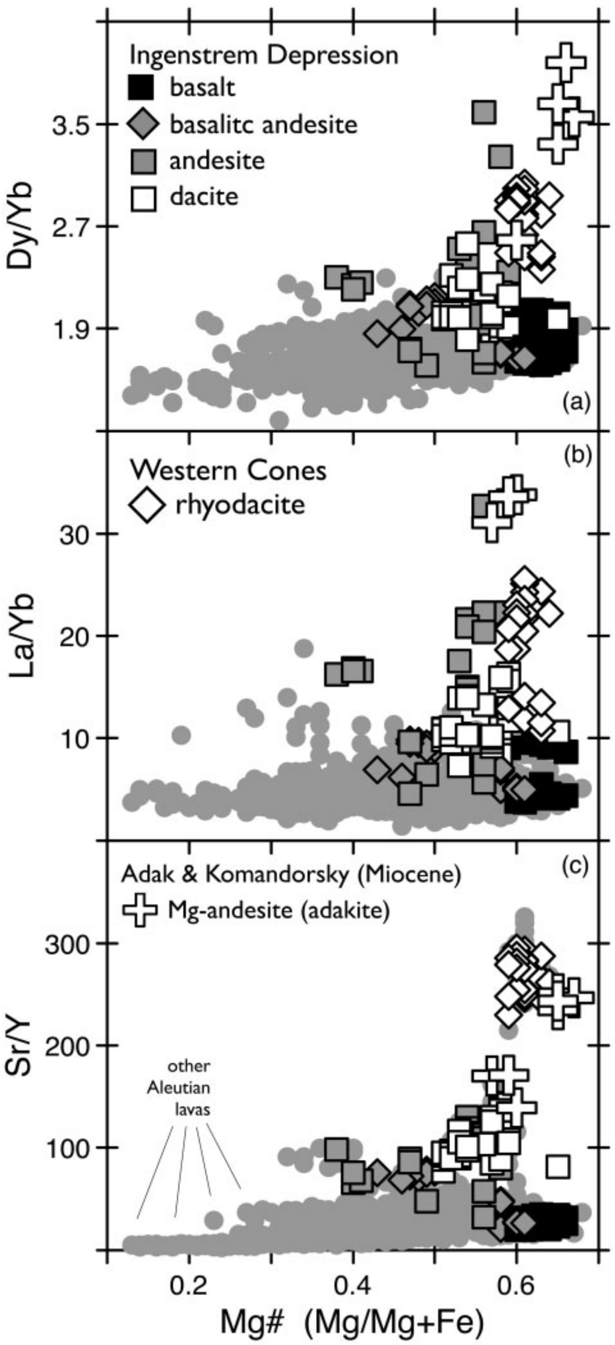

Fig. 9. Trace element ratios (a) Dy/Yb, (b) La/Yb and (c) Sr/Y vs Mg# for Aleutian lavas. The Mg# value is the molar Mg content divided by the sum of molar Mg and total Fe. Symbols and data sources are the same as in Fig. 4.

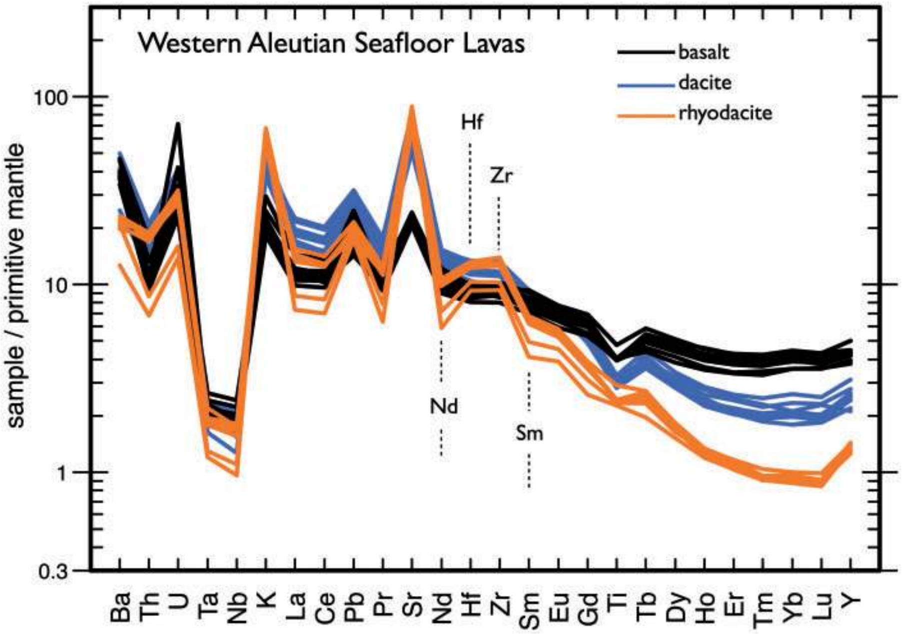

Fig. 10. Trace element abundances in western Aleutian seafloor lavas normalized to primitive mantle from McDonough and Sun (1995). Basalts and dacites (black and blue) are from the Ingenstrem Depression. Rhyodacites (orange) are from the Western Cones area. These data are from Table 5.

Adak and Komandorsky magnesian andesites (adakites), which are depleted in Y, Yb and Lu (3–6 times chondritic), but are also strongly enriched in Sr and LREE (Figs 6c, f and 8b). Only a small number of andesites from among the western Aleutian seafloor lavas have both elevated Sr and LREE abundances as well as fractionated REE patterns (La/Yb >30) and therefore closely resemble the Miocene-age Adak and Komandorsky adakites (Fig. 8). It is important to note that fractionated or adakitic trace element patterns in western seafloor andesites, dacites and rhyodacites are most clearly expressed in lavas with Mg# > 0·60 (Fig. 9). Thus, virtually all adakitic rocks in the Aleutians are primitive (Mg# > 0·60) and so differ from the broadly defined adakites of Defant & Drummond (1990), which include a wide variety of volcanic and plutonic rocks that are highly evolved, with Mg# commonly <0·50 (e.g. Drummond & Defant, 1990).

Enrichments in Ba and Th relative to the LREE (Ba/La, Th/La) are similar for all western seafloor lavas, and are less strongly expressed than in common Aleutian lavas, especially at intermediate and high silica (Fig. 7a and e). In contrast, the relative abundances of Sr, K, and Pb are more variable and are sometimes significantly different in western seafloor andesites, dacites and rhyodacites from those for common Aleutian lavas (e.g. Ce/Pb > 8; Fig. 7c).

Most of the seafloor andesites, dacites and rhyodacites are more strongly depleted in Ta and Nb than is normally observed in Aleutian lavas (La/Ta > 100, Fig. 7f). The strongest relative Ta–Nb depletions are present in the andesites, which have markedly higher La abundances (>20 ppm) and slightly lower Ta (<0·1 ppm) compared with common Aleutian lavas (Figs 6c, d and 7f). However, the lowest Ta and Nb abundances are in the dacites and rhyodacites (Fig. 6d). Also, Nb–Ta ratios in western seafloor lavas are similar to those in volcanic rocks throughout the Aleutians (Nb/Ta ~13–16), but the dacites and rhyodacites have systematically lower Nb/Ta than do the basalts and andesites (Fig. 7h). In contrast, Zr–Hf ratios in western seafloor lavas appear to be similar at all silica contents (Zr/Hf ~36, Fig. 7j).

Relative depletions of Hf and Zr in the seafloor lavas, which may be expressed as elevated Nd/Hf or Sm/Zr relative to MORB, are similar to those for common Aleutian lavas at all silica contents for all samples but one andesite, which has Nd/Hf > 7, similar to the Miocene Mg-andesites (Fig. 7i). The pattern of decreasing Nd/Hf with increasing silica (Fig. 7i), which is evident in island arc lavas worldwide (Handley *et al.*, 2011; Woodhead *et al.*, 2011), continues to high silica contents in the seafloor rhyodacites, which have relative abundances of Hf and Zr greater than Nd and Sm on primitive mantle-normalized plots (Fig. 10). The seafloor rhyodacites have Nd/Hf and Sm/Zr that are sub-chondritic, and therefore have small positive Hf–Zr abundance anomalies relative to Nd and Sm (Fig. 10).

The results indicate that incompatible trace element ratios in western seafloor andesites, dacites and rhyodacites are commonly distinct from those in lavas from emergent Aleutian volcanoes (Figs 7–10). An important exception is Ba/Th, which decreases slightly with increasing silica, but is generally similar in seafloor lavas of all compositions and in lavas from emergent volcanoes throughout the arc (Fig. 7b).

Consistent with their primitive, high-Mg# compositions, concentrations of compatible trace elements in

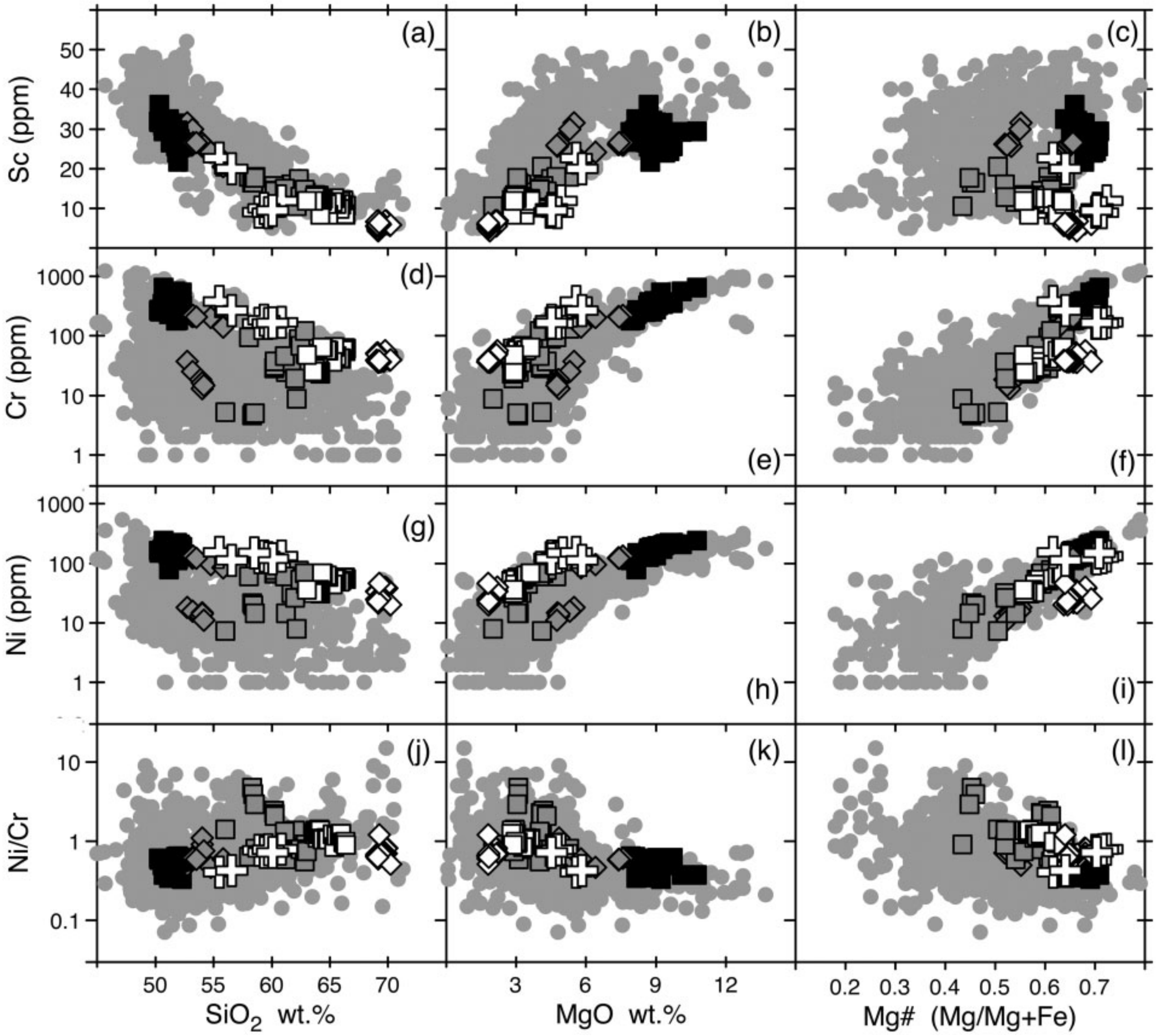

Fig. 11. Compatible trace element abundances and ratios vs weight per cent SiO_2, MgO and Mg# for Aleutian lavas. Symbols and data sources are the same as in Fig. 4.

western seafloor lavas are also relatively high. A few evolved basaltic andesites and andesites with <6% MgO and Mg# <0·56 have Cr and Ni abundances that are typical of Aleutian andesites, but Ni and Cr abundances in most western seafloor lavas are high relative to SiO_2 and MgO (Fig. 11d, e, g and h). Similarly high Ni and Cr are seen in the magnesian andesites (adakites) from Adak Island and the Komandorsky Straits, but with the exception of a few andesites, the Ni/Cr ratios in western seafloor lavas are similar to those of volcanic rocks throughout the Aleutian arc (Fig. 11j and l). Scandium abundances (Fig. 11a–c) are relatively low in western seafloor lavas. This is particularly clear for primitive andesites, dacites and rhyodacites with Mg# values >0·6 and Sc abundances often <15 ppm (Fig. 11c and l).

Isotopes (Hf, Nd, Pb)

For Hf and Nd isotopes, the western seafloor lavas cluster at the radiogenic end of Aleutian volcanic rock compositions, which are well correlated along the center of the terrestrial array in Hf–Nd isotope space (Fig. 12). Variability of Hf and Nd isotopes in western Aleutian seafloor lavas is limited. Total variation for Nd in 31 samples is only 1·5 ε_{Nd} units (8·3–9·8). Excluding one outlier at $\varepsilon_{Hf} = 16{\cdot}2$, the total variation for Hf in 26 western Aleutian seafloor samples is 1·6 ε_{Hf} units (13·6–15·2; Fig. 12). For Pb isotopes, the strong trend toward high $^{207}Pb/^{204}Pb$, which has long been interpreted to result from a source component for Pb in subducted sediment (Kay *et al.*, 1978; Kay, 1980), is reinforced by new thalium-normalized ICP-MS Pb isotope data presented here for western seafloor lavas (Table 6) and for samples collected from emergent volcanoes throughout the arc (Supplementary Data). The data form a steep trend of increasing $^{207}Pb/^{204}Pb$ with increasing $^{206}Pb/^{204}Pb$ (Fig. 13), which approaches the composition of Aleutian trench sediment from Deep Sea Drilling Project (DSDP) Site 183 (Peucker-Ehrenbrink *et al.*, 1994; Plank & Langmuir, 1998; Kelemen *et al.*, 2003*b*;

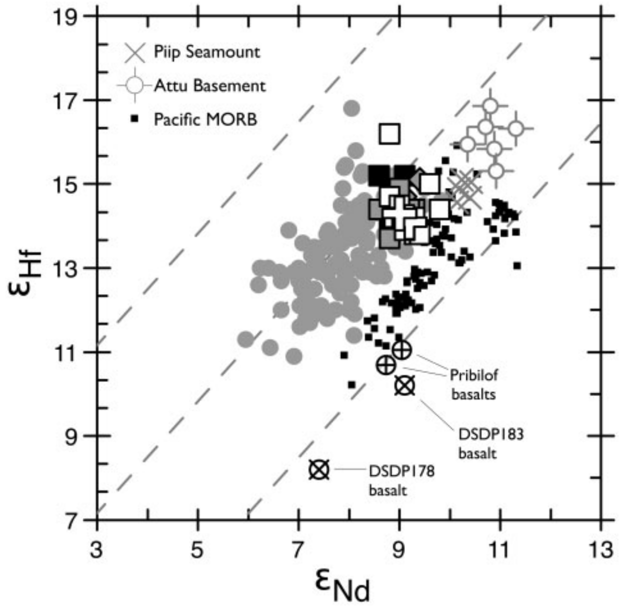

Fig. 12. Isotope correlation diagram for Hf and Nd (ε_{Hf}, ε_{Nd}) showing compositions of Aleutian lavas compared with Pacific MORB, Attu basement series basalts, DSDP basalts, and basalts from the Pribilof Islands, which are located in the Bering Sea (Fig. 1). Attu, Piip, Pribilof and DSDP data are from Yogodzinski *et al.* (2010). The Attu sample group includes geochemically similar depleted tholeiitic basalt from the Komandorsky Basin. Sample locations and symbols not defined on the graph are the same as in Fig. 4. Aleutian data shown are from Table 6 and from Jicha *et al.* (2004) and Yogodzinski *et al.* (2010). Pacific MORB data are from Sims *et al.* (2002), Hamelin *et al.* (2011) and Waters *et al.* (2011). Epsilon notations for Nd and Hf isotopes are defined in the footnotes to Table 6.

Vervoort *et al.*, 2011). Western seafloor lavas have relatively unradiogenic Pb, and so lie at the low $^{206}Pb/^{204}Pb$ end of this trend ($^{206}Pb/^{204}Pb = 18{\cdot}3$–$18{\cdot}6$; Fig. 13). The western seafloor lavas also have significantly more radiogenic Pb than lavas from Piip Seamount (Fig. 1), which have $^{206}Pb/^{204}Pb < 18{\cdot}1$ and fall above the regression line through the western seafloor lavas in Pb–Pb isotope plots (Fig. 13). Among the western seafloor lavas, there is a tendency toward more depleted isotopic compositions in higher-silica lavas, which is evident in Pb and Nd isotopes, but not for Hf (Fig. 14).

DISCUSSION

Extent of the Aleutian volcanic arc

The ages of Ingenstrem Depression lavas determined for this study, which are variable from 16 to 521 ka (Table 7; Fig. 3), are similar to ages obtained through detailed stratigraphic and geochronological studies of emergent Aleutian volcanoes (Jicha *et al.*, 2005, 2012; Coombs & Jicha, 2013). We interpret these ages to indicate that volcanic activity in the Ingenstrem Depression has been ongoing throughout the late Pleistocene and Holocene. Age data are not available for samples from the Western Cones, but the location and arc-parallel alignment of the cones indicates that volcanism is probably active along a volcanic front that spans the full 700 km distance from Buldir Volcano to Piip Seamount in the Komandorsky area (Fig. 1). The presence of an active volcanic front is consistent with trench depths of 6000–6500 m along the western Aleutian arc and with geodetic measurements documenting significant trench-normal convergence near Attu Island, which lies between the Ingenstrem Depression and Western Cones areas (Cross & Freymueller, 2008). These observations, which are consistent with modeling of the Aleutian slab shape (Hayes *et al.*, 2012), clearly indicate that the Aleutian arc west of Buldir Island is an oblique subduction boundary (not a transform boundary). Thus, it is evident that subduction and arc magmatism are active and continuous along the full length of the Aleutian island arc from the Cold Bay area and Unimak Island in the east to Piip Seamount in the Komandorsky area in the west (Fig. 1).

It is important to note that Piip and at least one of the Western Cones are as large as many emergent Aleutian volcanoes, and that submergence of these features reflects displacement of the volcanic front into relatively deep water to the north of the thickened arc crust of the western Aleutian ridge. We assume that the location of the volcanic front is controlled by the shape and dynamics of the subducting plate (England *et al.*, 2004). It is also evident from geodetic data that the Komandorsky and Near Islands crustal blocks (Fig. 1b) are moving along the arc at rates of tens of kilometers per million years (Cross & Freymueller, 2008; see also Avé Lallemant & Oldow, 2000). Thus, the location of the volcanic front and the axis of thickened arc crust are controlled independently in the western Aleutians. As a result, it is not surprising that an offset between the two exists. Development of this offset must have been since ~6 Ma, when magmatism in the western Aleutian islands ended (Kay *et al.*, 2014). The main importance of these issues here is that volcanoes of the westernmost Aleutian arc, from the Western Cones area to Piip Seamount in the Komandorsky area, are constructed largely or entirely on oceanic lithosphere of the Bering Sea (see also Seliverstov *et al.*, 1990; Baranov *et al.*, 1991; Yogodzinski *et al.*, 1993). This physical setting for the volcanism of the Western Cones area is important because it helps to constrain the origin of their distinctive trace element patterns, which require a significant role for residual or cumulate garnet, as discussed below.

Origin of the western Aleutian seafloor lavas

Concentrations of Yb, Lu, Ta and Nb are lower in western Aleutian seafloor andesites, dacites and rhyodacites than in western seafloor basalts or in lavas of any composition from emergent Aleutian volcanoes (Figs 6–9). Low Yb and Lu in some andesites and dacites may be interpreted as an effect of amphibole removal by fractional crystallization (Romick *et al.*, 1992), but

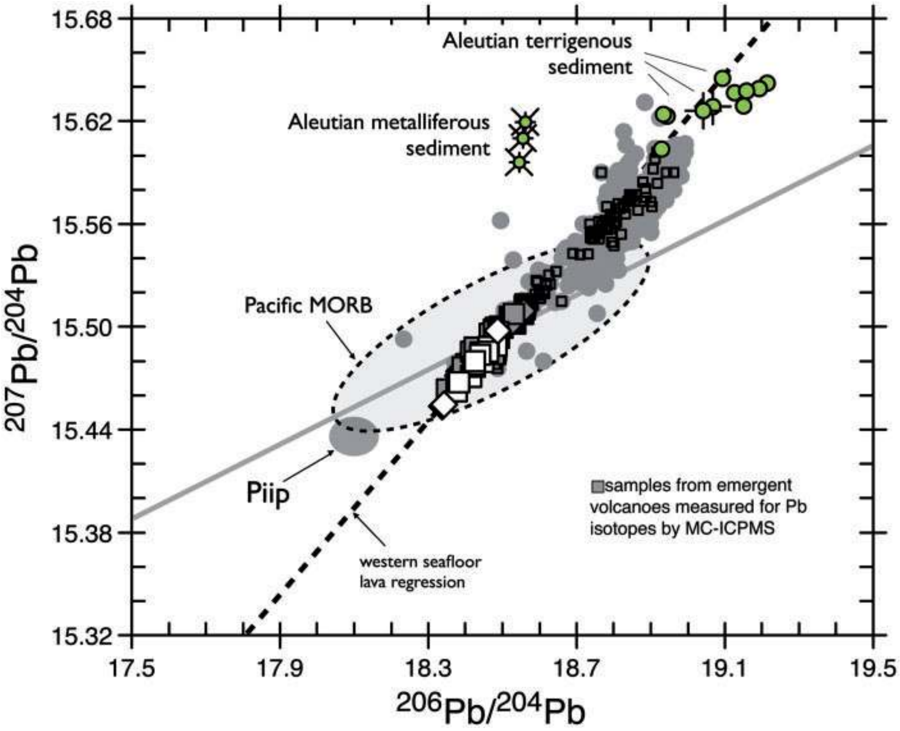

Fig. 13. Variation of ^{207}Pb/^{204}Pb vs ^{206}Pb/^{204}Pb for Aleutian lava and sediment samples compared with Pacific MORB. Sample locations and symbols not defined on the graph are the same as in Figs 4 and 12. Bold dashed black line is a major-axis regression through the western seafloor lavas, which passes through Aleutian terrigenous sediment and closely parallels the trend for all Aleutian lavas. Bulk sediment composition for the DSDP 183 core from Plank & Langmuir (1998) and an average composition for all DSDP 183 terrigenous sediments are shown by the sediment symbols with a cross through them. The continuous gray line is the northern hemisphere reference line (NHRL) from Hart (1984). Data for western seafloor lavas are from Table 6. Data for lavas from emergent volcanoes measured by Tl-normalized MC-ICP-MS are from the Supplementary Data. Sediment data are from McDermott & Hawkesworth (1991), Peucker-Ehrenbrink *et al.* (1994), Plank & Langmuir (1998), Kelemen *et al.* (2003*b*) and (Vervoort *et al.* 2011). Pacific MORB field shows the predominant compositional range based on data compiled from published sources (Hegner & Tatsumoto, 1987; Ito *et al.*, 1987; White *et al.*, 1987; Bach *et al.*, 1994; Mahoney *et al.*, 1994; Castillo *et al.*, 1998, 2000; Niu *et al.*, 1999, 2002; Regelous *et al.*, 1999; Vlastélic *et al.*, 1999; Wendt *et al.*, 1999; Chauvel & Blichert-Toft, 2001; Sims *et al.*, 2002; Davis *et al.*, 2008; Hahm *et al.*, 2009; Hamelin *et al.*, 2011; Waters *et al.*, 2011).

fractionation of the middle to heavy part of the REE pattern, as seen in rhyodacites from the Western Cones (Dy/Yb >2·0, Fig. 9), requires a role for garnet (e.g. Martin, 1994; Kelemen *et al.*, 2003*b*; Davidson *et al.*, 2007; Mamani *et al.*, 2010). Low relative abundances of Ta and Nb are similarly consistent with strong partitioning of these elements into rutile (Rapp *et al.*, 1991; Foley *et al.*, 2000; Schmidt *et al.*, 2004*a*; Klemme *et al.*, 2005; Xiong *et al.*, 2005). Trace element patterns in western Aleutian andesites, dacites and rhyodacites therefore reflect fractionation involving garnet + rutile, which is less evident in lavas from emergent Aleutian volcanoes.

Recent experimental studies of hydrous and oxidized silicate melt systems indicate that the low Yb–Lu character of western seafloor andesites, dacites and rhyodacites is unlikely to have been produced by fractional crystallization of a garnet-bearing mineral assemblage. Experiments by Müntener *et al.* (2001) and Alonzo-Perez *et al.* (2009) show that hydrous andesitic liquids will saturate in garnet at pressures of 1·2 GPa, and may, at that pressure, evolve by fractional crystallization to higher-silica liquids (see also Green, 1982). Such high-silica liquids evolving at low temperatures and under hydrous conditions may also be saturated in rutile (Ryerson & Watson, 1987). Co-saturation of garnet and rutile in basaltic and andesitic liquids undergoing fractional crystallization could therefore drive Y, Yb, Lu, Ta and Nb abundances downward, as seen in western Aleutian dacites and rhyodacites compared with lower silica lavas (Fig. 6). However, dacitic liquids produced in the Müntener *et al.* (2001) and Alonzo-Perez *et al.* (2009) and other experiments (Botcharnikov *et al.*, 2008) all have FeO*/MgO > 2·0, and so are unlike the highly calc-alkaline dacites and rhyodacites that we see among the western seafloor lavas (Fig. 4b). Berndt *et al.* (2005) and Sisson *et al.* (2005) showed that basaltic and andesitic liquids may evolve by fractional crystallization under highly oxidizing conditions [3–4 log units above nickel–nickel oxide (NNO)] to high-silica compositions with FeO*/MgO <2. However, evolved liquids in these experiments commonly contain <1·0 wt % MgO at 63–76% SiO_2, and so are also unlike high-silica western Aleutian seafloor lavas, which contain ~2% MgO at 69% SiO_2 and 3–4% MgO at 63–66% SiO_2. The absence of plagioclase phenocrysts from some Ingenstrem Depression andesites is a clear indication of high pre-eruptive water contents (see Luhr *et al.*, 1989; Carmichael, 2002). Based on this it seems likely that

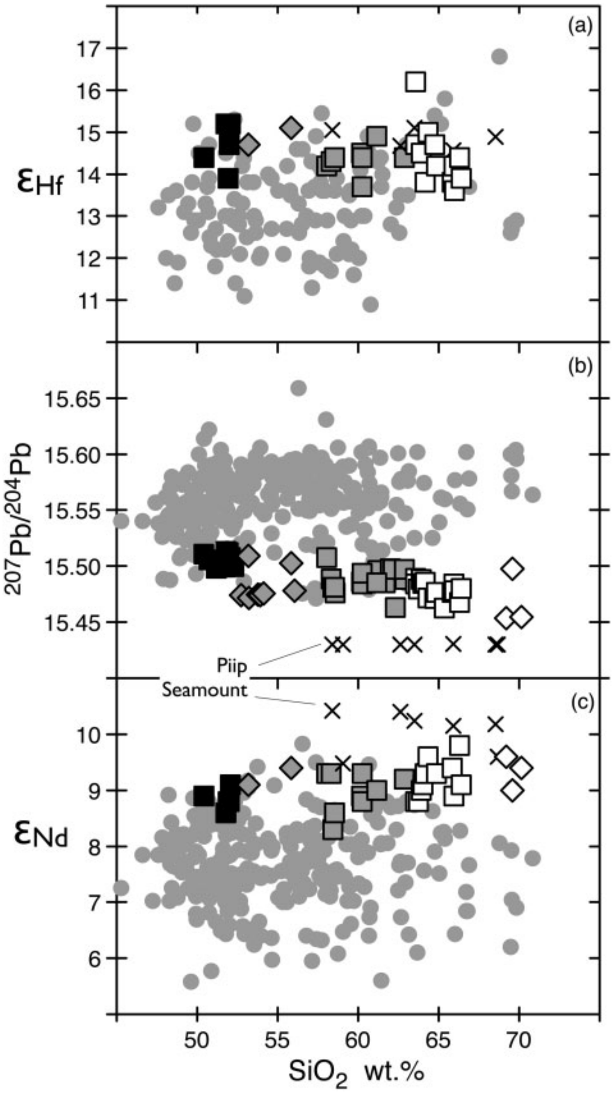

Fig. 14. Lead (Pb), Nd and Hf isotope compositions (ε_{Nd}, ε_{Hf}) vs SiO$_2$ for western Aleutian seafloor lavas from the Ingenstrem Depression and Western Cones area compared with those from Piip Seamount and lavas from other Aleutian volcanoes. Sample locations and symbols are the same as in Figs 4 and 12. Epsilon notation for Nd and Hf isotopes is defined in the footnotes to Table 6.

high water contents have played a role in controlling the highly calc-alkaline nature of the western Aleutian igneous series (e.g. Sisson & Grove, 1993; Zimmer *et al.*, 2010). Nonetheless, we find no experimental results showing that fractional crystallization from basalt can drive liquids to high-silica and magnesian compositions (high Mg#, low FeO*/MgO), such as those that we see in western Aleutian seafloor dacites and rhyodacites. This leads us to conclude that the low-Yb–Ta character of the western seafloor lavas must have been produced because garnet and rutile (or perhaps some other Ta–Nb-rich mineral) were left as residual phases in the melt source.

Some aspects of the highly calc-alkaline igneous series defined by the western Aleutian seafloor lavas (Fig. 4b) may be attributed to extensive melting and reactive transport of basalt through depleted peridotite under low-pressure and hydrous conditions (Kelemen *et al.*, 1990; Yogodzinski *et al.*, 1994). Experimental observations indicate that such processes may leave an olivine–orthopyroxene residual mineralogy and produce hydrous magnesian andesites, with up to 55–57% SiO$_2$ (Tatsumi, 1982; Grove *et al.*, 2003; Wood & Turner, 2009). Evolution of those primitive andesitic magmas by fractional crystallization may then produce dacitic lavas with higher silica and lower Mg# (Grove *et al.*, 2005). Magnesian andesites from Piip Volcano have been interpreted to be the products of primitive basalt reaction with depleted peridotite under low-pressure and hydrous conditions (Yogodzinski *et al.*, 1994). Dacites at Piip were likewise interpreted to reflect fractional crystallization of magnesian andesites (Yogodzinski *et al.*, 1994). However, Piip lavas do not have elevated Dy/Yb and therefore are unlike dacites and rhyodacites from the Ingenestrem Depression and Western Cones, which have higher silica and show adakitic trace element patterns, including elevated Dy/Yb that requires a role for residual garnet (Fig. 8b). The need for residual garnet and some mechanism to produce high silica therefore rules out peridotite melting as a model for the origin of the highly calc-alkaline series defined by seafloor lavas of the western Aleutian arc.

Melting of garnet-bearing deep crust is often cited as a mechanism capable of producing high-silica magmas with strongly fractionated trace element patterns (e.g. Lopez-Escobar *et al.*, 1977; Hildreth & Moorbath, 1988; Petford & Atherton, 1996). However, this process cannot have produced residual garnet control over trace element patterns in western Aleutian seafloor lavas because those samples with the strongest garnet signatures are rhyodacites from the Western Cones area, which are submerged in water depths of >3400 m and are built on oceanic lithosphere of the Bering Sea (Fig. 2). Under these conditions, the crust beneath the Western Cones is probably <10 km thick, because such thicknesses are typical of oceanic crust. This implies that pressures in the deep crust beneath the Western Cones must be <0·3 GPa, and so unlikely to stabilize garnet during crust melting reactions, which usually requires pressures of 1 GPa or more (Wolf & Wyllie, 1994; Rapp, 1995; Muentener *et al.*, 2001; Alonzo-Perez *et al.*, 2009). Physical conditions in the crust beneath the Western Cones (<0·4 GPa) are therefore inappropriate for garnet stabilization.

As noted above and in previous studies, isotope data rule out a significant contribution of incompatible trace elements from subducted, continentally derived sediment in western Aleutian magmas (Yogodzinski *et al.*, 1994, 1995; Kelemen *et al.*, 2003*b*). Figures 15–17, which are discussed in detail below, also show that many Aleutian lavas are more strongly depleted in Ta and Yb relative to Th, Nd and Hf than Aleutian sediment from DSDP 183. This means that the low Ta–Yb character of the western seafloor lavas is not derived primarily from recycled sediment. Therefore, we interpret western Aleutian seafloor lavas to have inherited their radiogenic Hf and Nd isotopic compositions from a combination of subducting oceanic crust and mantle wedge. This leads us to conclude that residual garnet and rutile in the source of western seafloor lavas must have been left in the basaltic part of the subducting oceanic lithosphere, following melt extraction under eclogite-facies conditions.

This model is also consistent with Pb isotope data showing that western seafloor dacites and rhyodacites fall at the unradiogenic end of the well-correlated field of Aleutian lava compositions in Pb–Pb isotope space (Fig. 13). We interpret this trend to indicate that Pb in Aleutian lavas is primarily derived from subducted basalt and subducted sediment. This is consistent with previous interpretations of Aleutian lavas (Kay *et al*., 1978; Kay, 1980; Miller *et al*., 1994), and with recent work from a variety of arcs where the Pb isotope compositions are highly variable (Hoernle *et al*., 2008; Beier *et al*., 2010; Regelous *et al*., 2010).

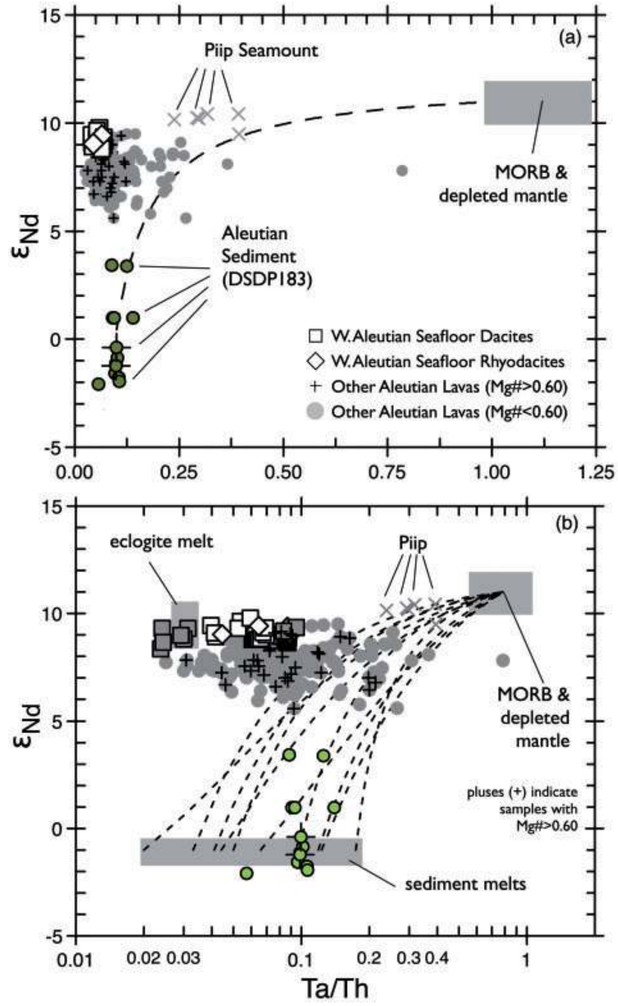

Fig. 15. Neodymium isotope composition (ε_{Nd}) vs Ta/Th for Aleutian lavas compared with sediment–mantle mixing lines. In (a) dashed line is a mixture between depleted mantle and bulk sediment. The mantle end-member in the mixture is from Salters & Stracke (2003) with Nd = 0·713 ppm, Th = 0·0137 ppm and Ta = 0·0138 ppm. The sediment end-member is average terrigenous sediment from DSDP 183 from Vervoort *et al.* (2011; ε_{Nd} = –1·0) and from Plank & Langmuir (1998; Nd = 19·1 ppm, Th = 5·49 ppm, Ta = 0·545 ppm). In (b), sediment melt end-members are model compositions based on experiments of Hermann & Rubatto (2009) and Skora & Blundy (2010). The eclogite melt is a model composition with Ta/Th = 0·031 (Table 8). The isotopic composition of the eclogite melt component ($\varepsilon_{Nd} \sim 9·5$) is estimated from the compositions of western seafloor dacites and rhyodacites. Sediment and eclogite melt models are also plotted in Fig. 18. Trace element ratios for the MORB and depleted mantle fields are based on average compositions from Sun & McDonough (1989), Salters & Stracke (2003) and Workman & Hart (2005). Isotopic compositions are set within narrow limits based on mixing trends inferred from the data trends, and on compositions of key sample sets, as described in the text. The eclogite melt shown here and in subsequent figures is the model composition in Table 8. (See footnotes to Table 8 and text for additional information.)

These interpretations are consistent with recent slab geometry models (Hayes *et al*., 2012), which indicate that subducting oceanic lithosphere is present beneath the Ingenstrem Depression and Western Cones areas, even though there is no deep seismic zone and there are few earthquakes to depths greater than 200 km west of Buldir Island (Levin *et al*., 2005; Ruppert *et al*., 2007). The lack of significant deep and intermediate depth seismicity in the area probably results from high temperatures in the subducting oceanic lithosphere beneath the western Aleutians, owing to the effects of oblique subduction (Yogodzinski *et al*., 1995; Kincaid & Sacks, 1997; Kelemen *et al*., 2003*b*; Lee & King, 2010). Geodetic observations show that the orthogonal subduction component beneath the western Aleutians is small compared with the arc-parallel component (Cross & Freymueller, 2008), so the motion of the subducting plate through the mantle beneath the western Aleutians is mostly horizontal. Resultant heating of the subducting lithosphere is probably enhanced by the effects of a breached slab or slab portal, brought on by tearing and/or thermal ablation of the slab (Yogodzinski *et al*., 2001; Levin *et al*., 2005). If this interpretation is correct, it means that incompatible trace element patterns in western Aleutian seafloor lavas are derived primarily from the residual mineralogy and processes related to the extraction of melts and/or fluids from subducting basalt in eclogite facies, and that their major and compatible trace element compositions reflect interactions of the resulting high-silica, low-Mg# liquid with peridotite in the mantle wedge prior to eruption (see Kay, 1978; Yogodzinski *et al*., 1994, 1995; Kelemen *et al*., 2003*b*; Portnyagin *et al*., 2007*a*, 2007*b*; Straub *et al*., 2008, 2011; Bryant *et al*., 2010). High Mg# in the andesites, dacites and rhyodacites, and high Cr and Ni abundances in many of these rocks relative to SiO_2 and MgO (Fig. 11), are interpreted to reflect interaction between high-Si melts from the subducting plate and peridotite in the overlying mantle wedge. These interpretations also imply that the dominant process controlling geochemical variation among the western seafloor lavas is mixing of different primitive magma types, which are widely variable in SiO_2 but which also have Mg# >0·6,

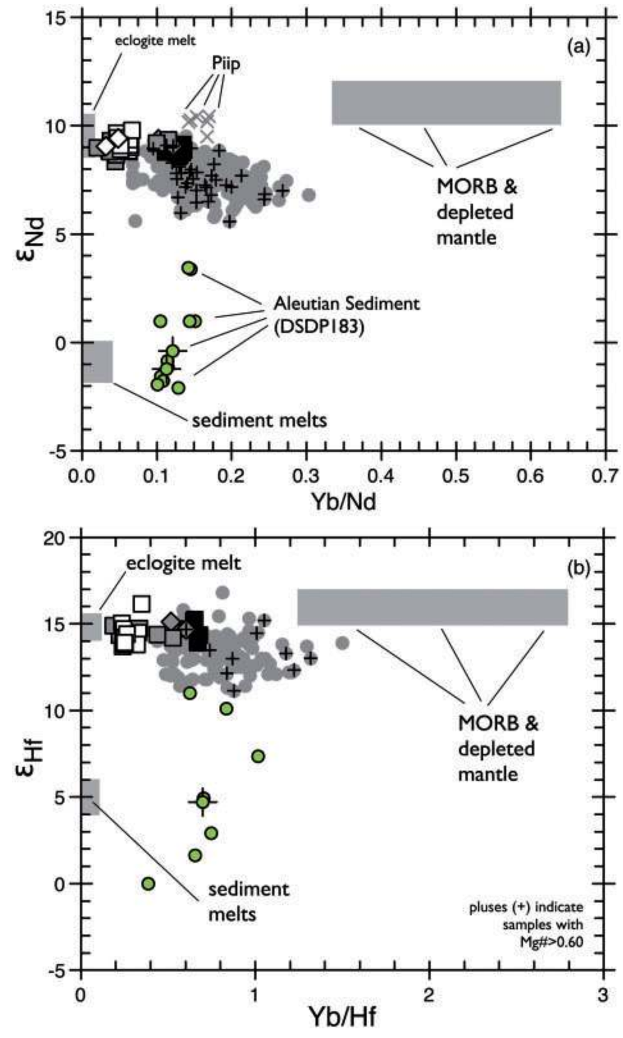

Fig. 16. Neodymium and Hf isotope variations (ε_{Nd}, ε_{Hf}) vs Yb/Nd and Yb/Hf for Aleutian volcanic rocks and sediment. Symbols and data sources are the same as Figs 4 and 12. Compositions of lavas from Piip Volcano are shown in (a) but are obscured by other western seafloor lavas in (b) and are not shown. Mixing lines on these graphs (not shown) are straight. The MORB and depleted mantle field and eclogite melt composition are defined as in Fig. 15. Sediment and eclogite melts are model compositions (Table 8), also plotted in Fig. 18.

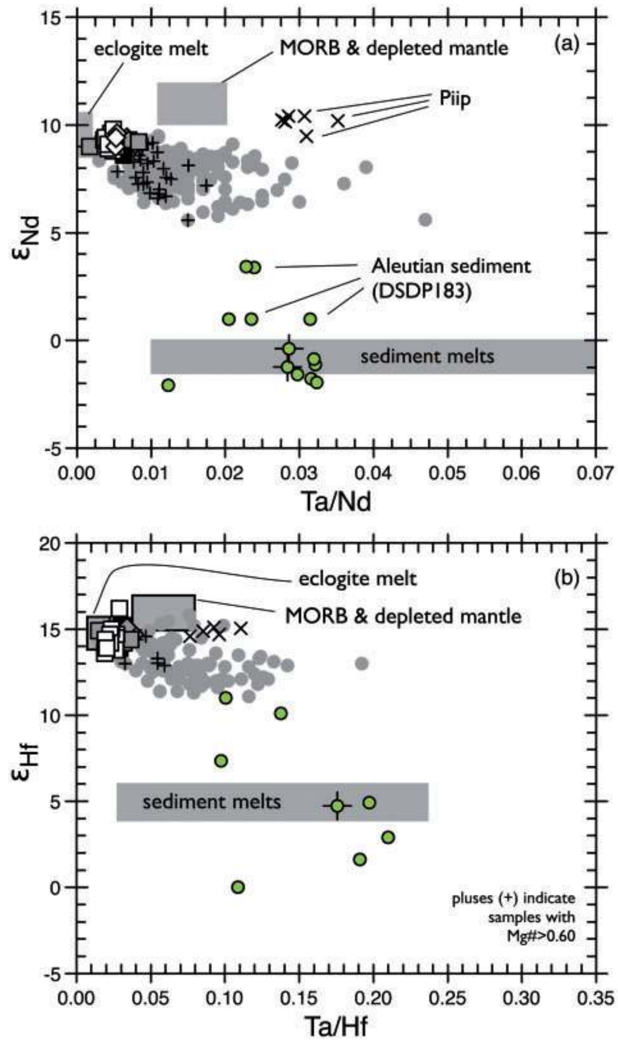

Fig. 17. Neodymium and Hf isotope variations vs Ta/Nd and Ta/Hf for Aleutian lavas. Symbols and data sources for Aleutian lavas and sediments are the same as in Figs 4 and 12. Mixing lines on these graphs (not shown) are straight. The MORB and depleted mantle field and eclogite melt composition are defined as in Fig. 15. Sediment and eclogite melts are model compositions (Table 8), also plotted in Fig. 18.

and which appear to have been produced in the subduction zone. Straub *et al.* (2008, 2011) offered similar interpretations of calc-alkaline volcanic rocks in central Mexico. It is likely that there have been some effects of shallow melt storage and fractional crystallization on the compositions of western seafloor lavas. These effects are evident for western seafloor basalts and some basaltic andesites and andesites, which form curved trends on Cr or Ni versus MgO plots, similar to those of lavas from emergent Aleutian volcanoes (Fig. 11e and h). However, for primitive western seafloor lavas that display widely variable incompatible element patterns at elevated Mg# (Fig. 9), the dominant geochemical effects appear to be those produced by partial melting and melt extraction processes in the subduction zone. These processes are discussed in detail below.

The eclogite source component in Aleutian volcanic rocks

The discussion so far has reiterated the conclusion reached previously, that the western Aleutians is a hot-slab subduction system (Yogodzinski *et al.*, 1994, 1995; Kelemen *et al.*, 2003*b*). Many distinctive characteristics of western Aleutian lavas are therefore shared with volcanic rocks from other hot-slab locations such as Patagonia (Kay *et al.*, 1993; Stern & Killian, 1996); Baja (Rogers *et al.*, 1985), Costa Rica and Panama (Abratis & Wörner, 2001), the southern Cascades (Grove *et al.*, 2002), Central Mexico (Cai *et al.*, 2014), South Island, New Zealand (Reay & Parkinson, 1997) and the Soloman Islands (König *et al.*, 2007).

The broader significance of the western Aleutian seafloor lavas is that they define a geochemical source component, which can be recognized in volcanic rocks

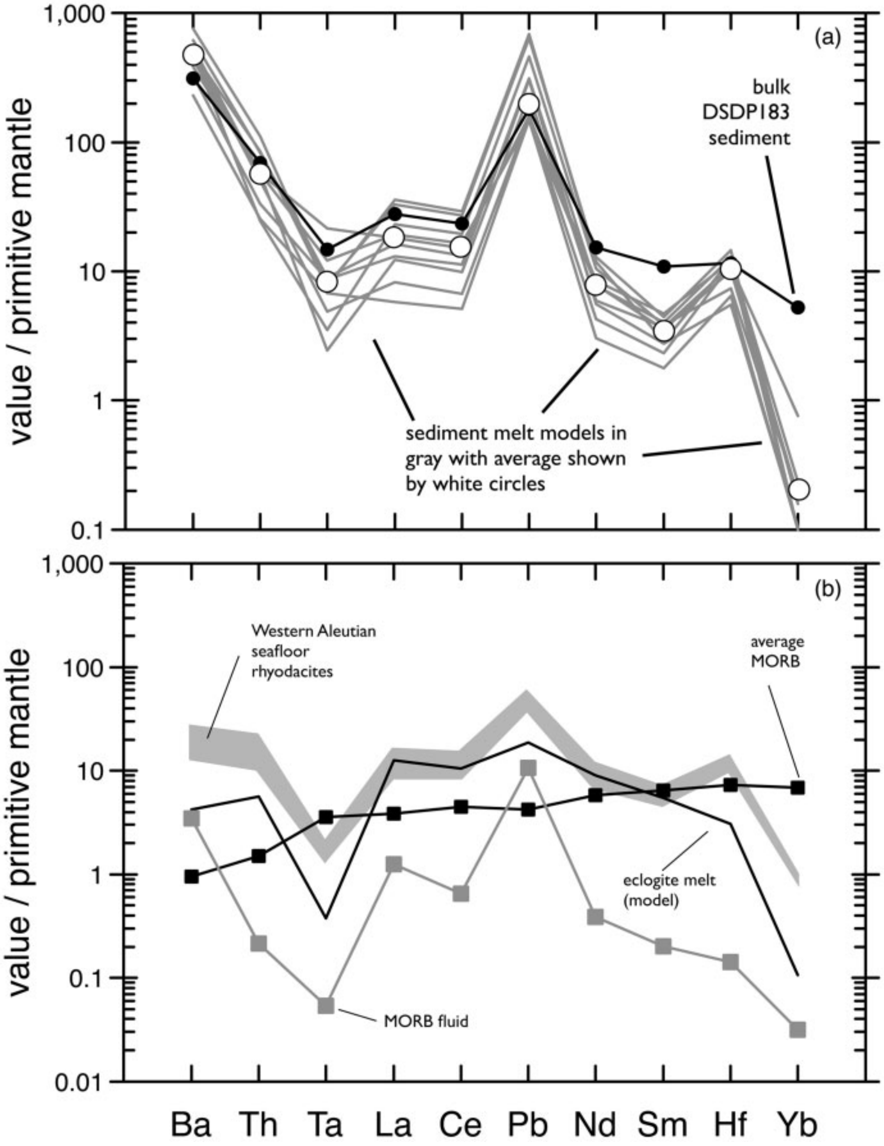

Fig. 18. Sediment and MORB eclogite melt models and related data. In (a), the sediment melt models shown by the gray lines are based on enrichment factors (melt/bulk sediment) from 10 sediment melting experiments at 2·5–3·5 GPa and 800–950°C from Hermann & Rubatto (2009) and Skora & Blundy (2010). The average sediment melt model, which is produced by the average of the enrichment factors from the 10 experiments, is shown by the open circles. The sediment melt starting composition is the average composition of DSDP 183 terrigenous sediment from Plank & Langmuir (1998). Average enrichment factors and sediment melts are listed in Table 8. In (b) the eclogite melt model is based on element mobility data (partitioning) from the 4 GPa experiments of Kessel *et al.* (2005) shown in Fig. 21. The eclogite melt source is an average MORB composition based on TiO_2 of 1·50 wt % and using MORB ratios (Sun & McDonough, 1989) with Ti to derive the abundances of the elements shown (see also Table 8). Gray field is the average western seafloor rhyodacite ± 1SD. The MORB and eclogite melt composition are defined as in Fig. 15.

produced throughout the Aleutians. The key relationships can be illustrated in graphs of Nd and Hf isotopes plotted against trace element ratios such as Ta/Th and Yb/Th, which are strongly fractionated by garnet and rutile. For the purpose of characterizing source compositions Ta/Th is best because it appears to be largely unaffected by fractional crystallization and related processes that occur in shallow parts of the subduction system. Bulk mixtures between depleted mantle (high ε_{Nd} and Ta/Th) and average Aleutian sediment (low ε_{Nd} and Ta/Th) fail to pass through the main cluster of Aleutian lava compositions (Fig. 15a). Class *et al.* (2000) showed that the Aleutian mixing trends on isotope plots versus trace element ratios sometimes point toward sediment melt compositions that are offset from bulk sediment (Class *et al.*, 2000, fig. 5). We estimate the compositions of Aleutian sediment melts based on enrichment factors (melt/bulk sediment) from 10 experimental runs at 800–950°C and 2·5–3·5 GPa from Hermann & Rubatto (2009) and Skora & Blundy (2010). Application of these enrichment factors to average Aleutian sediment (DSDP 183) produces the sediment melt models illustrated in Fig. 18a. The sediment melt models have widely variable Ta/Th that is often lower than bulk Aleutian sediment, but mixing lines from depleted mantle to these sediment melt compositions nonetheless fail to encompass the compositions of most Aleutian volcanic rocks (Fig. 15b).

As an alternative to binary mixing between mantle and sediment or sediment melt components, we hypothesize that a third end-member exists in the upper-left corner of Fig. 15, at high ε_{Nd} and low Ta/Th. We interpret this end-member to be a partial melt of subducted basalt in the eclogite facies. Throughout the remainder of this paper we refer to this as an eclogite component or eclogite melt component. This usage is similar to that adopted by Portnyagin *et al.* (2007*a*), who argued that such a component is present in volcanic rocks of the Central Kamchatka Depression (see also Portnyagin *et al.*, 2007*b*; Bryant *et al.*, 2010). Western seafloor andesites, dacites and rhyodacites have compositions that fall closer to this end-member than any other Aleutian lavas, but the same component is important throughout the arc. Three-way mixtures of depleted mantle, sediment or sediment melt and eclogite source components (Kay, 1980), which are discussed in detail below, readily encompass the compositions of Aleutian lavas in Fig. 15. Similar conclusions can be drawn from plots of Nd and Hf isotopes against Yb/Nd, Yb/Hf, Ta/Nd and Ta/Hf (Figs 16 and 17). Aleutian data on these plots show broad patterns of increasing ε_{Nd} and ε_{Hf} with decreasing Yb/Nd, Yb/Hf, Ta/Nd and Ta/Hf (Figs 16 and 17). Because mixing lines on these plots are straight, and assuming that mantle melting does not stabilize abundant residual garnet (which would fractionate Yb/Nd and Yb/Hf), it is clear that no binary mixture of depleted mantle and Aleutian sediment can explain the compositions of Aleutian lavas. It is important to emphasize that three-way mixing relationships are present not only in plots involving fluid-soluble trace elements (e.g. Sr, Ba, Pb) which are widely recognized to be sourced in seawater-altered subducted basalt (e.g. Turner *et al.*, 1996; Elliott *et al.*, 1997; Hawkesworth *et al.*, 1997) but also in plots involving Th, Nd, Hf and other relatively insoluble elements that are present in aqueous subduction fluids only in low abundances.

Three-way mixing patterns are also expressed in plots of Pb isotopes versus Ce/Pb (Miller *et al.*, 1994) and other incompatible trace element ratios, which separate the eclogite melt and mantle source components based on their relative Pb abundances (Fig. 19). Figure 19 highlights the end-member character of western Aleutian seafloor dacites and rhyodacites, and because mixing lines on these plots are straight they demonstrate the need for three end-member mixing to explain the compositions of Aleutian lavas (Miller *et al.*, 1994). Although Miller *et al.* (1994) argued that the component with unradiogenic Pb and low Ce/Pb was a hydrous fluid from altered oceanic crust (a MORB fluid) such a fluid cannot produce fractionation of trace element ratios such as Yb/Hf and Ta/Hf (Figs 16 and 17). Therefore, we believe that a melt from oceanic crust (and eclogite melt component) is required and probably also contributes a low Ce/Pb component with unradiogenic Pb (Fig. 19a). This, in turn, indicates that apparent binary mixing on Pb–Pb isotope plots (Fig. 13) must actually reflect mixing between radiogenic Pb in subducted sediment and a combination of unradiogenic Pb sources in the eclogite and MORB or depleted mantle source components

Mixing lines on Hf–Pb and Nd–Pb isotope plots are also consistent with the involvement of an eclogite source component in three-component mixtures (Fig. 20). The relationships on these plots highlight a general problem with interpretations of isotope correlation diagrams, which is that the data may appear to reflect mixing between two components, when, in fact, the data trends are produced by mixing in a three-component system in which two components lie at the isotopically depleted end of the data array. The same problem arises when Nd or Hf isotopes are plotted against ratios such as Th/Ce or Th/Nd because fractionation of Th from the LREE offsets the seafloor dacites and rhyodacites only a small amount from MORB, so the mantle and eclogite source components lie in the same corner of the graph.

The only Aleutian lavas that fall significantly outside these mixing patterns are from Piip Volcano, the hydrothermally active seamount in the far western Aleutian Komandorsky area (Fig. 1). The overall trace element patterns in Piip lavas have been interpreted to reflect a relatively large contribution from the mantle end-member compared with typical lavas from emergent Aleutian volcanoes (Yogodzinski *et al.*, 1994, 1995; Kelemen *et al.*, 2003*b*). For this reason, the Piip lavas are displaced toward possible mantle compositions in Figs 15–17. Piip lavas also have highly unradiogenic Pb isotope compositions, which are characteristic of the Komandorsky region and which appear to fall off the main mixing trend for Aleutian lavas' Pb–Pb isotope space (Fig. 13).

Modeling the eclogite source component

In the previous discussion we showed that data trends for Aleutian volcanic rocks in a variety of isotope and trace element ratio plots (Figs 15–20) point to an eclogite melt source component with a depleted (MORB-like) Hf, Nd and Pb isotopic composition and fractionated (arc-like) trace element ratios. Each plot (Figs 15–20) shows compositions for eclogite melt, sediment melt and depleted mantle or MORB end-members. Trace element ratios for the end-members are defined within narrow limits based on eclogite melt and sediment melt modeling summarized below, and by average MORB and depleted mantle compositions (Sun & McDonough, 1989; Salters & Stracke, 2003; Workman & Hart, 2005). The isotopic composition of the sediment end-member is assumed to be that of average Aleutian sediment (Vervoort *et al.*, 2011). The isotopic composition of the depleted mantle or MORB end-member is assumed to be similar to Attu basement series basalts and similar basalts from the Komandorsky Basin, which are

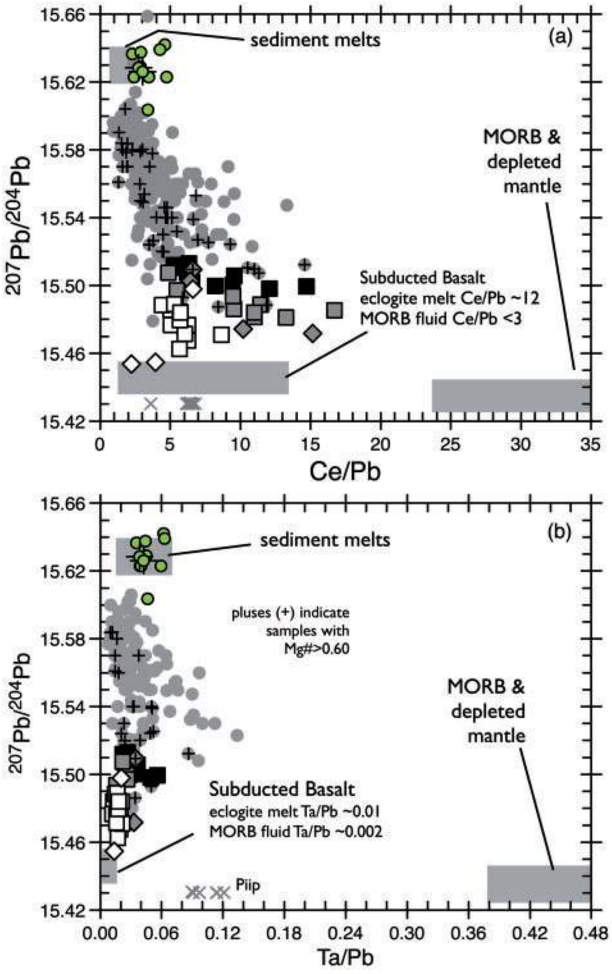

Fig. 19. Variation of ^{207}Pb/^{204}Pb vs (a) Ce/Pb and (b) Ta/Pb, modified from Miller *et al.* (1994). Symbols not defined in the figure are the same as in Figs 4 and 12. The end-member from subducted basalt is interpreted to be a mixture of MORB fluid and isotopically similar eclogite melt. The MORB fluid, sediment and eclogite melts are model compositions shown in Table 8 and Fig. 18. The MORB and depleted mantle field and eclogite melt composition are defined as in Fig. 15.

depleted tholeiites that have the most radiogenic Hf and Nd isotopic compositions in the Aleutian system (Fig. 12). The isotopic composition of the eclogite melt source component is assumed to be close to the cluster of data created by the western Aleutian seafloor lavas, which show relatively little influence of subducted sediment in their source. These choices of end-member compositions do not depict all possible variations in mantle and subducted basalt compositions that could be present in the Aleutian system. They are simply reasonable estimates that provide a basis for testing the hypothesis through modeling that an eclogite melt source component, with geochemical characteristics similar to western Aleutian seafloor lavas, is present in volcanic rocks throughout the Aleutian arc.

Formation of the eclogite melt source component can be modeled based on partitioning data from Kessel *et al.* (2005), whose experiments produced hydrous fluids and melts from MORB eclogite at 4 GPa and 700–1000°C. Experiments by Klimm *et al.* (2008) at 2·5 GPa also produced hydrous melts of eclogite in this temperature range, but their experiments produced fractionation of some key trace element pairs (e.g. La/Ta), which are not observed in Aleutian volcanic rocks. Partitioning from anhydrous eclogite melting experiments run at 2–3 GPa and 1200–1400°C (Klemme *et al.*, 2002; Pertermann *et al.*, 2004) is inappropriate for modeling of subduction zone processes, where conditions for melting and fluid extraction from subducting MORB eclogite probably occur at less than 1100°C.

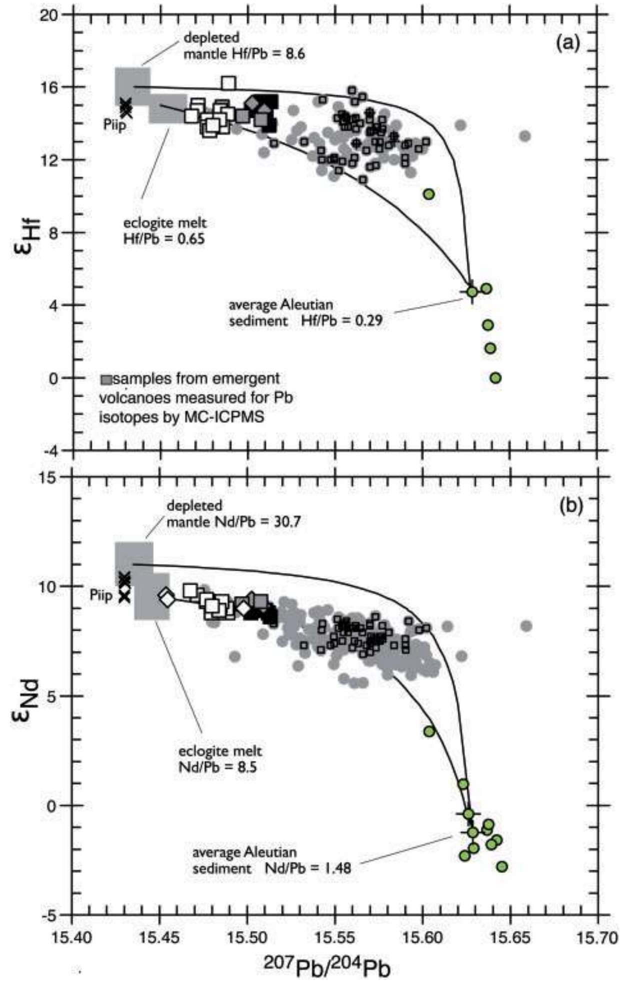

Fig. 20. Hafnium and Nd isotope (ε_{Nd}, ε_{Hf}) variations vs ^{207}Pb/^{204}Pb for Aleutian lava and sediment samples. Mixing lines are between average terrigenous Aleutian sediment from DSDP 183 and depleted mantle and between sediment and a model eclogite melt composition. Compositions of mixing end-members are given in Table 8. Data sources and symbols are the same as in Figs 4 and 12. Small square symbols are new Pb isotope data from emergent Aleutian volcanoes, provided in the Supplementary Data. Epsilon notations for Nd and Hf isotopes are defined in the footnotes to Table 6. The depleted mantle field and eclogite melt composition are defined as in Fig. 15.

Figure 21 shows bulk partitioning for selected trace elements measured at 4 GPa and 700–1000°C from Kessel *et al.* (2005). Partitioning is expressed as per cent mobility, which reflects the concentrations of the

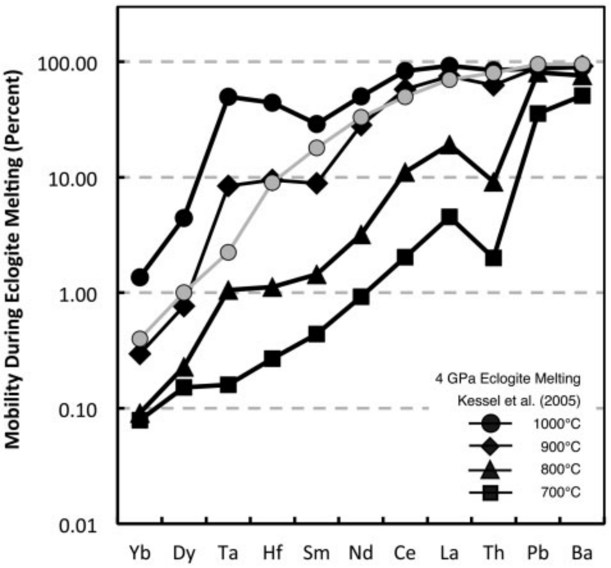

Fig. 21. Element mobility for selected trace elements observed during MORB eclogite melting experiments at 4 GPa from Kessel *et al.* (2005). Mobility is the concentration of the element in the fluid or melt multiplied by the per cent liquid present in the experiment and divided by the element abundance in the bulk system, expressed as a per cent (Table 6 Supplementary Data from Kessel *et al.*, 2005). Gray symbols show values used in eclogite melt modeling. Results of the eclogite melt model are shown in Table 8 and Fig. 18b.

elements in experimental liquids relative to the bulk residual solid. Values used to model the eclogite source component are plotted in gray symbols. For most elements, these values are close to those determined at 4 GPa and 900°C. This choice reflects relatively low Ba/Th in western seafloor dacites and rhyodacites (Fig. 7b), which is consistent with partitioning of Ba and Th during melting, but not during fluid extraction. The transition in experimental liquids from aqueous fluids to hydrous silicate melts is marked by a 13 times increase in Th mobility, from an average of 5·6% in 700 and 800°C experiment, to 73·7% in 900 and 1000°C experiments (Fig. 21). Using Ba and Th mobility values similar to those determined at 900°C and 4 GPa, and starting with a MORB eclogite that has Ba/Th = 52·5, the resulting model melt has Ba/Th ~73. Considering the total range for Ba/Th in island arc lavas (~50–1000, Labanieh *et al.*, 2012), this model agrees well with average Ba/Th of 101 ± 33 (1SD) in western seafloor rhyodacites (Fig. 18b). Brenan *et al.* (1995) measured even stronger fractionation of Ba from Th based on fluid–eclogite partitioning studies at 2 GPa and 900°C. All of the sub-solidus partitioning experiments predict Ba/Th above the typical range for Aleutian lavas, which have Ba/Th ~100–300 (Fig. 8b).

These characteristics for Ba/Th in the eclogite source component are broadly consistent with the compositions of lavas throughout the Aleutian arc, which exhibit Ba and Th enrichments that are highly correlated (Kay & Kay, 1994; Yogodzinski *et al.*, 1994; Kelemen *et al.*, 2003*b*). They are also consistent with the compositions of primitive (high-Mg#) island arc lavas worldwide, which display correlated enrichments for geochemically diverse elements such as Ba, Th, Pb and La, which are consistent with melt–rock partitioning and inconsistent with fluid–rock partitioning (Kelemen *et al.*, 2003*a*). This distinction will not vanish with the disappearance of the fluid–melt solvus at high pressures, where only the melt-like end-members, produced at 900°C and higher, have partitioning that can explain the Aleutian and global arc trends for Ba and Th (Kessel *et al.*, 2005). Based on these constraints we conclude that the eclogite source component in western Aleutian seafloor lavas is a hydrous silicate melt, produced at temperatures above the hydrous basalt solidus, which for MORB eclogite is 800–850°C under water-saturated conditions at 4 GPa, and 660–720°C at 2·0–3·0 GPa (Poli & Schmidt, 2002; Schmidt *et al.*, 2004*b*).

Results of eclogite melt modeling are shown in Fig. 18b and Table 8. Relative trace element abundances for the model, which are based on mobility values (partitioning) shown by the gray symbols in Fig. 21, are broadly similar to those of the rhyodacites, which are the western seafloor lavas that show the strongest effects of residual garnet, as discussed above. Deviations of the eclogite melt model from the observed rhyodacite compositions, which cannot be explained by variability in bulk partitioning determined from basalt–water experiments under eclogite conditions (Kessel *et al.*, 2005; Klimm *et al.*, 2008), are discussed further below.

Model concentrations for La, Ce, Nd and Sm are close to those observed in western seafloor rhyodacites whereas concentrations for Ta, Hf and Yb are below those in the rhyodacites (Fig. 18b). We assume that this difference reflects a significant contribution from the depleted mantle source component (MORB-source), which is present in the rhyodacites but not in the model eclogite melt. Kelemen *et al.* (2003*b*) showed this effect in their modeling of reactions between eclogite melt and peridotite, which produced increasing MREE and HREE and Hf abundances in resulting melt compositions [see Kelemen *et al.* (2003*b*) fig. 21 and related text]. Relatively low Ba and Th concentrations in the model cannot be explained in this way. This may indicate that the subducting oceanic crust beneath the western Aleutians is less depleted in these elements than in the average MORB composition that is used as the model melt source. Alternatively, there may be sources for these elements in western seafloor rhyodacites that are not accounted for in the model.

It is evident from Fig. 21 that we used a relatively low mobility for Ta in our model. This is because the compositions of western seafloor dacites and rhyodacites, combined with mixing relationships in Figs 15–17, require lower Ta/Nd, Ta/Hf and Ta/Th in the eclogite source component than would be predicted based on partitioning data from Kessel *et al.* (2005) or from other studies of bulk partitioning during eclogite melting (Klemme *et al.*, 2002; Pertermann *et al.*, 2004), or from studies of Ta partitioning into rutile and other eclogite minerals (e.g. Foley *et al.*, 2000; Klemme *et al.*, 2005;

Table 8: Parameters used in modeling

	Ba	Th	Ta	La	Ce	Pb	Nd	Sm	Hf	Dy	Yb	^{206}Pb/ ^{204}Pb	^{207}Pb/ ^{204}Pb	ε_{Nd}	ε_{Hf}
Eclogite melt partitioning	95·0	80·0	2·24	65·0	45·0	95·0	33·0	18·0	9·00	1·00	0·400				
MORB fluid partitioning	76·3	9·1	1·06	19·3	11·1	81·1	3·2	1·4	1·12	0·23	0·091				
Eclogite melt source	7·65	0·146	0·160	3·04	9·11	0·364	8·87	3·20	2·49	5·53	3·05	18·380	15·445	9·5	15·0
Eclogite melt model	28·0	0·449	0·014	7·59	15·8	1·33	11·3	2·21	0·862	0·213	0·047				
MORB fluid model	22·9	0·017	0·002	0·811	1·09	0·762	0·483	0·082	0·040	0·049	0·014				
Mantle melt	6·30	0·120	0·132	2·50	7·50	0·300	7·30	2·63	2·05	4·55	3·05	18·200	15·435	11·0	16·0
Average enrichment factors	1·52	0·850	0·571	0·668	0·659	1·04	0·512	0·317	0·898	0·080	0·038				
Average sediment	2074	5·49	0·545	18·0	39·0	12·9	19·1	4·34	3·26	4·12	2·31	19·050	15·628	–1·0	5·0
Average sediment melt model	3156	4·67	0·311	12·0	25·7	13·5	9·76	1·38	2·93	0·328	0·087				
Low sediment melt model	4140	2·33	0·156	6·00	12·9	6·74	4·88	0·688	1·46	0·164	0·044				
High sediment melt model	2172	7·00	0·467	18·0	38·6	20·2	14·63	2·06	4·39	0·492	0·131				

Partitioning for eclogite melt and MORB fluid modeling is expressed as per cent mobility. Values used in eclogite melting model are based on 900°C experiments at 4 GPa from Kessel *et al.* (2005), and are shown in Fig. 21. Partitioning used for MORB fluid modeling is from Kessel *et al.* (2005) experiments at 800°C and 4 GPa. The source (starting composition) for the eclogite melt and MORB fluid models is an average MORB with $TiO_2 = 1{\cdot}54\%$ and trace element ratios from Sun & McDonough (1989). The mantle melt composition is average MORB from Sun & McDonough (1989). The mantle melt, eclogite melt and MORB fluid models are also shown in Fig. 21. Enrichment factors used in sediment melt modeling are experimental sediment melt compositions divided by bulk sediment from 10 experimental runs at 800–900°C and 2·5–3·5 GPa from Hermann & Rubatto (2009) and Skora & Blundy (2010). Model sediment melts are average Aleutian sediments (Plank & Langmuir 1998; Vervoort *et al.* (2011) multiplied by average, high and low enrichment factors. High and low enrichment factors are the average ± 1SD. Isotopic compositions of all end-members are selected to match Aleutian data patterns, as discussed in the text.

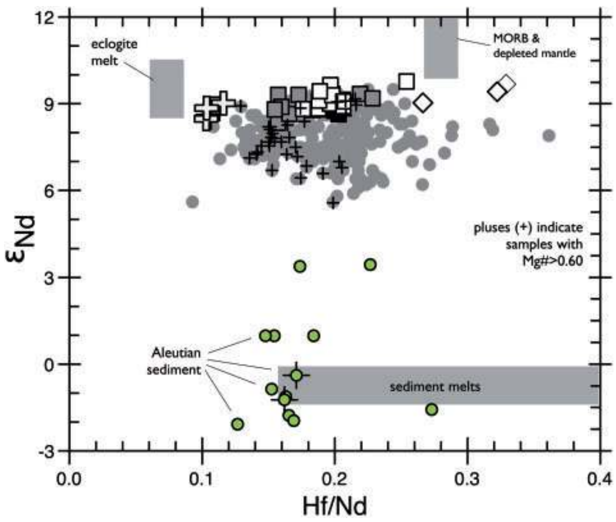

Fig. 22. Neodymium isotope variations (ε_{Nd}) vs Hf/Nd for Aleutian lavas and sediment, in comparison with MORB and model eclogite and sediment melts. Sediment and eclogite melts are model compositions shown in Table 8 and Fig. 18. Mixing lines on this plot are straight. Symbols for Aleutian lavas are defined in Figs 4 and 12. The MORB and depleted mantle field and eclogite melt composition are defined here as they are in Fig. 15.

Xiong *et al.*, 2005). This is a significant difference, which probably cannot be explained by large quantities of residual rutile, which should be <1% based on the composition of average MORB with TiO_2 ~1·5%. Data trends in Fig. 15b indicate that Ta/Th in the eclogite source component must be <0·05. Starting with a MORB eclogite that has Ta/Th = 1·1 (Sun & McDonough, 1989) and assuming that Th is perfectly incompatible during eclogite melting (100% mobile), the mobility of Ta needed to produce Ta/Th = 0·05 in an eclogite melt would be 2·1%. This value is 15 times lower than the mobility of 32% for Ta observed by Kessel *et al.* (2005) at 4 GPa and 1000°C (Fig. 21). Models using fluid–melt partitioning (which would produce Ba/Th far higher than what is observed) also fail to produce sufficiently low Ta/Th (<0·05) in the eclogite component.

These modeling results indicate that if residual rutile is what produces low Ta and Nb in Aleutian volcanic rocks then melting of subducted MORB beneath the arc must occur at moderate pressures and temperatures (<3·0 GPa and 900°C), which favor both larger quantities of residual rutile and stronger partitioning of Ta and Nb into rutile (Foley *et al.*, 2000; Klemme *et al.*, 2002, 2005; Schmidt *et al.*, 2004*a*; Xiong *et al.*, 2005). Alternatively, some other residual titaniferous mineral may also present in the Aleutian source. One possibility is titanite, but its main effect is to produce partial melts with high Nb/Ta (John *et al.*, 2011), which is inconsistent with the compositions of western Aleutian seafloor dacites and rhyodacites, which have low Nb/Ta (Fig. 7h). It is also possible that the effects of residual rutile are compounded by residual, low-Mg# amphibole, which produces partial melts with low Nb/Ta, low Ta/La and high Zr and Hf relative Sm and Nd (Foley *et al.*, 2002). Interestingly, all of these characteristics are evident in western Aleutian dacites and rhyodacites (Figs 7 and 10). Thus, partial melting of subducted basalt leading to the creation of an eclogite melt source component may involve residual amphibole in addition to garnet and rutile.

Constraints from Hf–Nd isotopes and Hf–Nd abundance ratios

Mixing relationships in plots of Hf–Nd isotopes versus Hf–Nd abundance ratios (Nd/Hf or Hf/Nd) also require three-component mixing in the Aleutian source. This is because Aleutian lavas have widely variable Nd–Hf abundance ratios across all Hf and Nd isotopic compositions, with no possible mixtures between mantle and sediment end-members able to explain the compositions of common Aleutian volcanic rocks (Brown *et al.*, 2005). This is shown most clearly in a plot of ε_{Nd} versus Hf/Nd (Fig. 22). Wide variation in Hf/Nd in Fig. 22 is interpreted to reflect three-component mixing combined with the effects of fractional crystallization, which increases Hf/Nd in evolved magmas (Handley *et al.*, 2011; Woodhead *et al.*, 2011). An eclogite melt source component with relatively low Hf/Nd (Fig. 22) can be modeled, as described above, using the 900°C and 4 GPa partitioning data shown in Fig. 21. However, western Aleutian dacites and rhyodacites have relatively high Hf/Nd, similar to MORB, and so appear to be unlike the eclogite melt component, which has relatively low Hf/Nd (Fig. 22). This probably indicates that eclogite melting beneath the western Aleutians is occurring at temperatures above 900°C, where Hf and Nd are similarly incompatible (Fig. 21), and melting of MORB eclogite will produce liquids with Nd–Hf abundance ratios close to those of MORB. This leads us to conclude that Nd–Hf abundance ratios in an eclogite source component will vary widely along the Aleutian arc, reflecting the highly variable and temperature-dependent partitioning of Hf and Nd in garnet (Kessel *et al.*, 2005; Klimm *et al.*, 2008).

Contributions from Aleutian source components

Data trends in plots of isotopic composition versus key trace element ratios (e.g. Miller *et al.*, 1994) provide a basis for estimating the relative contributions of different source components in Aleutian volcanic rocks throughout the Aleutian arc. Source contribution estimates discussed here, which are plotted against sample location in Fig. 23, are based simply on the geometric location of rock compositions relative to the vertices of the triangles formed by the three end-members in Figs 17 and 19. Selection of subducted basalt, sediment melt and mantle end-member compositions, which is guided by the data trends and by modeling of the eclogite melt component described above, is defined only by their isotopic and trace element ratios. A mass-balance calculation for selected trace elements, which provides a more fully

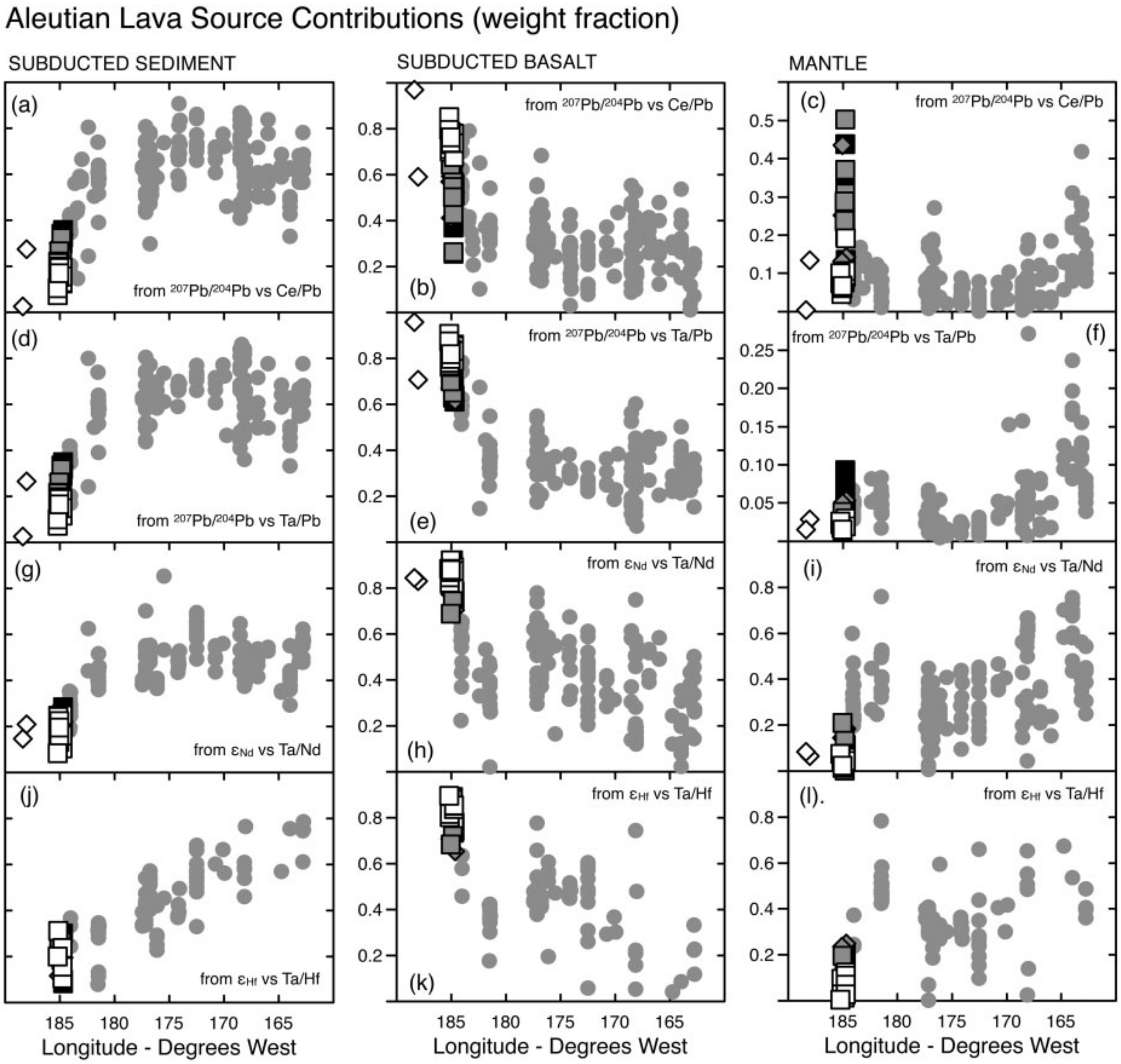

Fig. 23. Predicted weight fraction of sediment, subducted basalt and mantle source contributions for Aleutian lavas versus sample location in degrees west longitude. Vertical axes on these plots are the weight fractions contributed from each of the source components. Source contributions are estimates based on the location of data points for all Aleutian volcanic rocks falling within the three end-member systems shown in Figs 17 and 19. Source contributions in (a)–(c) are based on analysis of $^{207}Pb/^{204}Pb$ vs Ce/Pb (Fig. 19a). Source contributions in (d)–(f) are based on $^{207}Pb/^{204}Pb$ vs Ta/Pb (Fig. 19b). Those in (g)–(i) and (j)–(l) are based on ε_{Nd} vs Ta/Nd and ε_{Hf} vs Ta/Hf respectively (Fig. 17a and b).

quantitative estimate of source component contributions, is treated separately below.

Along-arc changes in source component contributions are qualitatively similar whether they are based on Pb, Nd or Hf isotope variability. This is particularly clear for the sediment component (first column in Fig. 23). However, the quantity of sediment is higher when it is based on Pb isotopes (~60% for typical, eastern Aleutian lavas) than when it is based on Nd or Hf isotopes (20–30%). This must reflect the geochemical behavior of Pb compared with Nd and Hf, as well as the high relative concentration of Pb in Aleutian sediment. All of the plots show generally decreasing contributions of sediment from east to west, reflecting along-arc shifts toward more depleted isotopic compositions and the absence of subducted sediment from lavas of the westernmost Aleutian arc, owing to the effects of oblique subduction (Yogodzinski *et al.*, 1994, 1995; Kelemen *et al.*, 2003*b*). The reverse is true for the subducted basalt component, which generally increases from east to west (second column in Fig. 23). The mantle component (third column in Fig. 23) is high in some eastern Aleutian locations, reflecting relatively high Ce/Pb and Ta/Pb in some eastern Aleutian samples (Fig. 23c and f). The mantle component also generally decreases from east to west, as expected from lower mantle temperatures under oblique-convergence conditions in the western arc (Kelemen *et al.*, 2003*b*). An east to west decrease in mantle temperatures beneath the Aleutians is also consistent with the decreasing size of Aleutian volcanoes as shown by Fournelle *et al.* (1994).

Some basalts, basaltic andesites and andesites from the Ingenstrem Depression have variable trace element ratios that lead to contradictory conclusions about their source. These samples have elevated Ce/Pb (Fig. 19a), which may be interpreted to indicate a relatively large contribution from the depleted mantle (Fig. 23c), but also low Ta relative to Pb (Fig. 19b), which may be interpreted to indicate an enhanced role for the eclogite melt component (Fig. 23e). These lavas, which include some andesites and basaltic andesites with high Sr abundances (>700 ppm) and other adakitic trace element characteristics, appear to be hybrid compositions produced by mixing and/or melt–rock reactions between high-silica/low-Mg# end-members derived predominantly from subducting oceanic crust and low-silica/high-Mg# end-members derived predominantly from the mantle wedge (Kay, 1978; Yogodzinski *et al*., 1995; Kelemen *et al*., 2003*b*). Strontium and La concentrations in these samples are often much higher than in primitive Aleutian basalts or in western seafloor dacites and rhyodacites (Fig. 6f). These characteristics may indicate a shift in accessory mineral stability (monazite or allanite) at very high slab temperatures, and/or the effects of melt–rock reactions. Our view is that where such geochemically variable and Sr-rich samples are observed, and where they have MORB-like isotope compositions, they may be interpreted as indicators for the presence of a substantial eclogite melt source component. However, they are not themselves the outstanding examples of lavas produced dominantly by melting of eclogite (western seafloor dacites and rhyodacites are), nor are they volumetrically important products of subduction magmatism.

Mass-balance modeling of the Aleutian source

Here we present mass-balance calculations, with the goal of quantifying the contributions of the source components needed to produce isotope ratios like those of common volcanic rocks from emergent Aleutian volcanoes, and trace element abundances and ratios like those observed in primitive Aleutian basalts, with Mg# >0·60. We do the mass balance simply by mixing sediment melts and melts of a depleted mantle wedge (MORB) with a third component from subducted basalt, which may be a fluid or an eclogite melt. This approach relies on bulk partitioning data from recent experimental work (Kessel *et al*., 2005; Hermann & Rubatto, 2009; Skora & Blundy, 2010) to produce reasonable compositions for melts and fluids of the type that are widely interpreted to contribute to the formation of arc magmas. This approach avoids the complexities of melting regime shape (Plank & Langmuir, 1992) and mechanisms of melt extraction (Kelemen *et al*., 1995), which can have a significant impact on trace element abundances in model compositions but are poorly understood for subduction systems. This approach does not address complexities of arc magmatism, such as pyroxenite formation, which are likely to occur when silica-rich fluids and melts from the subducting plate interact with peridotite in the mantle wedge (Straub *et al*., 2008).

End-member compositions used in the mass-balance calculation are listed in Table 8. The mantle melt component is normal MORB of Sun & McDonough (1989). We assume that the subducted basalt component may be an eclogite melt or a fluid or both. Modeling of the eclogite melt source component was discussed previously. The MORB fluid is modeled in the same way, except that mobility values (partitioning) were used from Kessel *et al*. (2005) experiments at 800°C and 4 GPa (triangles in Fig. 21). Sediment melt compositions are modeled from experimental data as described previously. To account for the widely variable trace element abundances produced in sediment melting experiments we do the mass-balance calculation three times for each model, using sediment melt compositions with average, high and low trace element abundances. Results of three mass-balance models are illustrated in Fig. 24.

Mass-balance Model-1 takes the source contributions determined from Nd and Hf isotopes, which call for approximately 20% sediment, 48% MORB fluid and 32% mantle melt (MORB). This model predicts Pb isotopic compositions that are slightly more radiogenic than observed in average Aleutian lavas, and Hf and Nd isotope compostions that are less radiogenic (Fig. 24a). This means that Model-1 has too much Pb, Nd and Hf from the subducted sediment source component. Model-1 also predicts REE abundances below those observed in primitive Aleutian lavas. In Model-2, we raise the mantle melt component to 48% and adjust the sediment downward to 10%. This leaves the MORB fluid component at 42%. The resulting mixture has appropriate isotopic compositions and HREE abundances similar to those in primitive Aleutian volcanic rocks (Yb~1·5 ppm), but the LREE abundances still fall well below those expected in primitive Aleutian magmas (Fig. 24b).

More importantly, Model-1 and Model-2 both produce a source mixture with a Nd/Hf ratio of ~3·6, which is similar to MORB and well below primitive Aleutian lavas, which have an average Nd/Hf of 5·80 ± 1·04 (1SD, $n = 84$). The creation of mixtures such as these, with inappropriately low Nd/Hf, is a persistent feature of models that rely heavily on MORB fluids, which carry low abundances of Nd and Hf, and therefore result in a mass balance where the dominant sources of Nd and Hf are sediment melts and depleted mantle, which both have Nd/Hf <4·0 (Table 8). Thus, a key constraint on the arc magma source mixture comes from recent experimental studies (Hermann & Rubatto, 2009; Skora & Blundy, 2010), which predict Nd/Hf values in sediment melts below those of bulk sediment (Fig. 18). Using these constraints, it appears that no mixture of MORB, sediment melt and MORB fluid will produce both elevated Nd/Hf and Nd, Hf and Pb isotope compositions like those observed in Aleutian lavas.

The main problems of Model-1 and Model-2 are resolved if the subducted basalt component is assumed

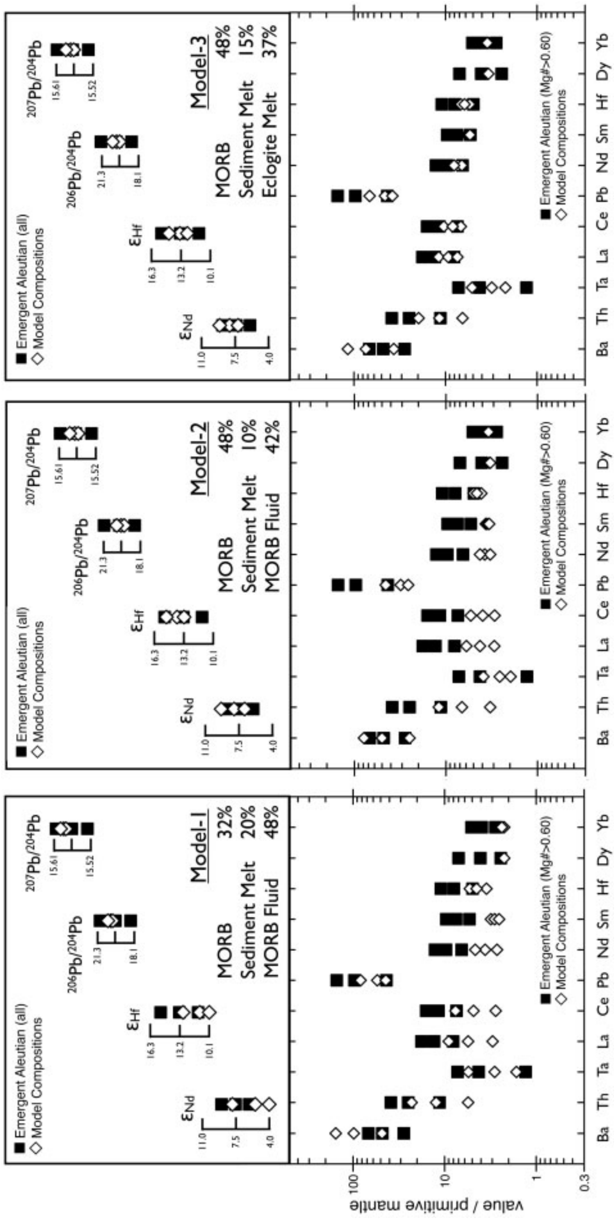

Fig. 24. Trace element abundances and isotope ratios for model melts, shown by open diamond symbols, compared with Aleutian volcanic rocks from emergent volcanoes, shown by filled squares. Model melts are produced by mixing of sediment melt and MORB with a third component from subducted basalt, which is either a MORB fluid or an eclogite melt. Mixing proportions of the three components are shown on the graphs. The three model compositions shown reflect the use of average, low and high trace element abundances in the sediment melt component. Compositions of the mixing end-members are plotted in Fig. 18 and listed in Table 8. Average isotope ratios plotted in the upper panels include all published data for samples from emergent Aleutian volcanoes (Buldir and east in Fig. 1). The low, average and high values for Nd isotopes are 6·1, 7·5 and 9·2 ε_{Nd} units ($n = 255$). For Hf isotopes they are 10·9, 13·2 and 15·8 ε_{Hf} units ($n = 99$). For ^{206}Pb/^{204}Pb they are 18·620, 18·830 and 18·992 ($n = 254$). For ^{207}Pb/^{204}Pb they are 15·520, 15·556 and 15·602 ($n = 254$). Average trace element abundances plotted in the lower panels include all published data for primitive samples from emergent Aleutian volcanoes, which have Mg# >0·60. The high and low values are the average ± 1SD.

to be an eclogite melt, instead of MORB fluid. This is seen in Model-3, which is 48% mantle melt, 37% eclogite melt and 15% sediment melt. This mixture predicts Nd, Hf and Pb isotope compositions, and abundances for most incompatible elements similar to those observed in Aleutian lavas (Fig. 24c). A key effect of the eclogite melt component is the creation of a mixture with Nd/Hf of ~5·2, which is close to the average of 5·8 ± 1·0 (1SD) observed in primitive Aleutian lavas. Again, this reflects the experimental results of Kessel *et al.* (2005), which predict both high Nd/Hf and relatively high abundances for Nd and Hf in melts of MORB eclogite at 900°C and 4 GPa (Fig. 21).

An important caveat for Model-3 is that although it predicts an average Ce/Pb of ~5·2, which is close to the observed average for primitive Aleutian lavas (Ce/Pb = 4·4 ± 2·2), it does so with an eclogite melt end-member that has Ce/Pb ~13. This is a problem because western seafloor dacites and rhyodacites have Ce/Pb of 5–6, which is close to the composition of the subducted basalt end-member, which should have Ce/Pb <5, based on the data in Fig. 19. This probably means that a significant quantity of unradiogenic Pb from a MORB fluid is present in the source mixture, which is in addition to the eclogite melt component. This means that for Pb, and probably for other fluid-soluble trace elements, especially K (see Kay, 1980), the source mixture requires four source components instead of three. This issue cannot be resolved if MORB fluid is substituted for eclogite melt as in Model-1 and Model-2, which produces poor agreement for trace element abundances, in particular for Nd/Hf, which is persistently low for source mixtures that do not include a significant quantity of eclogite melt.

It is interesting to note that all of the models predict stronger Ba enrichments in Aleutian lavas than are observed. Excess Ba in the models probably reflects the use of bulk sediment compositions as the source of the sediment melts, which is the dominant source of Ba. It is likely, for example, that by the onset of melting, dehydration and fluid loss imposed on the sediment column beneath the arc has removed large quantities of Ba, which is far higher in Model-3 (Ba/Th ~527, Ba/La ~81, Ba/Pb ~183) than in primitive Aleutian volcanic rocks (Ba/Th = 183 ± 46, Ba/La = 37 ± 6 and Ba/Pb = 64 ± 33). Class *et al.* (2000) encountered similar issues in their mass balance, and they also suggested that the sediment source for Aleutian lavas might have been depleted by fluid extraction, prior to melting.

The main effect of the eclogite component on the mass balance is that it adds a significant source of radiogenic Nd and Hf, which is in addition to the mantle component, and which offsets the contribution from sediment melts, which contain relatively high abundances of unradiogenic Nd and Hf. This is evident in the mass balance for Model-3 (Table 9), which shows that a large proportion of the LREE is derived from the eclogite melt (36–50% for Sm–La), compared with similar contributions from the mantle (55–20%) and somewhat lower contributions from sediment (9–30%). The eclogite melt

Table 9: Model-3 mass-balance tabulation by element

	Eclogite melt (ppm)	Sediment melt (ppm)	MORB melt (ppm)	Eclogite melt (%)	Sediment melt (%)	MORB melt (%)	Model melt (ppm)
Ba	10·3	473	3·02	2·1	97·3	0·6	487
Th	0·17	0·70	0·06	18·0	75·8	6·2	0·92
Ta	0·01	0·05	0·06	4·4	40·5	55·0	0·12
La	3·03	1·80	1·20	50·2	29·9	19·9	6·03
Ce	6·48	3·86	3·60	46·5	27·7	25·8	13·9
Pb	0·49	2·02	0·14	18·5	76·1	5·4	2·66
Nd	4·16	1·46	3·50	45·6	16·0	38·4	9·13
Sm	0·82	0·21	1·26	35·8	9·0	55·2	2·29
Hf	0·32	0·44	0·98	18·3	25·2	56·5	1·74
Dy	0·08	0·05	2·18	3·4	2·1	94·5	2·31
Yb	0·02	0·01	1·46	1·2	0·9	98·0	1·49

End-member contributions for Model-3 are 48% MORB melt, 37% eclogite melt and 15% sediment melt. End-member compositions are shown in Table 8. Full results of mass balance are illustrated in Fig. 24.

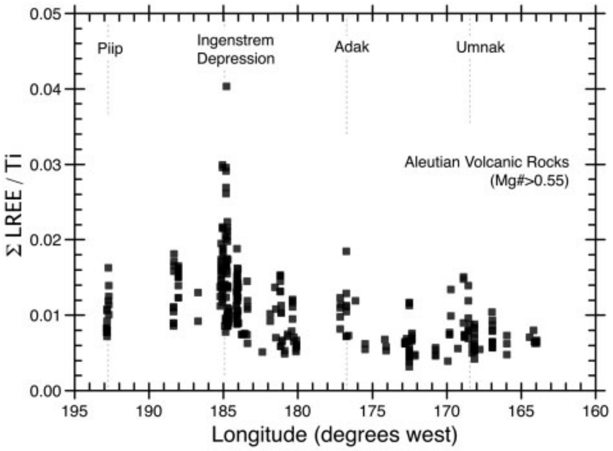

Fig. 25. Sum of the LREE divided by Ti for Aleutian lavas plotted against location in the arc, in degrees west longitude. Only samples with Mg# >0·55 are shown. Summed LREE are La, Ce, Nd and Sm.

contributes somewhat less Hf (18%) compared with sediment (25%) and the mantle (56%). If this result can be extended to other arc systems (e.g. Tollstrup *et al.*, 2010) it will mean that high-charge and relatively insoluble trace elements cannot be modeled as binary mixtures between subducted sediment and depleted mantle end-members, as is commonly inferred (Elliott *et al.*, 1997; Hawkesworth *et al.*, 1997; Class *et al.*, 2000; Walker *et al.*, 2001; Straub *et al.*, 2004; Plank, 2005; Duggen *et al.*, 2007; Singer *et al.*, 2007; Woodhead *et al.*, 2012). More broadly, the presence of abundant Nd, Hf and other insoluble trace elements from subducted basalt in arc magmas is inconsistent with models that call on the selective transport of fluid-mobile over fluid-immobile elements as the main process controlling the formation of subduction-related trace element patterns (e.g. Perfit *et al.*, 1980; Tatsumi *et al.*, 1986; Miller *et al.*, 1994; Turner *et al.*, 1996; Pearce *et al.*, 1999).

Origin of the arc magma trace element signature

A variety of recent studies have shown that melts of subducted basalt and sediment may be saturated in accessory minerals capable of fractionating trace elements in ways that may exert primary control over the distinctive trace element patterns expressed in subduction-related volcanic rocks. A role for accessory rutile has long been implicated in the control of low Ta and Nb abundances in arc magmas (e.g. Perfit *et al.*, 1980; Tatsumi *et al.*, 1986; Miller *et al.*, 1994; Turner *et al.*, 1996; Pearce *et al.*, 1999), but experimental studies show that slab-top melting conditions may stabilize a variety of accessory phases, including allanite, monazite, apatite and zircon, in addition to rutile (Johnson & Plank, 1999; Klimm *et al.*, 2008; Hermann & Rubatto, 2009; Skora & Blundy, 2010).

Effects of accessory mineral saturation have been well illustrated by Klimm *et al.* (2008), who showed that partial melts of eclogite co-saturated in rutile and allanite will shift to higher LREE abundances compared with Ti at higher eclogite melt equilibration temperatures. This relationship, which provides the basis for estimating slab-top temperatures from Ce/H_2O (Plank *et al.*, 2009; Cooper *et al.*, 2012), is consistent with highly variable relative depletions in Ta among western Aleutian seafloor lavas (variable La/Ta; Fig. 7f), which are controlled primarily by variation in LREE abundances with little change in Ta (Fig. 6c and d). The patterns of Ta and LREE abundances, which are relatively low in rhyodacites and increase systematically in dacites and andesites (Fig. 7c and d), are consistent with increasing equilibration temperatures for eclogite melts saturated in rutile and allanite, as discussed by Klimm *et al.* (2008). In this context, the dramatic increase in LREE abundances in some western seafloor andesites and basaltic andesites compared with dacites and rhyodacites (Figs 7c and 8a) could be interpreted to reflect the loss of accessory allanite or monazite at unusually high eclogite melt equilibration temperatures. In fact, we observe a general east to west shift toward higher LREE/Ti for Aleutian lavas with Mg# >0·55 (Fig. 25). This pattern is consistent with experimental observations of eclogite partial melts that are co-saturated in rutile and allanite over a range of temperatures (Klimm *et al.*, 2008, fig. 17). However, it does not provide a quantitative estimate of slab-top temperatures, because

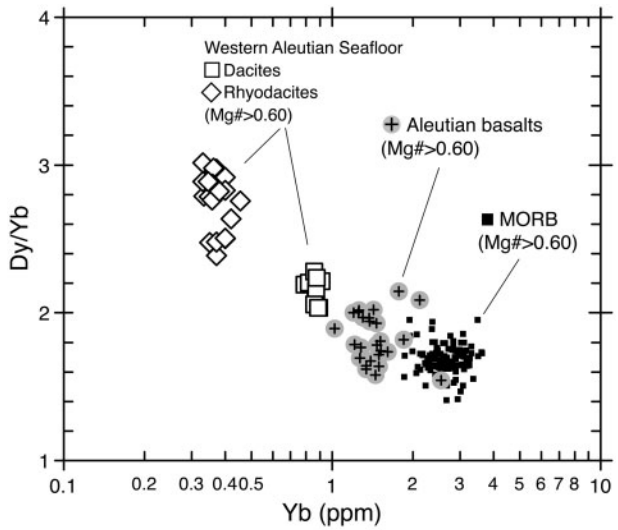

Fig. 26. Variation of Dy/Yb vs Yb for western Aleutian dacites and rhyodacites compared with primitive MORB and Aleutian basalts with Mg# >0·60. Primitive MORB data are from Class & Lehnert (2012). Other data sources are the same as in Fig. 4.

a significant quantity of LREE and Ti from the depleted mantle is present in all Aleutian volcanic rocks. It is important to note that LREE/Ti in primitive Aleutian lavas increases from east to west, despite the fact that Aleutian sediment has relatively high LREE/Ti (~0·019) and is a larger portion of the source mixture in the eastern part of the arc than in the west.

The role of residual garnet, which is well expressed in some western seafloor lavas, may also play an important role in the control of certain trace element features in arc magmas. It is often noted that island arc basalts have low abundances of MREE and HREE compared with MORB. This persistent trace element characteristic of arc magmas is commonly attributed to melting and depletion of sub-arc mantle beneath the back-arc, prior to melting beneath the volcanic front, as a consequence of subduction and corner-flow dynamics (McCulloch & Gamble, 1991). This pattern may also be interpreted to reflect higher degree melting beneath arcs than is typical for MORB (Kelley *et al.*, 2006). Interestingly, this depleted geochemical character is present in Aleutian lavas, even though the Aleutian mantle does not appear to be highly depleted (e.g. Class *et al.*, 2000, fig. 4) and there is no there is no spreading center behind the arc. Figure 26 shows Dy/Yb plotted against Yb abundance for primitive Aleutian basalts compared with primitive MORB. The primitive Aleutian and MORB lavas overlap broadly for Dy/Yb, which is mostly from 1·5 to 2·0 for both datasets (Fig. 26), indicating that fractionation of the middle to heavy parts of the REE pattern for Aleutian lavas and MORB are similar. The offset in Yb concentration between primitive Aleutian lavas (1–2 ppm Yb) and primitive MORB (2–3·5 ppm) is clearly evident (Fig. 26). We cannot rule out the possibility that low Yb in primitive Aleutian basalts may indicate that their mantle source was more depleted than that of MORB (McCulloch & Gamble, 1991) or that hydrous melting has produced higher-degree melting than is commonly seen in MORB (Kelley *et al.*, 2006); however, we note that average Dy/Yb appears to be slightly higher in primitive Aleutian basalts compared with primitive MORB, and that strongly fractionated Dy/Yb in the western Aleutian seafloor dacites and rhyodacites shows an inverse relationship for Dy/Yb and Yb with common Aleutian lavas (Fig. 26). These patterns suggests that low Yb abundances in Aleutian lavas may reflect the influence of the eclogite melt component on the source mixture, and therefore may not indicate that the Aleutian mantle wedge is more depleted than the average MORB source. Indeed, models of eclogite melt–peridotite reaction (Kelemen *et al.*, 2003*b*, fig. 21 and related text) show that low HREE concentrations are a characteristic of the resulting melts. Increasing reaction progress (decreasing melt/rock ratio) produces progressively lower Dy/Yb, approaching primitive mantle values, whereas HREE abundances in the melt remain low. Thus, we interpret low HREE concentrations in primitive Aleutian basalts to result from the addition of an eclogite melt component in the source, and not to be an indication of low HREE concentrations in the Aleutian mantle wedge. This interpretation is consistent with the conclusions of Class *et al.* (2000), who found that the Aleutian mantle wedge is no more deleted than the average MORB source, based on their measurements of Nb/Ta and Zr/Hf in Aleutian lavas, which they found to be indistinguishable from those in MORB (see also Kay & Kay, 1994). These results also indicate that it may be incorrect and misleading to use HREE concentrations in arc lavas to infer the degree of prior melt depletion, and/or the degree of sub-arc melting, in the arc mantle source.

Implications of high-Si magmas in the mantle wedge

We have modeled the trace element characteristics of western seafloor dacites and rhyodacites as partial melts of rutile-bearing eclogites, and suggested that their high-Mg# is a product of reaction with peridotite in the mantle wedge. Indeed, if 25% of the Fe in western seafloor dacites and rhyodacites is ferric iron, as is typical for arc lavas (Kelley & Cottrell, 2009), then these rocks have Mg/(Mg + Fe^{2+}) greater than 0·7, and thus are close to Fe^{2+}/Mg exchange equilibrium with typical residual mantle olivine and pyroxene compositions with Mg# values greater than ~0·89. However, their low MgO contents indicate that western Aleutian dacites and rhyodacites record relatively low magmatic temperatures, less than 1100°C (see Kelemen *et al.*, 2003*b*, fig. 3). These temperatures are especially low when compared with those for primitive basalts erupted nearby, with more than 8% MgO and with likely olivine-melt temperatures in excess of 1250°C. In some parts of the Ingenstrem Depression, we sampled primitive dacites and primitive basalts in the same dredge, indicating very different temperatures in the mantle source of spatially juxtaposed lavas. Furthermore,

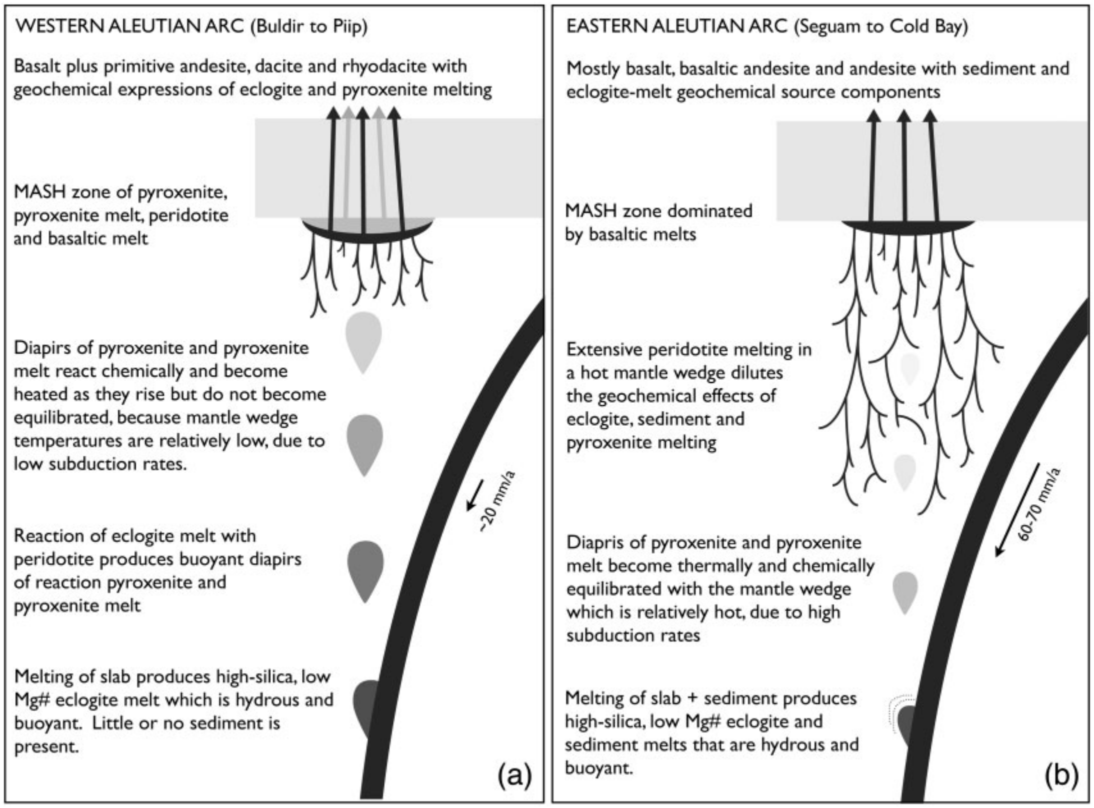

Fig. 27. Conceptual model comparing magmatic processes in the western and eastern Aleutian arc. Hydrous partial melts of MORB eclogite and sediment are shown rising from the subducting plate and interacting with a hotter, overlying mantle wedge (see Marsh, 1974; Ringwood, 1974; Myers *et al.*, 1985; Brophy & Marsh, 1986; Myers & Marsh, 1987). Black arrows in the subducting plate indicate relative trench-normal convergence rates. Slow convergence in the west produces a relatively cool and stagnant mantle wedge compared with the east, where advection of hot peridotite into the wedge is driven by high subduction rates and the corner-flow mechanism. Dendritic patterns in the mantle wedge depict basalt produced by partial melting of peridotite. Aqueous fluids from the subducting plate are not shown here but must be present to account for low Ce/Pb in western Aleutian seafloor lavas. Additional details of processes depicted here are discussed in the text. MASH: melting, assimilation, storage, and homogenization (from Hildreth & Moorbath, 1988).

although their high alkali contents and presumed high H_2O contents might stabilize relatively SiO_2-rich melts in equilibrium with olivine at ~1 GPa (Tatsumi, 1982; Draper & Johnston, 1992; Wood & Turner, 2009), dacites and rhyodacites with 60–70% SiO_2 cannot be in equilibrium with mantle olivine.

Thus, we think the most likely explanation for our observations, illustrated in Fig. 27a, is as follows. SiO_2-rich partial melts of subducting basalt in eclogite facies react with the overlying mantle wedge to form reaction pyroxenite (Straub *et al.*, 2008), which is relatively impermeable to porous flow of melt (Fujii & Oamura, 1986; Zhu & Hirth, 2003). Additional, low-density eclogite melts pond beneath this impermeable barrier until they reach sufficient size to form diapirs that rise through the mantle wedge (Marsh, 1974; Ringwood, 1974; Brophy & Marsh, 1986). For a density contrast of 400 kg m^{-3}, radii of 10–100 km, and mantle wedge viscosity between 10^{18} and 10^{20} Pa s, these diapirs are likely to rise at velocities of microns to meters per year. Larger diapirs, at the faster end of this range, would rise sufficiently rapidly that they would not thermally equilibrate with the mantle wedge. Smaller, slower diapirs would thermally equilibrate, but might be armored from chemical reaction with residual mantle peridotite via formation of impermeable, hybrid pyroxene reaction products along their margins (Myers *et al.*, 1985; Myers & Marsh, 1987). This limited wall-rock reaction might be sufficient to raise the Mg# within the melt-rich diapirs to values in Fe/Mg exchange equilibrium with mantle peridotite, while retaining high SiO_2 contents and other characteristics of hydrous partial melts of eclogite (Fig. 27a).

As they approach the base of arc crust such diapirs are likely to stall and pond, as they will encounter increasingly cold, high-viscosity mantle peridotite (Gerya & Yuen, 2003; Gerya *et al.*, 2004) and will have little or no density contrast with overlying arc crust. This will form a layer of SiO_2-rich, hydrous melt—perhaps as a porous mush—in the shallow mantle below the arc crust, where it will continue to partially react with the surrounding mantle, forming hybrid pyroxenites. Hot, basaltic magmas equilibrated with the high-temperature core of the mantle wedge may rise through this layer of low-temperature, relatively viscous, dacite and rhyodacite to feed basaltic volcanoes; more rarely, but over a wider region, small amounts of SiO_2-rich magma may also rise to form dacite and rhyodacite flows, as well as felsic plutons in the crust.

In the western Aleutians the mantle wedge is relatively cold and the subducting plate is relatively hot (Kelemen *et al.*, 2003*b*). These conditions are produced because low subduction rates limit the advection of hot mantle by the corner-flow mechanism, and because heating of the subducting plate has probably occurred in part, through cooling of the adjacent mantle (Kelemen *et al.*, 2003*b*). It also appears that the subducting plate beneath the western Aleutians has been torn or somehow breached, and so is probably being heated on three sides (Yogodzinski *et al.*, 2001; Levin *et al.*, 2005). Under these conditions, partial melting of peridotite in the wedge is limited, but partial melts of subducting eclogite are abundant, so the products of reactions between eclogite melt and mantle peridotite are clearly detectable in the surface volcanism (Fig. 27a). In the eastern Aleutians (Fig. 27b), which is a more typical arc setting, subduction rates are higher, so the mantle wedge is hotter owing to the advection of hot peridotite by the corner-flow mechanism. As a result, there is more melting of peridotite, so the arc produces mostly basalt (Fig. 27b). In this setting, eclogite and sediment melts are diluted and expressed only as geochemical source components (Fig. 27b).

Alternatively, it is possible that high-SiO_2, high-Mg# magmas with compositions like those of the western seafloor dacites and rhyodacites could be the products of basalt–peridotite reaction in the uppermost mantle, at 1 GPa or less (Kelemen, 1990; Kelemen *et al.*, 1990; Yogodzinski *et al.*, 1994; MacPherson *et al.*, 2006). If basaltic melts are cooled as they react with peridotite, this process could produce primitive andesites—and perhaps even dacites and rhyodacites—from initially basaltic melts (Kelemen, 1990). If the resulting melts became cool and SiO_2-rich enough to saturate in rutile (Ryerson & Watson, 1987), garnet (Müntener *et al.*, 2001) and allanite (Hermann, 2002) or some other LREE-rich accessory mineral, while retaining a high Mg# owing to reaction, this could produce primitive, SiO_2-rich liquids with geochemical characteristics similar to Aleutian andesites, dacites and rhyodacites. This view attributes the distinctive characteristics of high-Mg# western seafloor lavas to an assimilation–fractional crystallization (AFC; DePaolo, 1981) or melting, assimilation, storage, and homogenization (MASH; Hildreth & Moorbath, 1988) process occurring not in the crust, but in the uppermost mantle (Yogodzinski *et al.*, 1994). Recent experimental results have highlighted this model for creating primitive andesitic magmas (Weaver *et al.*, 2011; Weber *et al.*, 2011). However, we tentatively rule out this model on the basis of isotopic variation. Western Aleutian seafloor basalts have systematically less radiogenic Nd and more radiogenic Pb compared with the dacites and rhyodacites. Although extensive melt–rock reaction between a relatively isotopically enriched basalt parent and a highly depleted mantle peridotite could, in principle, produce this variation in isotopes with increasing reaction product, the required low melt/rock ratios (less than 0·001) would form melt compositions saturated in mantle olivine, very different from the primitive Aleutian dacites and rhyodacites.

CONCLUSIONS

Discovery of seafloor volcanism west of Buldir Volcano in the western Aleutian arc demonstrates that the surface expression of active Aleutian volcanism falls below sea level west of 175·9°E longitude, but is otherwise continuous from mainland Alaska to Kamchatka. Radioisotopic ages indicate that seafloor volcanism in the western Aleutians has probably been active throughout the late Pleistocene and Holocene. Western Aleutian seafloor lavas define a highly calc-alkaline igneous series from 50 to 70% SiO_2. This series was not produced by fractional crystallization of basalt. Strongly fractionated (adakitic) trace element patterns in andesites, dacites and rhyodacites (high La/Yb, Sr/Y, La/Ta, low Yb, Ta) appear to be effects of residual garnet and rutile left after partial melting of MORB eclogite in the subducting oceanic crust. High Mg# values in the andesites, dacites and rhyodacites, and high Cr and Ni abundances relative to SiO_2 and MgO, are interpreted to reflect interaction between high-Si melts from the subducting plate and peridotite in the overlying mantle wedge. Geochemical trends in isotope versus trace element ratio plots show that western seafloor lavas define end-member compositions with more strongly fractionated trace elements patterns (low Yb/Nd, Ta/Th, Ce/Pb) and more depleted (MORB-like) isotopic compositions than common volcanic rocks of the central and eastern Aleutian arc. This end-member is interpreted to be the expression of an eclogite melt source component, which is produced by partial melting of subducted basalt in the eclogite facies, and which appears to be present in all Aleutian lavas. Mass-balance modeling indicates that $\sim$15–50% of the LREE and Hf in Aleutian lavas is derived from this source component. Trace element patterns in Aleutian lavas are interpreted to be controlled by a residual mineralogy (garnet, rutile ± allanite/monazite) that is stabilized during eclogite-melting reactions over a range of temperatures. The presence of high-silica, eclogite melts in the Aleutian mantle wedge also suggests a role for pyroxenite formation by melt–rock reaction, and the formation of low-density diapirs of eclogite melt + reaction pyroxenite.

ACKNOWLEDGEMENTS

The authors thank G. Hart and C. Knaack for technical help at the ICP-MS facility at Washington State University. Thanks also go to C. Wyatt, J. Bryant, J. Turka, S. Arndt and M. Siegrist for their assistance with data collection at the University of South Carolina, and to J. Blusztajn for his assistance at Woods Hole. The cooperation of S. M. Kay, R. W. Kay and B. D. Marsh, who provided samples for this study, is also gratefully acknowledged. Thanks also go to T. Murray, T. Miller and others at the US Geological Society and Alaska Volcano Observatory for their generous support. Support for S.T.B., during manuscript preparation was provided by the Director, Office of Science, Office of Basic Energy Sciences, of the U.S. Department of Energy under Contract No. DE-AC02-05CH11231.

FUNDING

This work was supported by National Science Foundation grants EAR-0230261 to J.D.V.; EAR-0510671 to K.W.W.S.; EAR-0230145, EAR-0509922, EAR-0236481, OCE-0242585 and OCE-0728077 to G.M.Y.; and OCE-0242233, OCE-0533226, OCE-1144759, EAR-0727013, EAR-0961359 and EAR-0742368 to P.B.K. This work was also supported by the German Ministry for Education and Research grants Sonne cruise SO201 Leg1b and KALMAR B subproject 3B to K.A.H.

SUPPLEMENTARY DATA

Supplementary data for this paper are available from *Journal of Petrology* online.

REFERENCES

Abouchami, W., Galer, S. J. G. & Koschinsky, A. (1999). Pb and Nd iotopes in NE Atlantic Fe–Mn crusts: proxies for trace metal paleosources and paleocean circulation. *Geochimica et Cosmochimica Acta* **63**, 1489–1505.

Abratis, M. & Wörner, G. (2001). Ridge collision, slab-window formation, and the flux of Pacific asthenosphere into the Caribbean realm. *Geology* **29**, 127–130.

Alonzo-Perez, R., Müntener, O. & Ulmer, P. (2009). Igneous garnet and amphibole fractionation in the roots of island arcs: experimental constraints on andesitic liquids. *Contributions to Mineralogy and Petrology* **157**, 541–558.

Arculus, R. J. & Powell, R. (1986). Source component mixing in the regions of arc magma generation. *Journal of Geophysical Research* **91**, 5913–5926.

Armstrong, R. L. (1971). Isotopic and chemical constraints on models of magma genesis in volcanic arcs. *Earth and Planetary Science Letters* **12**, 137–142.

Avé Lallemant, H. G. & Oldow, J. (2000). Active displacement partitioning and arc-parallel extension of the Aleutian volcanic arc based on Global Positioning System geodesy and kinematic analysis. *Geology* **28**, 739–742.

Ayers, J. C. (1998). Trace element modeling of aqueous fluid–peridotite interaction in the mantle wedge of subduction zones. *Contributions to Mineralogy and Petrology* **132**, 390–404.

Bach, W., Hegner, E., Erzinger, J. & Satir, M. (1994). Chemical and isotopic variations along the superfast spreading East Pacific Rise from 6 to 30°S. *Contributions to Mineralogy and Petrology* **116**, 365–380.

Baranov, B. C., Seliverstov, N. I., Murav'ev, A. V. & Muzurov, E. L. (1991). The Komandorsky Basin as a product of spreading behind a transform plate boundary. *Tectonophysics* **199**, 237–269.

Beier, C., Turner, S. P., Sinton, J. M. & Gill, J. B. (2010). Influence of subducted components on back-arc melting dynamics in the Manus Basin. *Geochemistry, Geophysics, Geosystems* **11**, 21.

Berndt, J., Koepke, J. & Holtz, F. (2005). An experimental investigation of the influence of water and oxygen fugacity on differentiation of MORB at 200 MPa. *Journal of Petrology* **46**, 135–167.

Botcharnikov, R. E., Almeev, R. R., Koepke, J. & Holtz, F. (2008). Phase relations and liquid lines of descent in hydrous ferrobasalt—implication for the Skaergaard Intrusion and Columbia River Flood Basalts. *Journal of Petrology* **49**, 1687–1727.

Bouvier, A., Vervoort, J. D. & Patchett, P. J. (2008). The Lu–Hf and Sm–Nd isotopic composition of CHUR: constraints from unequilibrated chondrites and implications for the bulk composition of terrestrial planets. *Earth and Planetary Science Letters* **273**, 48–57.

Brenan, J. M., Shaw, H. F., Ryerson, R. J. & Phinney, D. L. (1995). Mineral–aqueous fluid partitioning of trace elements at 900°C and 2·0 GPa: constraints on trace element chemistry of mantle and deep crustal fluids. *Geochimica et Cosmochimica Acta* **59**, 3331–3350.

Brophy, J. G. & Marsh, B. D. (1986). On the origin of high-alumina arc basalt and the mechanics of melt extraction. *Journal of Petrology* **27**, 763–789.

Brown, S. T., Yogodzinski, G. M., Vervoort, J. D. & Gerseny, M. G. (2005). Hafnium in Aleutian lavas: isotopic and trace element evidence for slab melting. Abstract V34A-07 presented at the 2005 Fall Meeting, AGU, San Francisco, CA, 5–9 December.

Bryant, J. A., Yogodzinski, G. M. & Churikova, T. G. (2010). High-Mg# andesitic lavas of the Shisheisky Complex, Northern Kamchatka: implications for primitive calc-alkaline magmatism. *Contributions to Mineralogy and Petrology* **161**, 791–810.

Cai, Y., LaGatta, A. B., Goldstein, S. L., Langmuir, C. H., Gomez-Tuena, A., Martin-Del Pozzo, A. L. & Carrasco-Nunez, G. (2014). Hafnium isotope evidence for slab melt contributions in the Central Mexican Volcanic Belt and implications for slab melting in hot and cold slab arcs. *Chemical Geology* **377**, 45–55.

Carmichael, I. S. E. (2002). The andesite aqueduct: perspectives on the evolution of intermediate magmatism in west–central (105–99°W) Mexico. *Contributions to Mineralogy and Petrology* **143**, 641–663.

Castillo, P. R., Natland, J. H., Niu, Y. & Lonsdale, P. F. (1998). Sr, Nd, and Pb isotopic variation along the Pacific–Antarctic risecrest, 53°–57°S: implications for the composition and dynamics of the South Pacific upper mantle. *Earth and Planetary Science Letters* **154**, 109–125.

Castillo, P. R., Klein, E., Bender, J., Langmuir, C., Shirey, S., Batiza, R. & White, W. (2000). Petrology and Sr, Nd, and Pb isotope geochemistry of mid-ocean ridge basalt glasses from the 11.45°N to 15.00°N segment of the East Pacific Rise. *Geochemistry, Geophysics, Geosystems* **1**, doi:10.1029/1999GC000024.

Chauvel, C. & Blichert-Toft, J. (2001). A hafnium isotope and trace element perspective on melting of the depleted mantle. *Earth and Planetary Science Letters* **190**, 137–151.

Class, C. & Lehnert, K. (2012). PetDB Expert MORB (Mid-Ocean Ridge Basalt) Compilation. EarthChem Library. http://dx.doi.org/10.1549/IEDA/100060.

Class, C., Miller, D. M., Goldstein, S. L. & Langmuir, C. H. (2000). Distinguishing melt and fluid subduction components in Umnak Volcanics, Aleutian Arc. *Geochemistry, Geophysics, Geosystems*, doi:10.1029/1999GC000010.

Coombs, M. L. & Jicha, B. R. (2013). Geology and ^{40}Ar/^{39}Ar geochronology of Akutan Volcano, eastern Aleutian Islands. Abstract V21C-2747 presented at the Fall Meeting, AGU, San Francisco, CA, 9–13 December.

Cooper, L. B., Ruscitto, D. M., Plank, T., Wallace, P. J., Syracuse, E. M. & Manning, C. E. (2012). Global variations in H2O/Ce: 1. Slab surface temperatures beneath volcanic arcs.

Geochemistry, Geophysics, Geosystems **13**, doi:10.1029/2011GC003902.

Cross, R. S. & Freymueller, J. T. (2008). Evidence for and implications of a Bering plate based on geodetic measurements from the Aleutians and western Alaska. *Journal of Geophysical Research* **113**, doi:10.1029/2007JB005136.

Davidson, J., Turner, S., Handely, H., Macpherson, C. & Dosseto, A. (2007). Amphibole 'sponge' in arc crust? *Geology* **35**, 787–790.

Davis, A. S., Clague, D. A., Cousens, B. L., Keaten, R. & Paduan, J. B. (2008). Geochemistry of basalt from the North Gorda segment of the Gorda Ridge: evolution toward ultraslow spreading ridge lavas due to decreasing magma supply. *Geochemistry, Geophysics, Geosystems*, 9, doi:10.1029/2007GC001775.

Defant, M. J. & Drummond, M. S. (1990). Derivation of some modern arc magmas by melting of young subducted lithosphere. *Nature* **347**, 662–665.

DePaolo, D. J. (1981). Trace element and isotopic effects of combined wall rock assimilation and fractional crystallization. *Earth and Planetary Science Letters* **53**, 189–202.

Draper, D. S. & Johnston, A. D. (1992). Anhydrous *PT* phase relations of an Aleutian high-MgO basalt: an investigation of the role of olivine–liquid reaction in the generation of arc high-alumina basalts. *Contributions to Mineralogy and Petrology* **112**, 501–519.

Drummond, M. S. & Defant, M. J. (1990). A model for trondhjemite–tonalite–dacite genesis and crustal growth via slab melting: archean to modern comparisons. *Journal of Geophysical Research* **95**, 21503–21521.

Duggen, S., Portnyagin, M., Baker, J., Ulfbeck, D., Hoernle, K., Garbe-Schönberg, D. & Grassineau, N. (2007). Drastic shift in lava geochemistry in the volcanic-front to rear-arc region of the Southern Kamchatkan subduction zone: evidence for the transition from slab surface dehydration to sediment melting. *Geochimica et Cosmochimica Acta* **71**, 452–480.

Eggler, D. H. (1987). Solubility of major and trace elements in mantle metasomatic fluids: experimental constraints. In: Menzies, M. A. & Hawkesworth, C. J. (eds) *Mantle Metasomatism*. Academic Press, pp. 21–41.

Elliott, T., Plank, T., Zindler, A., White, W. & Bourdon, B. (1997). Element transport from slab to volcanic front at the Mariana arc. *Journal of Geophysical Research* **102**, 14991–15019.

England, P., Engdahl, R. & Thatcher, W. (2004). Systematic variation in the depths of slabs beneath arc volcanoes. *Geophysical Journal International* **156**, 377–408.

Foley, S., Tiepolo, M. & Vannucci, R. (2002). Growth of early continental crust controlled by melting of amphibolite in subduction zones. *Nature* **417**, 837–840.

Foley, S. F., Barth, M. G. & Jenner, G. A. (2000). Rutile/melt partition coefficients for trace elements and an assessment of the influence of rutile on the trace element characteristics of subduction zone magmas. *Geochimica et Cosmochimica Acta* **64**, 933–938.

Fournelle, J. H., Marsh, B. D. & Myers, J. D. (1994). Age, character, and significance of Aleutian arc volcanism. In: Plafker, G. & Berg, H. C. (eds) *The Geology of Alaska*. Boulder, CO: Geological Society of America, pp. 723–758.

Fujii, N. & Oamura, K. (1986). Effect of water saturation on the distribution of partial melt in the olivine–pyroxene–plagioclase system. *Journal of Geophysical Research* **91**, 9253–9259.

Galer, S. J. G. & Abouchami, W. (1998). Practical application of lead triple spiking for correction of instrumental mass discrimination. *Mineralogical Magazine* **62A**, 491–492.

Gerya, T. V. & Yuen, D. A. (2003). Rayleigh–Taylor instabilities from hydration and melting propel 'cold plumes' at subduction zones. *Earth and Planetary Science Letters* **212**, 47–62.

Gerya, T. V., Yuen, D. A. & Sevre, E. O. D. (2004). Dynamical causes for incipient magma chambers above slabs. *Geology* **32**, 89–92.

Gill, J. (1981). *Orogenic Andesites and Plate Tectonics*. Springer.

Green, T. H. (1982). Anatexis of mafic crust and high pressure crystallization of andesite. In: Thorpe, R. S. (ed.) *Orogenic Andesites and Related Rocks*. John Wiley, pp. 465–487.

Grove, T., Parman, S. W., Bowring, S. A., Price, R. & Baker, M. B. (2002). The role of an H_2O-rich fluid component in the generation of primitive basaltic andesites and andesites from the Mt. Shasta region, N California. *Contributions to Mineralogy and Petrology* **142**, 375–396.

Grove, T. L., Elkins-Tanton, L. T., Parman, S. W., Chatterjee, N., Müntener, O. & Gaetani, G. A. (2003). Fractional crystallization and mantle-melting controls on calc-alkaline differentiation trends. *Contributions to Mineralogy and Petrology* **145**, 515–533.

Grove, T. L., Baker, M. B., Price, T. D., Parman, S. W., Elkins-Tanton, L. T., Chatterjee, N. & Müntener, O. (2005). Magnesian andesite and dacite lavas from Mt. Shasta, northern California: products of fractional crystallization of H2O-rich mantle melts. *Contributions to Mineralogy and Petrology* **148**, 542–565.

Hahm, D., Castillo, P. R. & Hilton, D. R. (2009). A deep mantle source for high ^{3}He/^{4}He ocean island basalts (OIB) inferred from Pacific near-ridge seamount lavas. *Geophysical Research Letters* **36**.

Hamelin, C., Dosso, L., Hana, B. B., Moreira, M., Kositsky, A. P. & Thomas, M. Y. (2011). Geochemical portray of the Pacific Ridge: new isotopic data and statistical techniques. *Earth and Planetary Science Letters* **302**, 154–162.

Handley, H. K., Turner, S., Macpherson, C. G., Gertisser, R. & Davidson, J. P. (2011). Hf–Nd isotope and trace element constraints on subduction inputs at island arcs: limitations of Hf anomalies as sediment input indicators. *Earth and Planetary Science Letters* **304**, 212–223.

Hart, S. R. (1984). A large-scale isotope anomaly in the Southern Hemisphere mantle. *Nature* **309**, 753–757.

Hawkesworth, C. J., Gallagher, K., Hergt, J. M. & McDermott, F. (1993). Mantle and slab contributions in arc magmas. *Annual Review of Earth and Planetary Sciences* **21**, 175–204.

Hawkesworth, C. J., Turner, S. P., Peate, D. W., McDermott, F. & van Calsteren, P. (1997). Elemental U and Th variations in island arc rocks: implications for U-series isotopes. *Chemical Geology* **139**, 207–221.

Hayes, G. P., Wald, D. J. & Johnon, R. L. (2012). Slab 1.0: A three-dimensional model of global subduction zone geometries. *Journal of Geophysical Research* **117**, doi:10.1029/2011JB008524.

Hegner, E. & Tatsumoto, M. (1987). Pb, Sr, and Nd isotopes in basalts and sulfides from the Juan de Fuca Ridge. *Journal of Geophysical Research* **92**, 11380–11386.

Hermann, J. (2002). Allanite: thorium and light rare earth element carrier in subducted crust. *Chemical Geology* **192**, 289–306.

Hermann, J. & Rubatto, D. (2009). Accessory phase control on the trace element signature of sediment melts in subduction zones. *Chemical Geology* **265**, 512–526.

Hildreth, W. & Moorbath, S. (1988). Crustal contributions to arc magmatism in the Andes of central Chile. *Contributions to Mineralogy and Petrology* **98**, 455–489.

Hoernle, K., Abt, D. L., Fischer, K. M., Nichols, H., Hauff, F., Abers, G. A., van den Bogaard, P., Heydolph, K., Alvarado, G., Protti, M. & Strauch, W. (2008). Arc-parallel flow in the mantle wedge beneath Costa Rica and Nicaragua. *Nature* **451**, 1094–1097.

Ito, E., White, W. M. & Göpel, C. (1987). The O, Sr, Nd, and Pb isotope geochemistry of MORB. *Chemical Geology* **62**, 1957–1976.

Jicha, B., Coombs, M. L., Calvert, A. T. & Singer, B. S. (2012). Geology and ^{40}Ar/^{39}Ar geochronology of the medium- to high-K Tanaga volcanic cluster, western Aleutians. *Geological Society of America Bulletin* **124**, 842–856.

Jicha, B. R., Singer, B. S., Brophy, J. G., Fournelle, J. H., Johnson, C. M., Beard, B. L., Lapen, T. J. & Mahlen, N. J. (2004). Variable impact of the subducted slab on Aleutian Island Arc magma sources: evidence from Sr, Nd, Pb and Hf isotopes and trace element abundances. *Journal of Petrology* **45**, 1845–1875.

Jicha, B. R., Singer, B. S., Beard, B. L. & Johnson, C. M. (2005). Contrasting timescales of crystallization and magma storage beneath the Aleutian island arc. *Earth and Planetary Science Letters* **236**, 195–210.

John, T., Klemd, R., Klemme, S., Pfänder, J. A., Hoffmann, J. E. & Gao, J. (2011). Nb–Ta fractionation by partial melting at the titanite–rutile transition. *Contributions to Mineralogy and Petrology* **161**, 35–45.

Johnson, M. C. & Plank, T. (1999). Dehydration and melting experiments constrain the fate of subducted sediments. *Geochemistry, Geophysics, Geosystems* **1**, 26.

Kay, R. W. (1978). Aleutian magnesian andesites: melts from subducted Pacific ocean crust. *Journal of Volcanology and Geothermal Research* **4**, 117–132.

Kay, R. W. (1980). Volcanic arc magma genesis: implications for element recycling in the crust–upper mantle system. *Journal of Geology* **88**, 497–522.

Kay, R. W., Sun, S. S. & Lee-Hu, C. N. (1978). Pb and Sr isotopes in volcanic rocks from the Aleutian Islands and Pribilof Islands, Alaska. *Geochimica et Cosmochimica Acta* **42**, 263–273.

Kay, S. M. & Kay, R. W. (1994). Aleutian magmas in space and time. In: Plafker, G. & Berg, H. C. (eds) *The Geology of Alaska*. Boulder, CO: Geological Society of America, pp. 687–722.

Kay, S. M., Ramos, V. A. & Marquez, Y. M. (1993). Evidence in Cerro Pampa volcanic rocks for slab-melting prior to ridge–trench collision in southern South America. *Journal of Geology* **101**, 703–714.

Kay, S. M., Tibbetts, A. & Jicha, B. R. (2014). The magmatic and tectonic evolution of Attu Island in the Near Islands of the Aleutian arc. *Geological Society of America, Abstracts with Programs* **46**, 448.

Kelemen, P. B. (1990). Reaction between ultramafic rock and fractionating basaltic magma I. Phase relations, the origin of calc-alkaline magma series, and the formation of discordant dunite. *Journal of Petrology* **31**, 51–98.

Kelemen, P. B. (1995). Genesis of high Mg# andesites and the continental crust. *Contributions to Mineralogy and Petrology* **120**, 1–19.

Kelemen, P. B., Joyce, D. B., Webster, J. D. & Holloway, J. R. (1990). Reaction between ultramafic rock and fractionating basaltic magma IZI. Experimental investigation of reaction between olivine tholeiite and harzburgite at 1150–1050°C and 5 kb. *Journal of Petrology* **31**, 99–134.

Kelemen, P. B., Shimizu, N. & Salters, V. J. M. (1995). Extraction of mid-ocean-ridge basalt from the upwelling mantle by focused flow of melt in dunite channels. *Nature* **375**, 747–753.

Kelemen, P. B., Hanghøj, K. & Greene, A. R. (2003a). One view of the geochemistry of subduction-related magmatic arcs, with an emphasis on primitive andesite and lower crust. In: Holland, H. D. & Turekian, K. K. (eds) *Treatise on Geochemistry*. Elsevier, pp. 593–659.

Kelemen, P. B., Yogodzinski, G. M. & Scholl, D. W. (2003b). Along-strike variation in lavas of the Aleutian Island Arc: Implications for the genesis of high Mg# andesite and the continental crust. In: Eiler, J. (ed.) *Inside the Subduction Factory. American Geophysical Union, Geophysical Monograph* **138**, 223–276.

Kelley, K. A. & Cottrell, E. (2009). Water and oxidation state of subduction zone magmas. *Science* **325**, 605–607.

Kelley, K. A., Plank, T., Ludden, J. N. & Staudigel, H. (2003). Composition of altered oceanic crust at ODP Sites 801 and 1149. *Geochemistry, Geophysics, Geosystems* **4**, 21.

Kelley, K. A., Plank, T., Grove, T. L., Stolper, E. M., Newman, S. & Hauri, E. H. (2006). Mantle melting as a function of water content beneath back-arc basins. *Journal of Geophysical Research* **111**, B09208, doi:10.1029/2005JB003732.

Kessel, R., Schmidt, M. W., Ulmer, P. & Pettke, T. (2005). Trace element signature of subduction-zone fluids, melts and supercritical liquids at 120–180 km depth. *Nature* **437**, 724–727.

Kincaid, C. & Sacks, I. S. (1997). Thermal and dynamical evolution of the upper mantle in subduction zones. *Journal of Geophysical Research* **102**, 12295–12315.

Klemme, S., Blundy, J. D. & Wood, B. J. (2002). Experimental constraints on major and trace element partitioning during partial melting of eclogitie. *Geochimica et Cosmochimica Acta* **66**, 3109–3123.

Klemme, S., Prowatke, S., Hametner, K. & Günther, D. (2005). Partitioning of trace elements between rutile and silicate melts: implications for subduction zones. *Geochimica et Cosmochimica Acta* **69**, 2361–2371.

Klimm, K., Blundy, J. D. & Green, T. H. (2008). Trace element partitioning and accessory phase saturation during H_2O-saturated melting of basalt with implications for subduction zone chemical fluxes. *Journal of Petrology* **49**, 523–553.

König, S., Schuth, S., Münker, C. & Qopoto, C. (2007). The role of slab melting in the petrogenesis of high-Mg andesites: evidence from Simbo Volcano, Solomon Islands. *Contributions to Mineralogy and Petrology* **153**, 85–103.

Krogh, T. E. (1973). A low-contamination method for hydrothermal decomposition of zircon and extraction of U and Pb for isotopic age determinations. *Geochimica et Cosmochimica Acta* **37**, 485–494.

Labanieh, S., Chauvel, C., Germa, A. & Quidelleur, X. (2012). Martinique: a clear case for sediment melting and slab dehydration as a function of distance to the trench. *Journal of Petrology* **53**, 2441–2464.

Lee, C. & King, S. D. (2010). Why are high-Mg# andesites widespread in the western Aleutians? A numerical model approach. *Geology* **38**, 583–586.

Levin, V., Shapiro, N., Park, J. & Ritzwoller, M. (2005). Slab portal beneath the western Aleutians. *Geology* **33**, 253–256.

Lopez-Escobar, L., Frey, F. A. & Vergara, M. (1977). Andesites and high-alumina basalts from the central–south Chile High Andes; geochemical evidence bearing on their petrogenesis. *Contributions to Mineralogy and Petrology* **63**, 199–228.

Lugmair, G. W. & Carlson, R. W. (1978). The Sm–Nd history of KREEP. *Proceedings of the 9th Lunar and Planetary Science Conference. Geochimica et Cosmochimica Acta Supplement* 689–704.

Luhr, J. F., Allan, J. F., Carmichael, I. S. E., Nelson, S. A. & Hasenaka, T. (1989). Primitive calc-alkaline and alkaline rock types from the Western Mexican Volcanic Belt. *Journal of Geophysical Research* **94**, 4515–4530.

MacPherson, G. J., Dreher, S. & Thirlwall, M. F. (2006). Adakites without slab melting: high pressure differentiation of island arc magma, Mindanao, the Philippines. *Earth and Planetary Science Letters* **243**, 581–593.

Mahoney, J. J., Sinton, J. M., Kurz, M. D., Macdougall, J. D., Spencer, K. J. & Lugmair, G. W. (1994). Isotope and trace element characteristics of a super-fast spreading ridge: east

Pacific rise, 13–23°S. *Earth and Planetary Science Letters* **121**, 173–193.

Mamani, M., Wörner, G. & Sempere, T. (2010). Geochemical variations in igneous rocks of the Central Andean orocline (13°S to 18°S): tracing crustal thickening and magma generation through time and space. *Geological Society of America Bulletin* **122**, 162–182.

Marsh, B. D. (1974). Benioff zone magmatism. *Journal of Geophysical Research* **79**, 1196–1206.

Martin, H. (1994). The Archean grey gneisses and the genesis of continental crust. In: Condie, K. C. (ed.) *Archean Crustal Evolution*. Elsevier Science, pp. 205–259.

McCulloch, M. T. & Gamble, J. A. (1991). Geochemical and geodynamical constraints on subduction zone magmatism. *Earth and Planetary Science Letters* **102**, 358–374.

McDermott, F. & Hawkesworth, C. J. (1991). Th, Pb, and Sr isotope variations in young island-arc volcanics and oceanic sediments. *Earth and Planetary Science Letters* **104**, 1–15.

McDonough, W. F. & Sun, S. (1995). The composition of the Earth. *Chem Geol.* **120**, 223–253.

Miller, D. M., Goldstein, S. L. & Langmuir, C. H. (1994). Cerium/lead and lead isotope ratios in arc magmas and the enrichment of lead in the continents. *Nature* **368**, 514–520.

Miyashiro, A. (1974). Volcanic rock series in island arcs and active continental margins. *American Journal of Science* **274**, 321–355.

Morris, J. D., Leeman, W. P. & Tera, F. (1990). The subducted component in island arc lavas: constraints from Be isotopes and B–Be systematics. *Nature* **344**, 31–35.

Muentener, O., Kelemen, P. & Grove, T. (2001). The role of H_2O during crystallization of primitive arc magmas under uppermost mantle conditions and genesis of igneous pyroxenites: an experimental study. *Contributions to Mineralogy and Petrology* **141**, 643–658.

Münker, C., Weyer, S., Scherer, E. & Mezger, K. (2001). Separation of high field strength elements (Nb, Ta, Zr, Hf) and Lu from rock samples for MC-ICPMS measurements. *Geochemistry, Geophysics, Geosystems*, 2, doi:10.1029/2001GC000183.

Müntener, O., Kelemen, P. & Grove, T. (2001). The role of H_2O during crystallization of primitive arc magmas under uppermost mantle conditions and genesis of igneous pyroxenites: an experimental study. *Contributions to Mineralogy and Petrology* **141**, 643–658.

Myers, J. D. & Frost, C. D. (1994). A petrologic re-investigation of the Adak volcanic center, central Aleutian arc, Alaska. *Journal of Volcanology and Geothermal Research* **60**, 109–146.

Myers, J. D. & Marsh, B. D. (1987). Aleutian lead isotopic data: additional evidence for the evolution of lithospheric plumbing systems. *Geochimica et Cosmochimica Acta* **51**, 1833–1842.

Myers, J. D., Marsh, B. D. & Sinha, A. K. (1985). Strontium isotopic and selected trace element variations between two Aleutian volcanic centers (Adak and Atka): implications for the development of arc volcanic plumbing systems. *Contributions to Mineralogy and Petrology* **91**, 221–234.

Niu, Y., Collerson, K. D. & Batiza, R. (1999). Origin of enriched-type mid-ocean ridge basalt at ridges far from mantle plumes: the East Pacific Rise at 11°20′ N. *Journal of Geophysical Research* **104**, 7067–7087.

Niu, Y. L., Regelous, M., Wendt, I. J., Batiza, R. & O'Hara, M. J. (2002). Geochemistry of near-EPR seamounts: importance of source vs. process and the origin of enriched mantle component. *Earth and Planetary Science Letters* **199**, 327–345.

Patchett, J. P. & Tatsumoto, M. (1980). A routine high-precision method for Lu–Hf isotope geochemistry and chronology. *Contributions to Mineralogy and Petrology* **75**, 263–267.

Patchett, P. J. & Ruiz, J. (1987). Nd isotopic ages and crust formation and metamorphism in the Precambrian of eastern and southern Mexico. *Contributions to Mineralogy and Petrology* **96**, 523–528.

Pearce, J. A. & Norry, M. J. (1979). Petrogenetic implications of Ti, Zr, Y, and Nb variations in volcanic rocks. *Contributions to Mineralogy and Petrology* **69**, 33–47.

Pearce, J. A., Kempton, P. D., Nowell, G. M. & Noble, S. R. (1999). Hf–Nd element and isotope perspective on the nature and provenance of mantle and subduction components in western Pacific arc–basin systems. *Journal of Petrology* **40**, 1579–1611.

Perfit, M. R., Gust, D. A., Bence, A. E., Arculus, R. J. & Taylor, S. R. (1980). Chemical characteristics of island-arc basalts: implications for mantle sources. *Chemical Geology* **30**, 227–256.

Pertermann, M., Hirschmann, M. M., Hametner, K., Günther, D. & Schmidt, M. W. (2004). Experimental determination of trace element partitioning between garnet and silica-rich liquid during anhydrous partial melting of MORB-like eclogite. *Geochemistry, Geophysics, Geosystems* **5**, 23.

Petford, N. & Atherton, M. (1996). Na-rich partial melts from newly underplated basaltic crust: the Cordillera Blanca Batholith, Peru. *Journal of Petrology* **37**, 1491–1521.

Peucker-Ehrenbrink, B., Hofmann, A. W. & Hart, S. R. (1994). Hydrothermal lead transfer from mantle to continental crust: the role of metalliferous sediments. *Earth and Planetary Science Letters* **125**, 129–142.

Plank, T. (2005). Constraints from thorium/lanthanum on sediment recycling at subduction zones and the evolution of continents. *Journal of Petrology* **46**, 921–944.

Plank, T. & Langmuir, C. (1992). Effects of the melting regime on the composition of the oceanic crust. *Journal of Geophysical Research* **97**, 19749–19770.

Plank, T. & Langmuir, C. H. (1993). Tracing trace elements from sediment input to volcanic output at subduction zones. *Nature* **362**, 739–742.

Plank, T. & Langmuir, C. H. (1998). The chemical composition of subducting sediment and its consequences for the crust and mantle. *Chemical Geology* **145**, 325–394.

Plank, T., Cooper, L. B. & Manning, C. E. (2009). Emerging geothermometers for estimating slab surface temperatures. *Nature Geoscience* **2**, 611–615.

Poli, S. & Schmidt, M. W. (2002). Petrology of subducted slabs. *Annual Review of Earth and Planetary Sciences* **30**, 207–235.

Portnyagin, M., Bindeman, I., Hoernle, K. & Hauff, F. (2007a). Geochemistry of primitive lavas of the Central Kamchatka Depression: magma generation at the edge of the Pacific Plate. In: Eichelberger, J., Gordeev, E., Izbekov, P., Kasahara, M. & Lees, J. (eds) *Volcanism and Subduction: The Kamchatka Region. American Geophysical Union, Geophysical Monograph* **172**, 199–239.

Portnyagin, M., Hoernle, K., Plechov, P., Mironov, N. & Khubunaya, S. (2007b). Constraints on mantle melting and composition and nature of slab components in volcanic arcs from volatiles (H_2O, S, Cl, F) and trace elements in melt inclusions from the Kamchatka arc. *Earth and Planetary Science Letters* **255**, 53–69.

Rapp, R. P. (1995). Amphibole-out phase boundary in partially melted metabasalt, its control over liquid fraction and composition, and source permeability. *Journal of Geophysical Research* **100**, 15601–15610.

Rapp, R. P., Watson, E. B. & Miller, C. F. (1991). Partial melting of amphibolite/eclogite and the origin of Archean trondhjemites and tonalites. *Precambrian Research* **51**, 1–25.

Reay, A. & Parkinson, D. (1997). Adakites from Solander Island, New Zealand. *New Zealand Journal of Geology and Geophysics* **40**, 121–126.

Regelous, M., Niu, Y., Wendt, J. I., Batiza, R., Greig, A. & Collerson, K. D. (1999). Variations in the geochemistry of magmatism on the East Pacific Rise at 10°30′N since 800 ka. *Earth and Planetary Science Letters* **168**, doi:10.1016/S0012-821X(99)00048-5.

Regelous, M., Gamble, J. A. & Turner, S. P. (2010). Mechanism and timing of Pb transport from subducted oceanic crust and sediment to the mantle source of arc lavas. *Chemical Geology* **273**, 46–54.

Renne, P. R., Swisher, C. C., Deino, A. L., Karner, D. B., Owens, T. L. & DePaolo, D. J. (1998). Intercalibrations of standards, absolute ages and uncertainties in $^{40}Ar/^{39}Ar$ dating. *Chemical Geology* **145**, 117–152.

Ringwood, A. E. (1974). The petrological evolution of island arc systems. *Journal of the Geological Society, London* **130**, 183–204.

Rogers, G., Saunders, A. D., Terrell, D. J., Verma, S. P. & Marriner, G. F. (1985). Geochemistry of Holocene volcanic rocks associated with ridge subduction in Baja California, Mexico. *Nature* **315**, 389–392.

Romick, J. D., Kay, S. M. & Kay, R. W. (1992). The influence of amphibole fractionation on the evolution of calc-alkaline andesite and dacite tephra from the central Aleutians, Alaska. *Contributions to Mineralogy and Petrology* **112**, 101–118.

Rudnick, R. L. (1995). Making continental crust. *Nature* **378**, 571–577.

Rudnick, R. L. & Fountain, D. M. (1995). Nature and composition of the continental crust: a lower crustal perspective. *Reviews of Geophysics* **33**, 267–309.

Ruppert, N. A., Lees, J. M. & Kozyreva, N. P. (2007). Seismicity, earthquakes and structure along the Alaska–Aleutian and Kamchatka–Kurile subduction zones: a review. In: Eichelberger J., Gordeev, E., Kasahara, M., Izbekov, P. & Lees, J. (eds) *Volcanism and Subduction: The Kamchatka Region. American Geophysical Union, Geophysical Monograph* **172**.

Ryerson, F. J. & Watson, E. B. (1987). Rutile saturation in magmas: implications for Ti–Nb–Ta depletion in island-arc basalts. *Earth and Planetary Science Letters* **86**, 225–239.

Saha, A., Basu, A., Jacobsen, S., Poreda, R., Yin, Q. & Yogodzinski, G. M. (2005). Slab devolatilization and Os and Pb mobility in the mantle wedge of the Kamchatka arc. *Earth and Planetary Science Letters* **236**, 182–194.

Salters, V. J. M. & Stracke, A. (2003). Composition of the depleted mantle. *Geochemistry, Geophysics, Geosystems* **5**, doi:10.1029/2003GC000597.

Schmidt, M. W., Dardon, A., Chazot, G. & Vannucci, R. (2004a). The dependence of Nb and Ta rutile–melt partitioning on melt composition and Nb/Ta fractionation during subduction processes. *Earth and Planetary Science Letters* **226**, 415–432.

Schmidt, M. W., Vielzeuf, D. & Auzanneau, E. (2004b). Melting and dissolution of subducting crust at high pressures: the key role of white mica. *Earth and Planetary Science Letters* **228**, 65–84.

Scholl, D. W., Marlow, M. S., MacLeod, N. S. & Buffington, E. C. (1976). Episodic Aleutian Ridge igneous activity: implications of Miocene and younger submarine volcanism west of Buldir Island. *Geological Society of America Bulletin* **87**, 547–554.

Seliverstov, N. I., Baranov, B. V., Egorov, Y. O. & Shkira, V. A. (1990). New data on the structure of the southern Komandorsky Basin provided by cruise 26 of R/V VULKANOLOG. *Volcanology and Seismology* **10**, 499–524.

Sims, K. W., Goldstein, S. J., Blichert-Toft, J., Perfit, M. R., Kelemen, P. B., Fornari, D. J., Michael, P., Murrell, M. T., Hart, S. R., DePaolo, D. J., Layne, G. D., Ball, L., Jull, M. & Bender, J. (2002). Chemical and isotopic constraints on the generation and transport of magma beneath the East Pacific Rise. *Geochimica et Cosmochimica Acta* **66**, 3481–3504.

Singer, B., Jicha, B. R., Leeman, W. P., Rogers, N. W., Thirlwall, M. F., Ryan, J. & Nicolaysen, K. E. (2007). Along-strike trace element and isotopic variation in Aleutian island arc basalt: subduction melts sediments and dehydrates serpentine. *Journal of Geophysical Research* **112**, B06206.

Sisson, T. W. & Grove, T. L. (1993). Experimental investigations of the role of H_2O in calc-alkaline differentiation and subduction zone magmatism. *Contributions to Mineralogy and Petrology* **113**, 143–166.

Sisson, T. W., Ratajeski, K., Hankins, W. B. & Glazner, A. F. (2005). Voluminous granitic magmas from common basaltic sources. *Contributions to Mineralogy and Petrology* **148**, 635–661.

Skora, S. & Blundy, J. (2010). High-pressure hydrous phase relations of radiolarian clay and implications for the involvement of subducted sediment in arc magmatism. *Journal of Petrology* **51**, 2211–2243.

Stalder, R., Foley, S. F., Brey, G. P. & Horn, I. (1998). Mineral–aqueous fluid partitioning of trace elements at 900–1200°C and 3·0–5·7 GPa: new experimental data for garnet, clinopyroxene and rutile and implications for mantle metasomatism. *Geochimica et Cosmochimica Acta* **62**, 1781–1801.

Steiger, R. H. & Jäger, E. (1977). Subcommission on geochronology: convention on the use of decay constants in geo- and cosmochronology. *Earth and Planetary Science Letters* **36**, 359–362.

Stern, C. R. & Killian, R. (1996). Role of the subducted slab, mantle wedge and continental crust in the generation of adakites from the Andean Austral Volcanic Zone. *Contributions to Mineralogy and Petrology* **123**, 263–281.

Straub, S. M., Layne, G. D., Schmidt, A. & Langmuir, C. H. (2004). Volcanic glasses at the Izu arc volcanic front: new perspectives on fluid and sediment melt recycling in subduction zones. *Geochemistry, Geophysics, Geosystems* **5**, 40.

Straub, S. M., LaGatta, A. B., Martin-Del Pozzo, A. L. & Langmuir, C. H. (2008). Evidence from high-Ni olivines for a hybridized peridotite/pyroxenite source for orogenic andesites from the central Mexican Volcanic Belt. *Geochemistry, Geophysics, Geosystems* **9**, 33.

Straub, S. M., Gomez-Tuena, A., Stuart, F. M., Zellmer, G. F., Espinasa-Perena, R., Cai, Y. & Iizuk, Y. (2011). Formation of hybrid arc andesites beneath thick continental crust. *Earth and Planetary Science Letters* **303**, 337–347.

Sun, S. S. & McDonough, W. F. (1989). Chemical and isotopic systematics of oceanic basalts: implications for mantle composition and processes. In: Saunders, A. D. & Norry, M. J. (eds) *Magmatism in the Ocean Basins. Geological Society, London, Special Publications* **42**, 313–346.

Taras, B. D. & Hart, S. R. (1987). Geochemical evolution of the New England Seamount chain: isotopic and trace-element constraints. *Chemical Geology* **64**, 35–54.

Tatsumi, Y. (1982). Origin of high-magnesium andesites in the Setouchi volcanic belt, southwest Japan, II: Melting phase relations at high pressure. *Earth and Planetary Science Letters* **60**, 305–317.

Tatsumi, Y., Hamilton, D. L. & Nesbitt, R. W. (1986). Chemical characteristics of fluid phase released from a subducted lithosphere and origin of arc magmas: evidence from high-pressure experiments and natural rocks. *Journal of Volcanology and Geothermal Research* **29**, 293–309.

Taylor, R. S. & McLennan, S. M. (1995). The geochemical evolution of the continental crust. *Reviews of Geophysics* **33**, 241–265.

Tollstrup, D., Gill, J. B., Prinkey, D., Williams, R., Tamura, Y. & Ishizuka, O. (2010). Across-arc geochemical trends in the

Izu–Bonin arc: Contributions from the subducting slab, revisited. *Geochemistry, Geophysics, Geosystems* 11, 27.

Turner, S., Hawkesworth, C., van Calsteren, P., Heath, E., Macdonald, R. & Black, S. (1996). U-series isotopes and destructive plate margin magma genesis in the Lesser Antilles. *Earth and Planetary Science Letters* **142**, 191–207.

Vervoort, J. D. & Blichert-Toft, J. (1999). Evolution of the depleted mantle; Hf isotope evidence from juvenile rocks through time. *Geochimica et Cosmochimica Acta* **63**, 533–556.

Vervoort, J. D. & Patchett, P. J. (1996). Behavior of hafnium and neodymium isotopes in the crust: constraints from Precambrian crustally derived granites. *Geochimica et Cosmochimica Acta* **60**, 3717–3723.

Vervoort, J. D., Plank, T. & Prytulak, J. (2011). The Hf–Nd isotopic composition of marine sediments. *Geochimica et Cosmochimica Acta* **75**, 5903–5926.

Vlastélic, I., Aslanian, D., Dosso, L., Bougault, H., Olivet, J. L. & Geli, L. (1999). Large-scale chemical and thermal division of the Pacific mantle. *Nature* **399**, 345–350.

Walker, J. A., Patino, L. C., Carr, M. J. & Feigenson, M. D. (2001). Slab control over HFSE depletions in central Nicaragua. *Earth and Planetary Science Letters* **192**, 533–543.

Waters, C. L., Sims, K. W. W., Perfit, M. R., Blichert-Toft, J. & Blusztajn, J. (2011). Perspective on the genesis of E-MORB from chemical and isotopic heterogeneity at 9–10°N East Pacific Rise. *Journal of Petrology* **52**, 565–602.

Weaver, S. L., Wallace, P. J. & Johnston, A. D. (2011). A comparative study of continental vs. intraoceanic arc mantle melting: Experimentally determined phase relations of hydrous primitive melts. *Earth and Planetary Science Letters* **308**, 97–106.

Weber, R. M., Wallace, P. J. & Johnston, A. D. (2011). Experimental insights into the formation of high-Mg basaltic andesites in the trans-Mexican volcanic belt. *Contributions to Mineralogy and Petrology* **163**, 825–840.

Wedepohl, K. H. (1995). The composition of the continental crust. *Geochimica et Cosmochimica Acta* **59**, 1217–1232.

Wendt, J. I., Regelous, M., Niu, Y., Hekinian, R. & Collerson, K. D. (1999). Geochemistry of lavas from the Garrett Transform Fault: insights into mantle heterogeneity beneath the eastern Pacific. *Earth and Planetary Science Letters* **173**, 271–284.

Werner, R. & Hauff, F. (2009). *RV Sonne Fahrtbericht/Cruise Report SO201-1b: KALMAR (Kurile–Kamchatka and Aleutian Marginal Sea–Island Systems): Geodynamic and Climate Interaction in Space and Time, IFM-GEOMAR Report 32*. http://oeanrep.geomar.de/2923.

Wheller, G. E., Varne, R., Foden, J. D. & Abbott, M. J. (1987). Geochemistry of Quaternary volcanism in the Sunda–Banda arc, Indonesia, and three-component genesis of island-arc basaltic magmas. *Journal of Volcanology and Geothermal Research* **32**, 137–160.

White, S. M., Yogodzinski, G. M., Kelemen, P. B. & Scholl, D. W. (2007). Back-arc seamount distribution along the western Aleutian volcanic arc. Abstract V43D-1627 presented at 2007 Fall Meeting, AGU, San Francisco, CA, 10–14 December.

White, W. M., Hofmann, A. W. & Puchelt, H. (1987). Isotope geochemistry of Pacific mid-ocean ridge basalt. *Journal of Geophysical Research* **92**, 4881–4893.

White, W. M., Albarède, F. & Télouk, P. (2000). High-precision analysis of Pb isotope ratios using multi-collector ICP-MS. *Chemical Geology* **167**, 257–270.

Wolf, M. B. & Wyllie, P. J. (1994). Dehydration-melting of amphibolite at 10 kbar; the effects of temperature and time. *Contributions to Mineralogy and Petrology* **115**, 369–383.

Wood, B. J. & Turner, S. P. (2009). Origin of primitive high-Mg andesite: Constraints from natural examples and experiments. *Earth and Planetary Science Letters* **283**, 59–66.

Woodhead, J., Hergt, J., Greig, A. & Edwards, L. (2011). Subduction Hf-anomalies: mantle messenger, melting artifact or crustal process. *Earth and Planetary Science Letters* **304**, 231–239.

Woodhead, J., Stern, R. J., Pearce, J. A., Hergt, J. & Vervoort, J. D. (2012). Hf–Nd isotope variation in Mariana Trough basalts: The importance of 'ambient mantle' in the interpretation of subduction zone magmas. *Geology* **40**, 539–542.

Workman, R. K. & Hart, S. R. (2005). Major and trace element composition of the depleted MORB mantle (DMM). *Earth and Planetary Science Letters* **231**, 53–72.

Xiong, X. L., Adam, J. & Green, T. H. (2005). Rutile stability and rutile/melt HFSE partitioning during partial melting of hydrous basalt: implications for TTG genesis. *Chemical Geology* **218**, 339–359.

Yogodzinski, G. M. & Kelemen, P. B. (1998). Slab melting in the Aleutians: implications of an ion probe study of clinopyroxene in primitive adakite and basalt. *Earth and Planetary Science Letters* **158**, 53–65.

Yogodzinski, G. M., Rubenstone, J. L., Kay, S. M. & Kay, R. W. (1993). Magmatic and tectonic development of the western Aleutians: An oceanic arc in a strike-slip setting. *Journal of Geophysical Research* **98**, 11807–11834.

Yogodzinski, G. M., Volynets, O. N., Koloskov, A. V., Seliverstov, N. I. & Matvenkov, V. V. (1994). Magnesian andesites and the subduction component in a strongly calc-alkaline series at Piip Volcano, far western Aleutians. *Journal of Petrology* **35**, 163–204.

Yogodzinski, G. M., Kay, R. W., Volynets, O. N., Koloskov, A. V. & Kay, S. M. (1995). Magnesian andesite in the western Aleutian Komandorsky region: Implications for slab melting and processes in the mantle wedge. *Geological Society of America Bulletin* **107**, 505–519.

Yogodzinski, G. M., Lees, J. M., Churikova, T. G., Dorendorf, F., Wörner, G. & Volynets, O. N. (2001). Geochemical evidence for the melting of subducting oceanic lithosphere at plate edges. *Nature* **409**, 500–504.

Yogodzinski, G. M., Vervoort, J. D., Brown, S. T. & Gerseny, M. (2010). Subduction controls of Hf and Nd isotopes in lavas of the Aleutian island arc. *Earth and Planetary Science Letters* **300**, 226–238.

Zhu, W. & Hirth, G. (2003). A network model for permeability in partially molten rocks. *Earth and Planetary Science Letters* **212**, 407–416.

Zimmer, M. M., Plank, T., Hauri, E. H., Yogodzinski, G. M., Stelling, P., Larsen, J., Singer, B., Jicha, B., Mandeville, C. & Nye, C. J. (2010). The role of water in generating the calc-alkaline trend: new volatile data for Aleutian magmas and a new tholeiitic index. *Journal of Petrology* **51**, 2411–2444.